EXPERIMENTAL INVESTIGATION AND FORCE MODELING OF ORTHOGONAL CUTTING WITH THE EFFECT OF THIRD DEFORMATION ZONE

by

Ceren Çelebi

Submitted to the Graduate School of Engineering and Natural Sciences

in partial fulfillment ofthe requirements for the degree of

Master of Science

Sabancı University

January, 2014

i

EXPERIMENTAL INVESTIGATION AND FORCE MODELING OF ORTHOGONAL CUTTING WITH THE EFFECT OF THIRD DEFORMATION ZONE

Ceren ÇELEBİ

Industrial Engineering, MSc. Thesis, 2014

Thesis Supervisor: Prof. Dr. Erhan Budak

Abstract

Metal cutting is the most common manufacturing method used in various industries. There have been many investigations on the interaction between the cutting edge and the material in the first and the second deformation zones in order to understand the mechanics of the process. Investigations on the third deformation zone, on the other hand, have been limited although it may have significant effects on the process and the machined part. Especially in finishing operations where slow feed rates are used, the contributions of the edge and flank contacts on the total cutting force can be substantial. Furthermore, the third zone determines the surface quality and the integrity due to its direct contact with the finished surface. Despite of these important effects of the third zone, there is lack of analytical and practical methods for modeling and predictions of the third deformation zone in metal cutting which is the focus of the thesis.

In this study, an experimental analysis of cutting forces along with the thermal investigation of third deformation zone is presented. An orthogonal cutting model including a thermo-mechanical model with sticking and sliding contact zones is developed in order to determine the effects of hone radius and flank contact on cutting forces. Different approaches such as full and elastic recovery of the material are considered for contact length calculations. Predictions of the proposed model are compared with the measurements and. it is shown that the model predictions are reasonably comparable to the experimental data with close trends.

ÖZET

Ceren ÇELEBİ

Endüstri Mühendisliği, Yüksek Lisans Tezi, 2014

Tez Danışmanı: Prof. Dr. ErhanBudak

AnahtarKelimeler: Dik Kesme Mekaniği, Kesme Ucu Yarıçapı, Talaşlı İmalat, Kenar Kuvvetleri

Üretim methodlarının en yaygını metal kesme işlemidir.Kesme mekaniğini anlamak amacıyla kesme ucu iş parçası etkileşimi ve birinci ve ikinci deformasyon bölgeleri hakkında bir çok araştırma yapılmıştır. Halbuki kesme işlemi ve kesilmiş iş parçası üzerinde önemli etkileri olmasına rağmen üçüncü deformasyon bölgesi hakkındaki araştırmalar sınırlıdır. Özellikle küçük ilerleme değerlerinin kullanıldığı ince işlemede kesici uç yuvartlatmasının ve boşluk açısı yüzeyinin kuvvetler üzerindeki etkisi çok önemlidir. Ayrıca bitmiş yüzey ile etkileşim halinde olduğundan yüzey kalitesi ve sürekliliği üzerinde de etkilidir. Bütün bu önemli etkilerine rağmen üçüncü deformasyon bölgesinin analitik modelleme ve deneysel çalışmalar konusunda eksik alanlar bulunmaktadır.

Bu çalışmada üçüncü deformasyon bölgesi kesme ucu yarıçapının etkisini görmek amacıyla mekanik ve termal deneylerle incelenmiştir. Kesme ucu yuvarlatması ve boşluk açısı yüzeyinin etkilerini göz önüne alıp termomekanik malzeme modelini veyapışan ve kayar sürtünme bölgelerini kapsayan bir dik kesme modeli oluşturulmuş ve farklı temas uzunluğu varsayımları yapılmıştır. Sunulan modelin sonuçları deneysel verilerle karşılaştırılmıştır. Modelin kuvvet trendlerini ve toplam kuvvetleriiyi tahmin ettiği görülmüştür.

Acknowledgement

to loved ones…

TABLE OF CONTENTS

List of Figures

List of Tables

xiv

NOMENCLATURE

Y: shear strain

$\dot{Y}$: shear strain rate

$\dot{Y}_0$: reference shear strain rate

T_m: melting temperature of the material

T_{ref}: reference temperature

T: absolute temperature

P: normal pressure distribution

P_0: normal pressure constant

θ_s : stagnation angle

ɤ : clearance angle

χ: distance from the stagnation point

l_{ce}: contact length after stagnation point

ℓ_{ce}': measured contact length

ζ: stress distribution exponent

τ_0: shear stress at the beginning of the primary shear zone

μ : sliding friction coefficient between tool and workpiece

l_{pe} :sticking contact length

V_c: cutting speed

h_p: ploughing depth

h_f: final height

CHAPTER 1 INTRODUCTION

1.1. Introduction & Literature Review

Machining is the most common manufacturing technique which can be applied to various materials (wood, metals, polymers etc.) in a wide range of industrial areas (automotive, aerospace, electronics etc.). It involves several methods including turning, milling, drilling, broaching and others, all work in a similar principle that material removing by a cutting tool.

Being one of the most important parameters in cutting tools, hone radius have important effects on the cutting mechanics, dynamics, surface quality, tool life and overall production efficiency. The common assumption of the cutting edge to be sharp is not possible when it comes to application, there is roundness on the edge which can be controlled but cannot be eradicated. Some brands purposely round the tool edge based on observations such as a large hone radius preventing chipping of the tool edge and also being useful for vibration damping [1, 2].

The basic orthogonal cutting model with a hone radiused tool is shown in Figure 1.1.Point A is defined as the stagnation point, where the material just above this point creates a chip while the lower sections plough under the tool and form the flank contact. Region above stagnation point (AB) represents the primary and secondary shear zones whereas below stagnation point (AC) represents the third deformation zone.
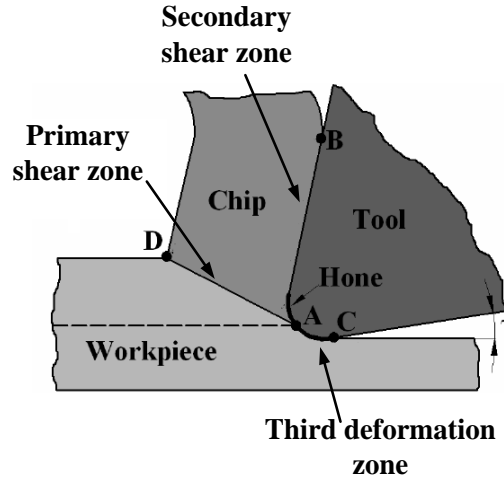
Figure 1.1. Deformation zones in orthogonal cutting. [3]

Different deformation zones result in forces with two components, cutting forces and edge (third deformation zone) forces.Cutting forces can be calculated most basically as follows [4]:

$$F_t = F_{tc} + F_{te} \tag{1.1}$$

$$F_t = F_{tc} + F_{te} \tag{1.2}$$

where, F_t is the tangential force, $F_f$is the feed force, F_{tc} is the tangential cutting force, F_{fc} is the feed cutting force, F_{fe} is the feed edge force and F_{te} is the tangential edge force.

Many aspects of the cutting process are investigated by researchers for many years; and mechanical modeling of the orthogonal cutting has been the most common challenge since orthogonal cutting is the base for many other cutting processes. In one of the earlier studies, Merchant [5] developed a mathematical model for the orthogonal cutting process. Although numerous models have been proposed for primary and secondary shear zones, there are few models covering the third deformation zone and edge forces. Albrecht [6] introduced hone radiused tools in his studies and presented a force diagram including ploughing forces to Merchant's conventional force diagram. Later, Manjunathaihah and Endres [7] developed an analytical model which includes the effect of hone radius explicitly by studying deformation under the hone edge. In a later study Kountanya and Endres [8] used high magnification experiments in order to verify the aforementioned model. It is found out that the basic model is not sufficient in order to represent the deformation in front of the hone radius and a model which includes the deformation precisely is needed. Waldorf et al. [9] compared forces which are obtained from the models based on stagnation angle and stable build up edge for 6061-T6

2

Aluminum. As the result of indentation and cutting tests, it is found that stable build up edge model gives better results. Shatla et al. [10], on the other hand, introduced Oxley's theory [11], and implemented a computerized methodology for flow stress determination at high strains, strain rates and temperatures with a sharp tool assumption where Shatla et al. [12] compared the model results with the FEA solutions considering different edge geometries. The results indicated that chamfered edge has the lowest temperatures, and smaller hone radius decreases the possibility of chipping. In another study, Guo and Chou [13] experimentally investigated non-cyclic forces and stated that with flow stress correction linear regression fitting is acceptable to be used to estimate ploughing forces. In a recent study, Salvatore et al. [14] analytically modeled third deformation zone with side burr formation, calibratingploughing and elastic recovery by used FEA and experimental analysis of disc cutting.

Slip-line field modeling has been widely used in modeling of third deformation zone. Fang [15] for instance, integrated previously developed slip-line models into a unified model, which accounts for different effects (shear zone cutting edge roundness, etc.) and can predict several machining parameters (forces, ploughing, contact length etc.). However the developed model was not verified. Waldorf [1], on the other hand, modified his slip line field model to make it compatible with 3D turning conditions, and compared experimental results of cutting with different edge geometries to model predictions. The results showed that increasing hone radius increases forces and process damping ratio. Budak and Tunç [2] also studied the effect of hone radius as well as other various tool geometry parameters and cutting conditions on process damping showing that bigger hone radius resulted in increased specific process damping. In a later study, Özel and Karpat [16] developed a slip line model for orthogonal cutting considering the dead metal zone for chamfered tools, and also a moving heat source model is proposed. The force model is compared with the experiments, where the temperature model is verified with FEM results yielding promising predictions. Moreover, Özel and Karpat [17] used artificial neural network (ANN) approach to predict surface roughness and tool flank wear in hard turning using tools with different edge preparations and obtained promising results. Also, Karpat and Özel [18] studied the effects of different edge preparations while trying to obtain tool chip friction characteristics using slip-line model. The results indicated that increased hone radius results in more serration of the chip, and waterfall hone gives the lowest forces.

Experimental studies are also carried out to understand the cutting process with honed cutting edge. Thiele and Melkote [19] conducted experiments using tools having different hone radii and chamfered edges in hard turning of AISI 52100 steel. It was observed that large hone radii increased average surface roughness due to higher ploughing forces. In another study, Kountanya and Endres [20] investigated the effects of the combinations of nose and hone radii on the tool flank wear experimentally. In order to improve the tool life it is recommended to use larger hone radius for large nose radiused tools. In a later study, Özel [21] conducted cutting experiments on AISI H13 tool steel using CBN cutting tools with two different edge preparations (honed and chamfered) where chamfered edge preparation resulted in higher stresses and cutting forces. Moreover, Özel et al. [22] experimentally and statistically investigated the effects of hone radius and feed rate in hard turning of AISI H13 steel with CBN tools, where honed edge gives better surface finish and smaller hone radius results in smaller edge forces. Later, Ranganath et al. [23] carried out tube turning tests with hone radiused tools and developed a mechanistic model for force prediction which includes the effects of chip thickness and rake angle. Model was calibrated for the tube turning of grey cast iron. In another study, Ceau et al. [24] experimentally investigated the temperature at the hone radius with thermocouples, infrared cameras and pyrometers to obtain an empirical relationship between temperature and cutting parameters. In a recent study, Wyen and Wegener [25] investigated the effect of hone radius on cutting forces and tool face friction in turning process of titanium experimentally. Ploughing forces were obtained by linear fitting of the thrust and feed forces. The results implied that both ploughing forces and friction coefficients are increasing with hone radius. It was also reported that increasing speed increases feed forces at large hone radii and decreases feed forces at smaller hones. Bassett et al. [26], investigated how the method of shaping cutting edge influences the thermo-mechanical load profile on the wedge, wear behavior and tool life in orthogonal turning process. It was indicated that choosing hone radius larger than the critical size results in heat induction with higher wear rates. The forces are found to be increasing with cutting speed and hones radii.

Finite element analysis has also been used widely used, mostly to see the effect on stress and strain conditions, and also temperature on the third deformation zone. For instance; Yen et al. [27] used FE simulations to investigate how hone geometry affects chip shape, cutting temperatures and forces. It was found out that due to increased

plastic deformation near chip-tool interface large hone radii and increased chamfer width resulted in increased tool rake temperatures. The results also showed that the hone geometry does not affect stress components significantly; and increasing chamfer width increases force components. In another study, Hua et al. [28] used numerical analysis to see the effect of hone radius and chamfer angle on residual stresses on machined surfaces of AISI 52100 steel. It was observed that increased hone radius resulted in increased maximum compressive residual stress and increased tool temperature; but the profile depth was almost unchanged. Also, it was stated that hone radius has more effect on cutting edge temperature than chamfered tool. Umbrello et al. [29] stated that residual stresses were affected by machining conditions, work piece material properties, cutting edge geometry; and introduced an ANN approach combined with FEM to predict residual stresses in hard turning more efficiently. It was reported that increased hone radii and chamfer angles result in higher compressive residual stresses in the subsurface, and an increase in the temperature and penetration depth. Fang and Fang [30], on the other hand, compared experiments with slip-line model and FEA results for finish turning of 6061-Al considering a rounded edge tool. It was indicated that a large stress and strain rate exists in the primary and tertiary deformation zones, and maximum temperature was observed around hone. Furthermore, Özel [31] performed FEM analysis (of 3D turning) and experiments with PCBN tools on turning of AISI 4340 steel, as a continuation to previous research in 2008 [32]. The effects of uniform and variable micro edge geometry on tool wear, chip formation, tool stresses, strain, and temperature fields are compared. It was found out that hone with variable micro geometry reduces heat generation, improves surface integrity and decreases wear rate. Moreover, Kountanya et al. [33] investigated effect of hone radius on chip morphology cutting forces with experiments and FEM analysis. It was reported that increasing hone radius increases forces and normal stress. Also, it was found that hone radius has no effect on the chip morphology.

1.2. Objective & Organization of the Thesis

As concluded from the aforementioned studies, previous researchers showed that cutting hone radius affects various aspects of the cutting process. Most of these studies are experimental or simulation based where slip-line model is used commonly for analytical modeling. Also it is interpreted that there is no unity between third deformation zone modeling when slip-line models are used and in most of the models

total forces are verified instead of third deformation zone forces. Studies are continuing in order to identify the third deformation zone using FEM analysis which can give more insight about the cutting process; however, the solution of process is limited with the software capabilities. Besides, the true friction between the tool and workpiece material cannot be identified both in the simulation programs and the force models. The objective of this research is to understand the mechanical and thermal behavior of the third deformation zone under different hone radii better; and to present a more clear third deformation representation including material behavior under the hone with friction state on tool-workpiece contact.

Experimental investigation of the cutting process with hone radiused tool and model representing the third deformation zone forces are presented in this thesis with the first time implementation of thermo-mechanical model with sticking and sliding contact zones. For the first and secondary deformation zones modeling the analytical model proposed by Özlü [3] is adopted.

The thesis structure is organized as follows: A detailed experimental investigation of the mechanical and temperature behavior of the third deformation zone is presented in Chapter 2. Modeling of the third deformation zone is presented in Chapter 3.The model results are compared to experimental data and the data taken from the literature and discussed in Chapter 4.Further verification of the implemented model in terms of thermal, frictional and stress behavior is presented in Chapter 4. Concluding remarks and future work are discussed in Chapter 5.

CHAPTER 2 EXPERIMENTAL INVESTIGATION WITH HONE RADIUSED TOOLS

In this section experimental studies about the orthogonal cutting process with hone radiused tools are presented. Measurement methods are explained and effects of different cutting conditions on total forces and edge forces are examined. Furthermore, thermal investigation of orthogonal cutting process is presented.

2.1. Experimental Investigation of Effect on Forces

2.1.1. Experimental Setup & Parameters

Orthogonal tube cutting tests using a coolant are conducted on Mori Seiki Lathe. AISI 1050 steel tube with 2 mm wall thickness is selected as the workpiece, while TPGN type 610 grade uncoated carbide tools having 5° rake angle, 6° clearance angle are used. To see the effect; four different hone radii (6, 20, 40, and 60 μm); four different cutting speed(30, 60, 100 and 250 m/min);and four different feed rates (0.05, 0.1, 0.15 and 0.2 mm/rev) are used. Tangential and feed forces are measured by Kistler table type dynamometer. Force data is collected with using LabVIEW software. Test setup and cutting process can be seen in Figure 2.1.

(a)

(b)
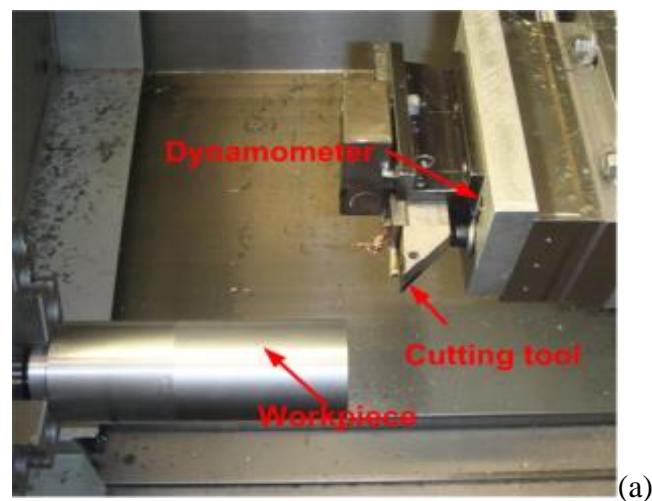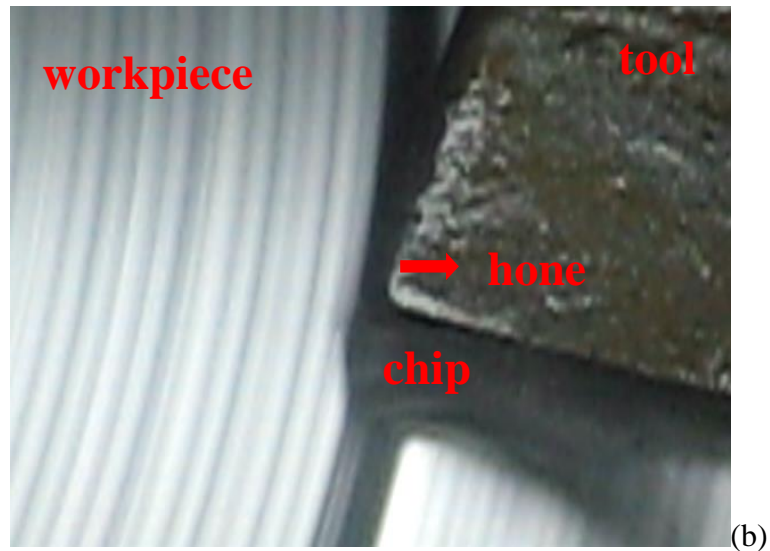
Figure 2.1. (a) Experimental Setup (b)Cutting process with hone radiused tool.

2.1.2. Hone Radius Measurements

It is essentially important to measure hone radius (Figure 2.2) precisely for each cutting experiment to understand the effect on cutting forces and modeling simulations. Also wear should be avoided for each test since it can increase hone radius at the cut region. Therefore, tool is measured along its cutting edge and in each test a new part of the tool is used.
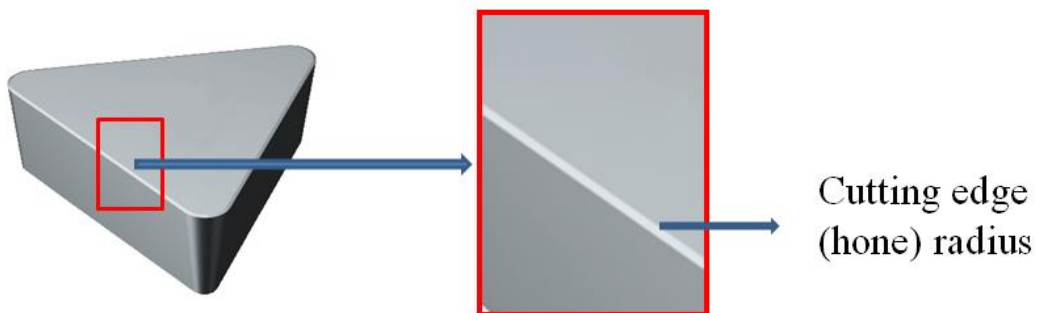
Figure 2.2.TPGN Tool cutting edge and hone radius.

Figure 2.3. Nanofocus μsurf explorer.

The measurements on the cutting edge were performed using Nanofocus μsurf Explorer (Figure 2.3). Firstly three dimensional (3D) profile of the tool (Figure 2.4) is extracted. Then sectional profile (Figure 2.5) of the tool edge is obtained from 3D profile. Finally a circle is fitted at the tool tip to determine hone radius. Hone radius is varying along the cutting edge, thus average of measurements are taken into consideration for each cutting region (Figure 2.6).

(a)   (b)
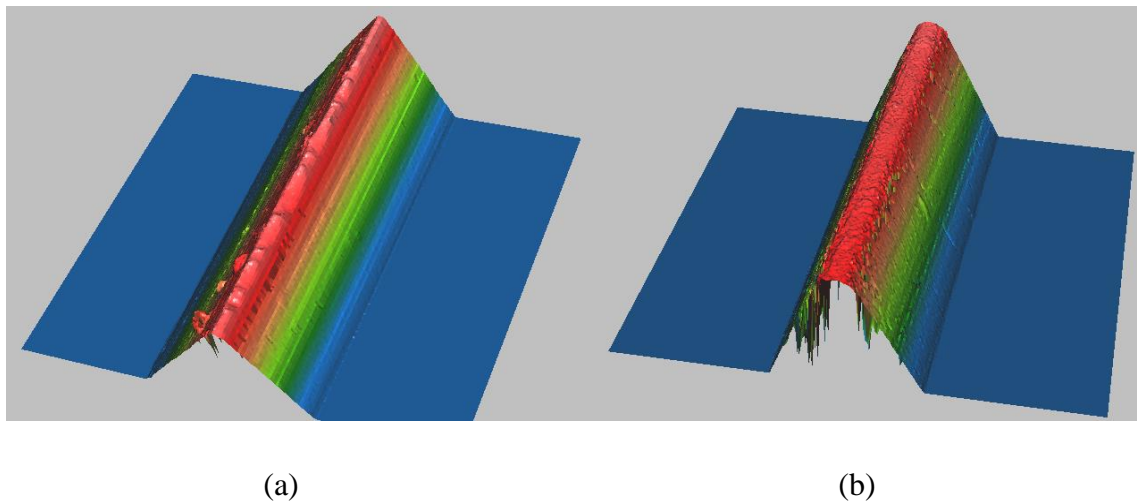
Figure 2.4. 3D profile of cutting edge of the cutting tools for (a) Tool with sharp edge (~10μm) (b)Tool with large hone radiused edge (~60μm)

9
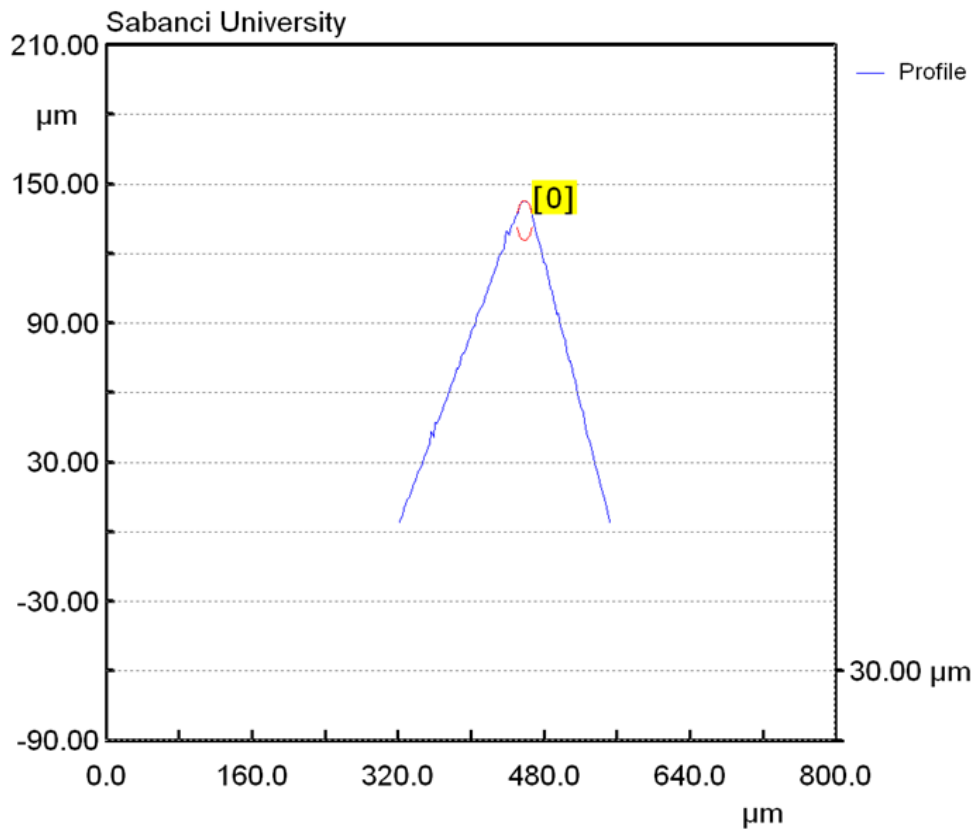
Figure 2.5. Section profile of the cutting edge.

Profile values
Radius = 6.20 µm

(a)

Profile values
Radius = 8.49 µm

b)
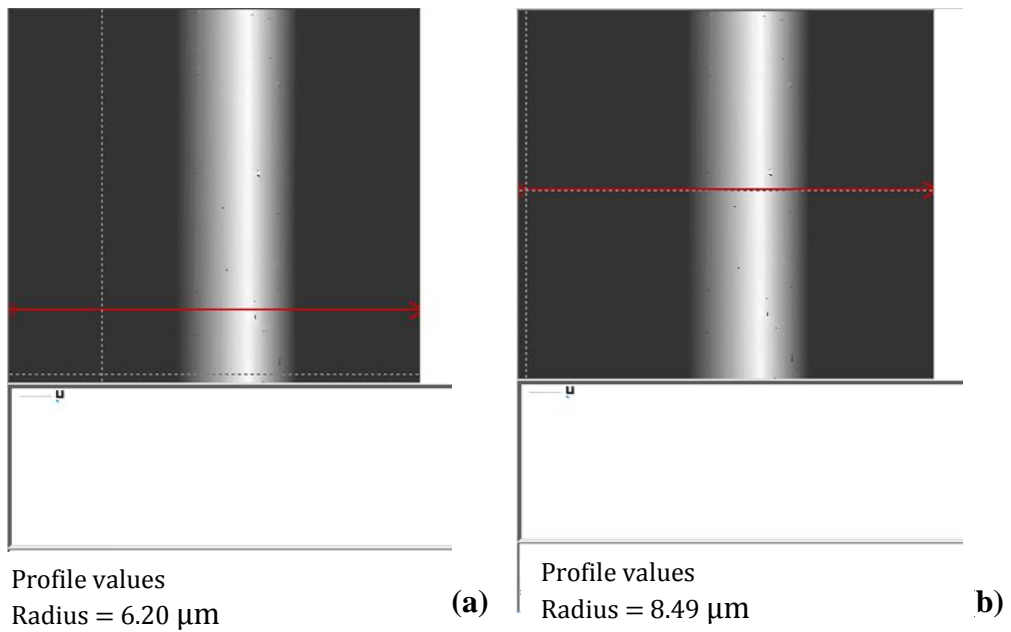
Figure 2.6. Varying hone radius at the cutting edge (a) Measured hone radius: 6.20µm
(b) Measured hone radius: 8.49µm.

2.1.3. Effect on Total Forces

The effects of feed and hone radius are examined for four different speeds (30, 60,100 and 250 m/min).The change of tangential and feed forces with hone radius, feed and speed are presented in Figure 2.7, Figure 2.8, Figure 2.9 and Figure 2.10. It is observed that both tangential and feed forces are increased with increased feed independent of speed and hone radius. It is also observed that increasing hone radius generally results in increase in the both tangential and feed forces; however the change is insignificant especially for smaller cutting speeds of 30 and 60 m/min (Figure 2.7 and Figure 2.8). The increase in forces is more observable at higher cutting speeds, which is still small due to increase rate of hone radius. For example, the maximum effect is observed on the test conducted with 250 m/min cutting speed at 0.2 mm/rev feed rate. Increasing hone radius from 6µm to 20µm (approximately 200% increase) changes feed forces to increase from 270 N to 355 N (23% increase) and tangential forces to increase from 300 N to 360 N (16% increase) (Figure 2.10). Also a force variation with hone radius is observed at 100 m/min (Figure Figure 2.9). This may be a result of higher forces with built-up edge formed due to rounder cutting edge and thermal softening at high speed. At 250 m/min feed forces (Figure 2.10 (b)) are observed to be high at small feed rates. At high speeds because of the coolant may not have time to reach the tool tip workpiece contact; the process behaves like a dry cutting and friction is increased more; increasing forces in small feed rates.

(a)　　　　　　　　　　　　　　　(b)
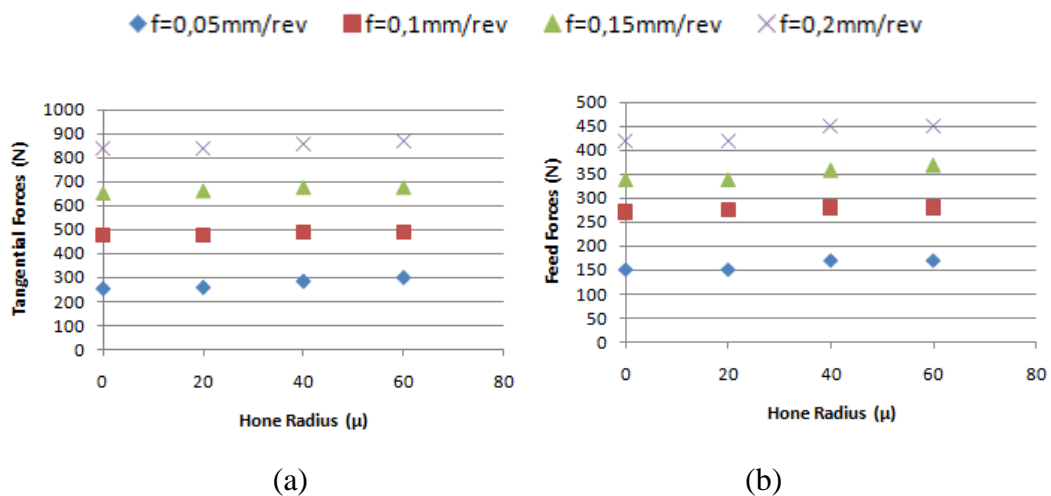
Figure 2.7. Change of (a) Tangential Forces (b) Feed Forces with hone radius at 30 m/min cutting speed.
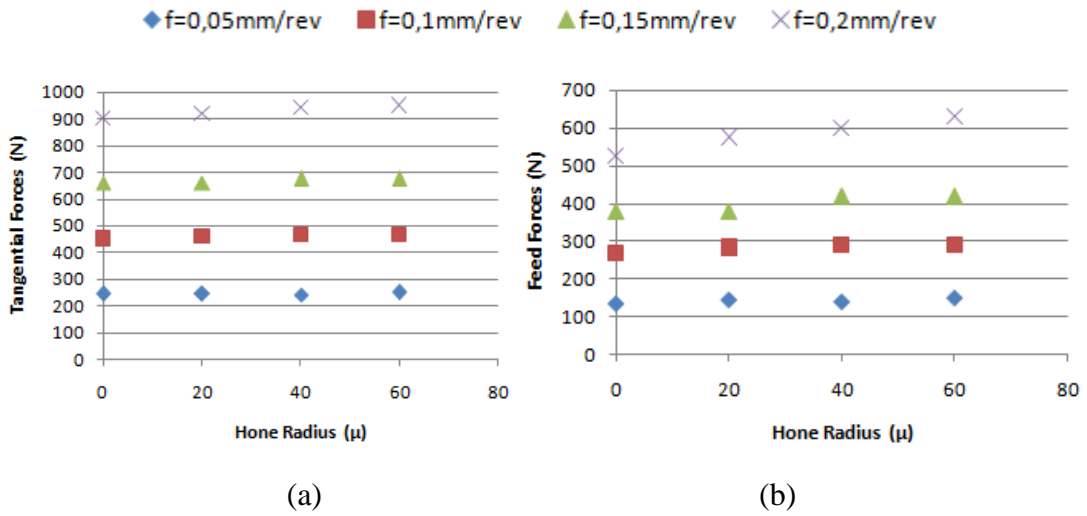
Figure 2.8. Change of (a) Tangential Forces (b) Feed Forces with hone radius at 60 m/min cutting speed.
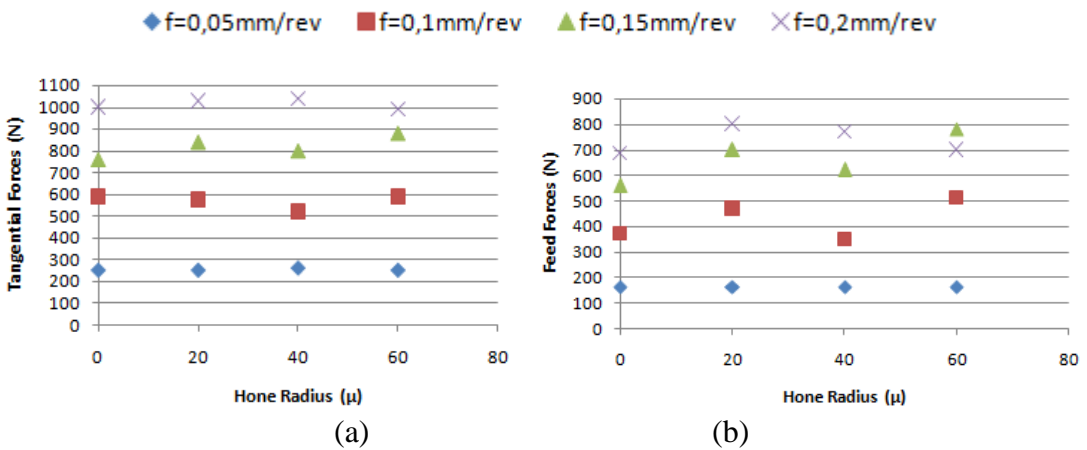
Figure 2.9. Change of (a) Tangential Forces (b) Feed Forces with hone radius at 100 m/min cutting speed.
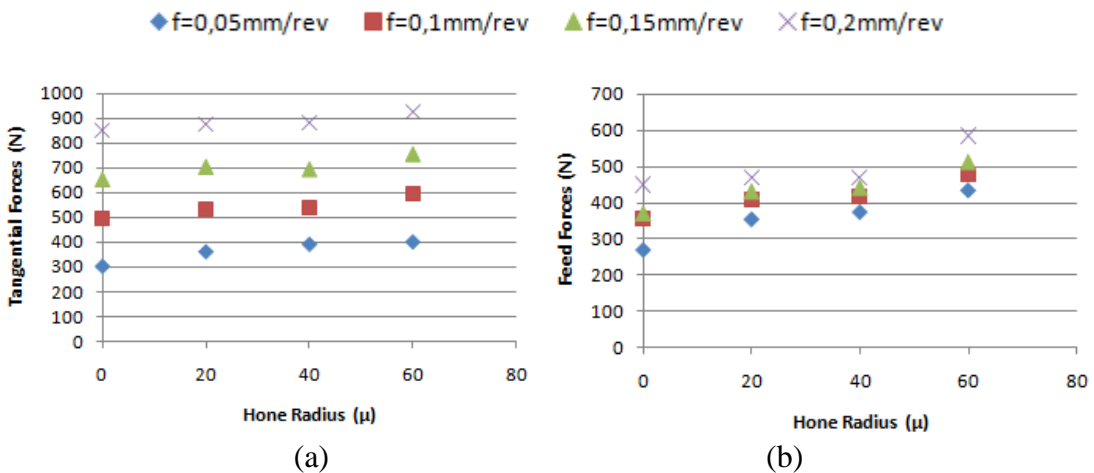
Figure 2.10. Change of (a) Tangential Forces (b) Feed Forces with hone radius at 250 m/min cutting speed.

12

For the repeatability of the forces example repeated data results can be seen in Figure 2.11. Also the % difference in all measurements is presented in the chart below (Figure 2.12). It is seen that the difference between forces is not exceeding 30 %.

(a)   (b)
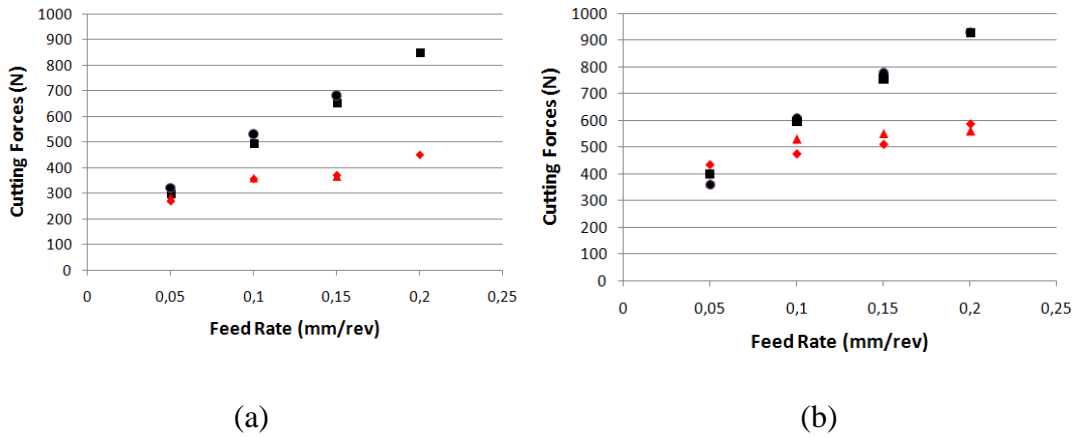
Figure 2.11. Feed (red markers) and Tangential (black markers) cutting forces for (a)6μm (b) 60 μm hone radius and250 m/min cutting speed.
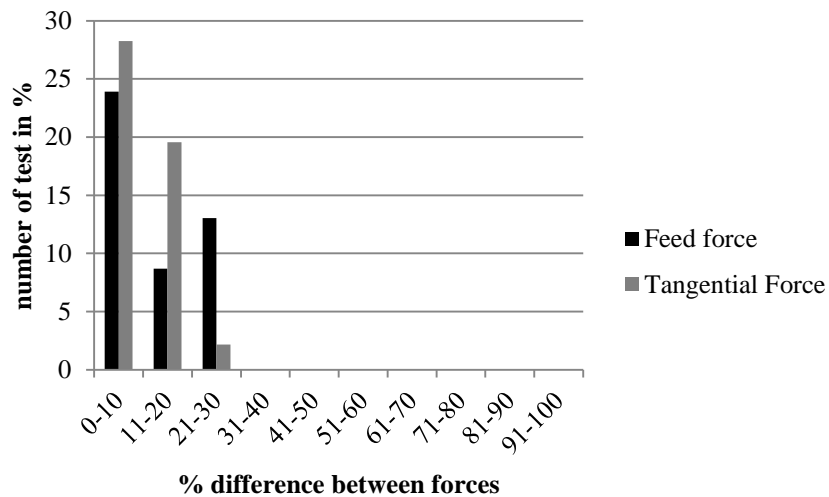
Figure 2.12. Overall comparison of the difference in the measured forces.

2.14. Edge Forces

In this study, two different approaches are considered for edge force determination. The first assumption is linear regression method where edge forces are obtained by extrapolating the total forces to zero feed. It is assumed that at zero feed the remaining forces resemble the non cutting part of the total tangential and feed forces. As shown in Figure 2.13; edge forces are determined for single cutting speed covering multiple feed rates. Thus resulting edge forces are independent of the feed rate.

13
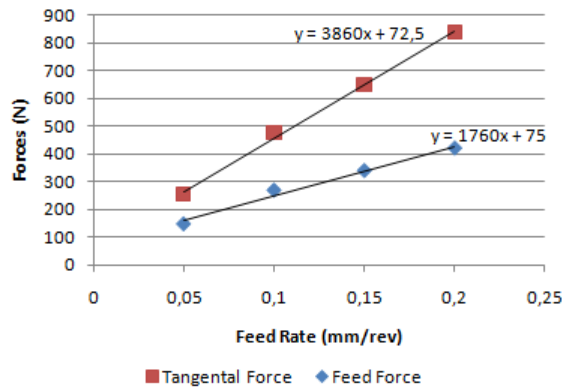
Figure 2.13. Forces vs. feed rate for 6µm hone radius and 30 m/min cutting speed.

In the second approach it is assumed that at very small feed rates the forces will make a peak at the point where the tool starts cutting and then a steep decrease. The force measured at that point is edge force. Orthogonal tube cutting tests with 20 μm hone radiused tool on2 mm depth of cut are performed with 0.001, 0.002, 0.003, 0.004, 0.005, 0.008 and 0,015 mm/rev feed rates and 150 m/min cutting speed. All of the feed rates are smaller than the hone radius to clearly see the behavior before cutting.

As seen from the

Figure 2.14, Figure 2.15, Figure 2.16 and Figure 2.17 the trend in the measured forces are not comparable with the aforementioned approach. The force behavior at the non cutting part of each test is expected to be similar. However; at the smallest feed the force increase is more uniform while the higher feeds give different force trends. Lathe's accuracy on small feeds may be a cause of the discrepancy in this force trends. It is not possible to obtain accurate edge forces with the second approach. Thus linear regression assumption is used for edge force determination and the modeling comparison throughout the thesis.

14
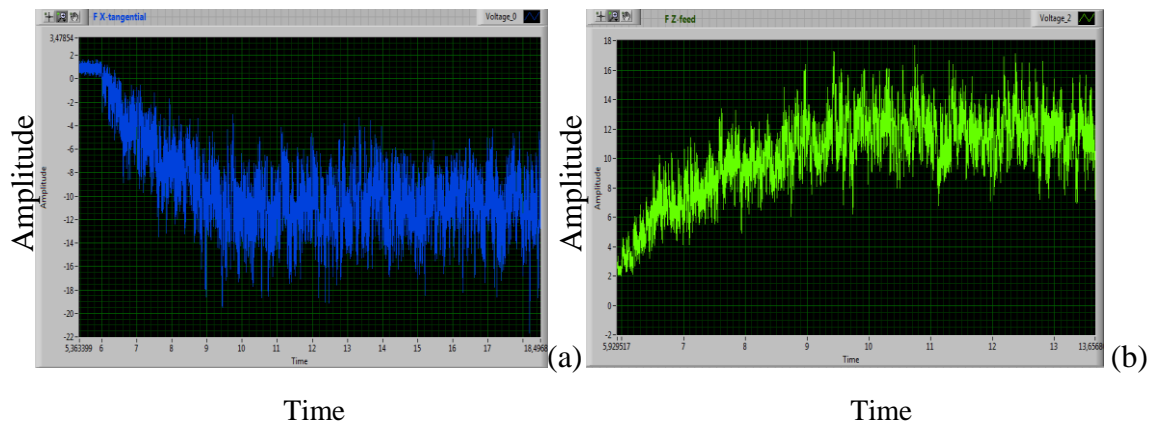
Figure 2.14. (a) Tangential (b) Feed Force measurements from the LabView software for 0.001 m/rev feed.

Time   Time
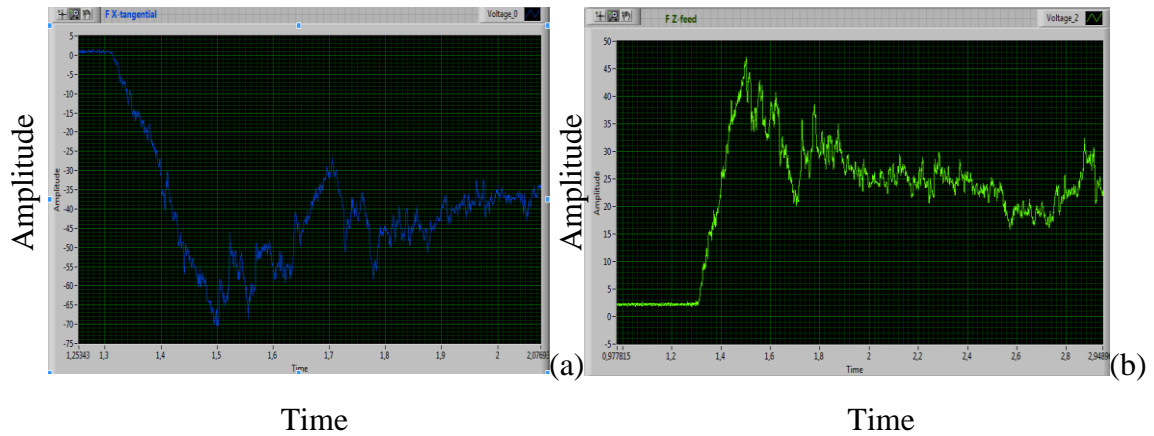
Figure 2.15. (a) Tangential (b) Feed Force measurements from the LabView software for 0.005 m/rev feed.

Time   Time
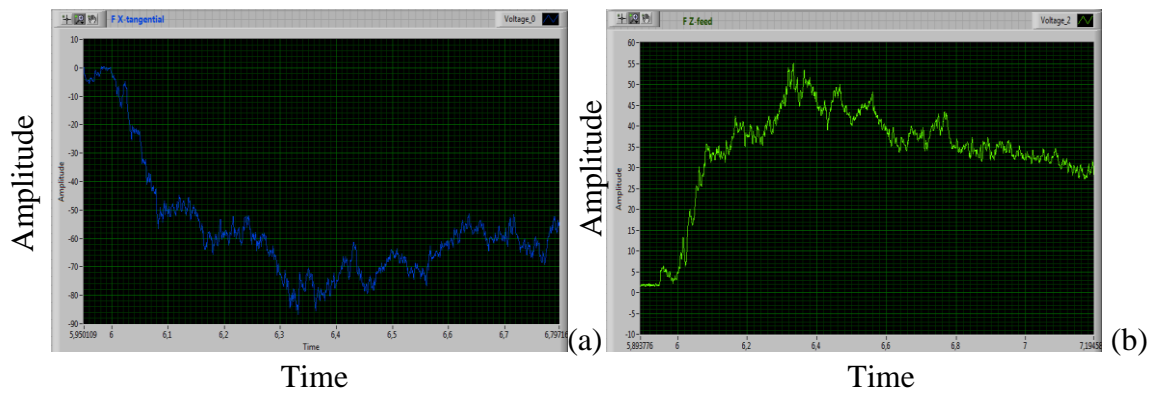
Figure 2.16. (a) Tangential (b) Feed Force measurements from the LabView software for 0.005 m/rev feed.

Time   Time
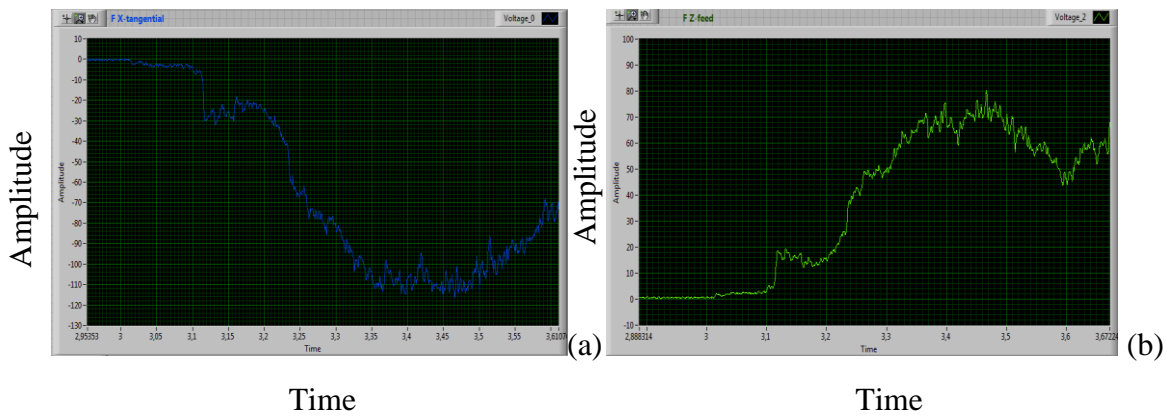
Figure 2.17. (a) Tangential (b) Feed Force measurements from the LabView software for 0.015 m/rev feed.
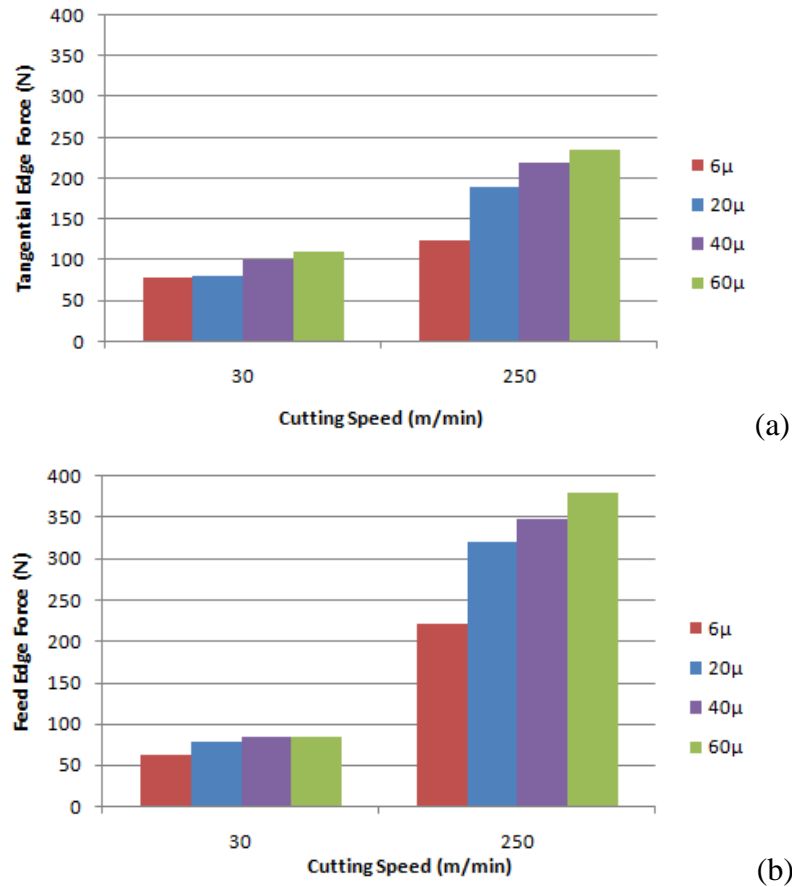
Figure 2.18. Change of (a) Tangential Edge Forces (b) Feed Edge Forces with hone radius at 30 m/min and 250 m/min cutting speed.

Changes in tangential and feed edge forces with hone radius are shown in Figure 2.18 for 30 and 250 m/min cutting speeds. It is observed that increasing cutting speed also increases edge forces, and forces are more affected when large hone radiused tools are used. As cutting speed remains constant it is seen that higher hone radius results in higher edge forces. The rise in the forces is the result of increased ploughing of the tool edge by large hone radius or thermal material softening with increased cutting temperature. Also, feed edge forces are more sensitive to speed change; since forces in direction the feed are directly affected by the material under the hone. At 30 m/min the maximum rise is 19% while at 250 m/min it is 35% when hone radius is increased from 6 µm to 20 µm. The rise of the forces are 19% and 15% for tangential and feed edge forces, respectively for the same test parameters when hone radius is increased from 20 µm to 60 µm. The results indicate there is a nonlinear relationship between the force and the hone radius.

2.1.5. Contact Length Measurements

The contact length on the flank surface is measured by a stereomicroscope (Nikon Eclipse ME600) with up to100x magnification. Image taken from the microscope can be seen in Figure 2.19.
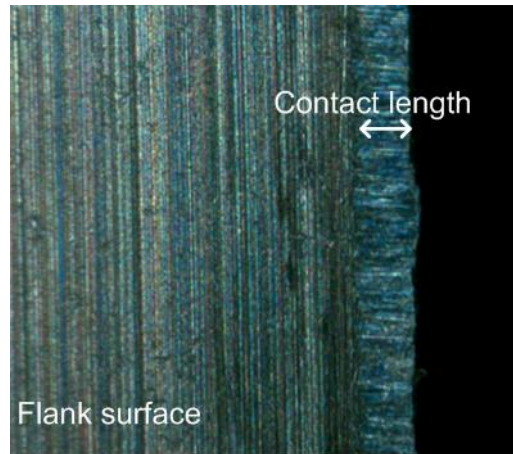
Figure 2.19. Microscope image of the flank surface.

Figure 2.20 shows the change of contact length with speed and feed when 60μm hone radiused tool is used. It is observed that the change is small when the cutting process is done at lower speeds. However at higher speeds feed rate has more dominant effect on contact lengths. Also, it is observed at 0.1 mm/rev feed rate contact lengths are seen to be longer which is the result of build-up edge and can be taken as outliers.
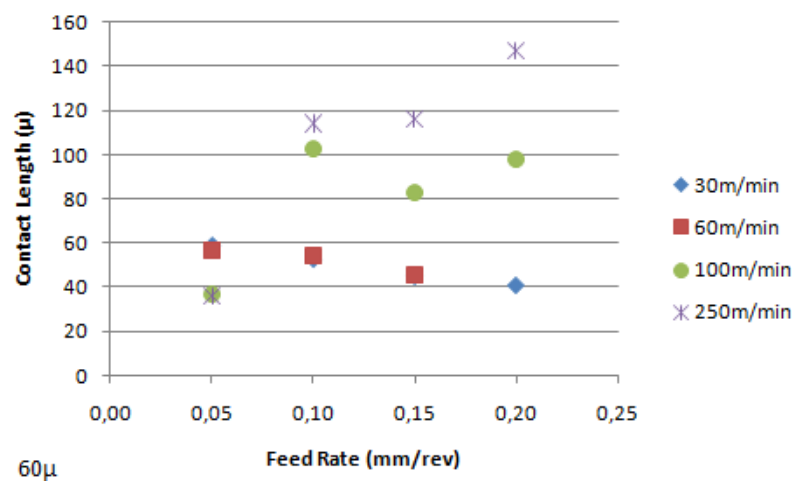
Figure 2.20. Variation of the contact length with feed and cutting speed for 60μm hone radiused tool.

Also, a wider set of contact length data is acquired from the literature [34] in addition to the presented study. Figure 2.21 shows the change in the average measured contact

length with feed and speed. Originally the contact lengths are obtained for 12 μm, 30 μm and 60 μm hone radiused tools.
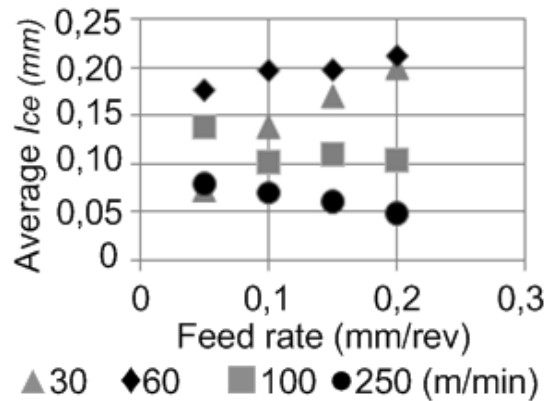
Figure 2.21. Variation of the average contact length with feed and cutting speed.

It is observed that with increased feed the contact length increases at low speeds and decreases at high speeds. Also, it can be seen that there is a critical speed at which the behavior changes. For instance at a certain feed rate increasing speed leads to an increase in the contact length at low speeds, but for higher speeds the opposite is true. Also, feed has more dominant effect on the contact length at low speeds.

When the measured data and the data taken from the literature are compared it is observed that the trends are the opposite of each other. This may be the result of subjectivity of the measurements to the researchers. Also, machining conditions may vary such as stiffness of the tool may be different that affects the cutting process or workpiece tool interaction could be different for the same material but different grade tools. Moreover, since the average of the measured data is taken; some tools having hone radii around 55 μm while the others have around 65 μm. Cutting process is affected by this change; which eventually affect contact length measurements.

2.2. Thermal Investigation

It is important to accurately measure temperature at the tool tip for better understanding of the thermal aspects of cutting process and their effect on the third deformation zone. Thus, investigation of temperature behavior is essential for the third deformation zone. In order to do that; experiments are conducted and temperature is monitored during cutting using a thermal camera. Various methods are available and widely used for temperature measurements such as thermocouples and visual monitoring pyrometer [24]. In this research thermal measurements via an infrared camera are taken an initial

reference. With visual monitoring there is no need of a modified tool or workpiece. Measured temperature at the tool tip can be used in the Johnson-Cook model in order to estimate the stress at the start of third deformation zone.

2.2.1. Experimental Studies

The grooving tests are conducted on AISI 1050 Steel workpiece to simulate orthogonal cutting. Uncoated carbide grooving tools are used with hone radii of 6, 20 and 60 μm and rake angle of 5º. Due to a previous study [38] the temperature change is found to be insignificant at different feed rates. Thus feed rate is selected as 0.01 mm/rev. Three different speeds of 30, 100 and 250 m/min are considered to see the effect for the experiments. Workpiece is designed with 2 mm grooves and peaks to simulate 2 mm depth of cut for each test(Figure 2.22). The peaks are cut with a grooving tool in each test and grooves are cleared for the next test preparation. For instance with the part below; three tests can be performed.
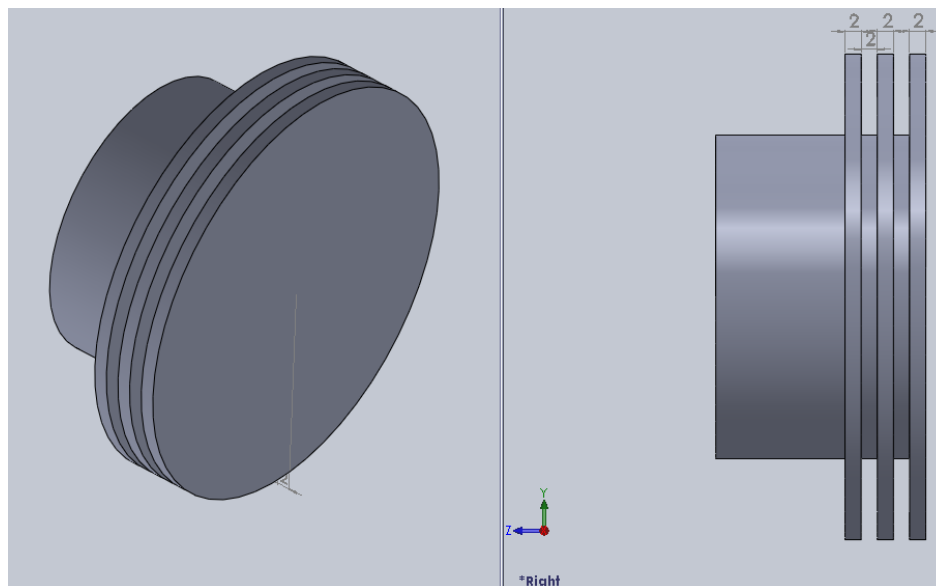
Figure 2.22.Workpiece model used in thermal experiments.

A FLIR A325 SC IR thermal camera is used for thermal measurements of orthogonal cutting on the Mori Seiki Lathe. A special fixture is designed to place the camera in the lathe. Chip formed usually heads towards the camera. Thus, a special lens which conducts infrared lights is used for the protection of camera lens. It is seen that the measurements with and without protective lens give the same results. Experimental setup and lens fixture can be seen in Figure 2.23 and Figure 2.24.

19
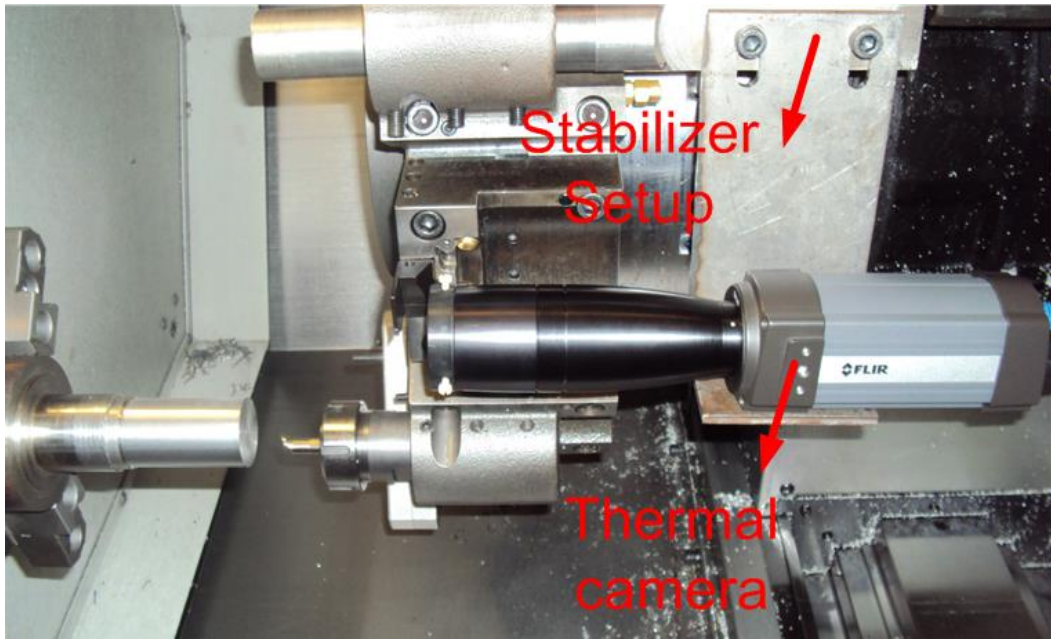
Figure 2.23.Experimental setup for thermal investigation.
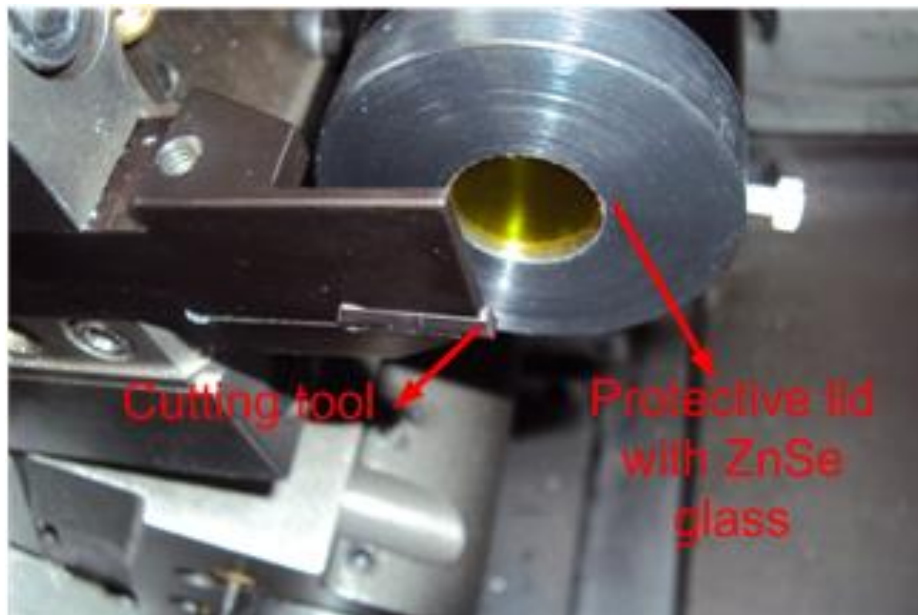
Figure 2.24.The cutting tool edge and the protective lens.

2.2.2. Experimental analysis

Figure 2.25 shows the screenshot of video-measurement of temperature as a sample. A point or an area on the image is defined for temperature data collection, which can be seen in Figure 2.26. At the measurement window different values such as maximum, average, or minimum temperature for an area can be obtained as a graph. Also instant

temperature of the selected point can be seen at the right of the window while the measurement video is played. More than one point or area can be defined in the screen to compare temperatures.
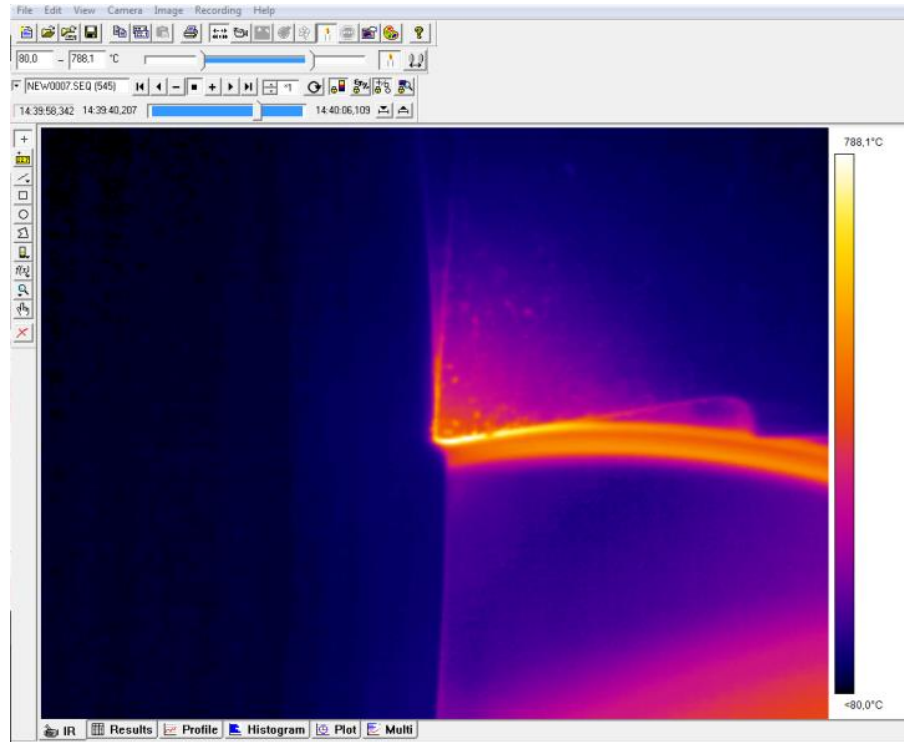
Figure 2.25. Screenshot of the measurement for 2 mm depth of cut, 100 m/min and 0.1 mm/rev feed rate.
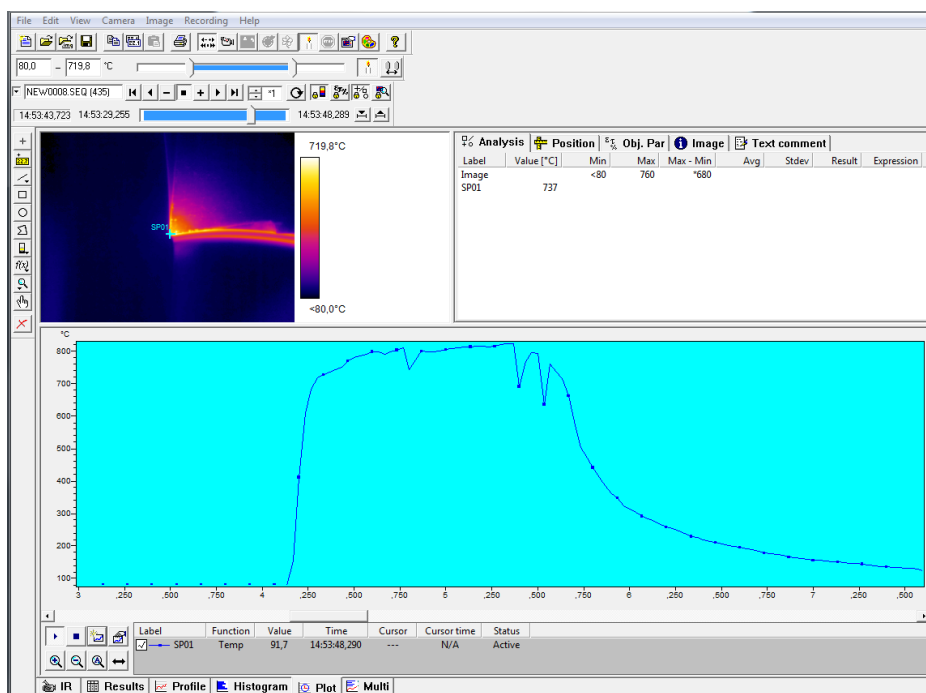
Figure 2.26.Data extraction from the measurement video.

2.2.3. Thermal distribution along tool tip

In this section the temperature differences among rake face, tool tip and the flank face are included. For a tool with large hone radius (60µm) five different data points are taken into consideration to obtain temperatures on the rake face, along the tool tip and on the flank surface as seen in the Figure 2.27. It is observed (Figure 2.28) that the temperature is gradually decreases from the beginning of the rake face to flank face; as the graph of the rake face is at the top, tool tip is in the middle and the flank face is positioned at the bottom. Due to large hone radius larger contact allows heat to dissipate easier thus temperature is reduced at the tool tip. The maximum temperature difference between the chip contact and tool tip is determined around 80˚C. Due to small vibrations of the camera during cutting; the temperature data may not be represented by a straight line or curve. Apart from the spikes, temperature data is extracted from the part of the cutting process that becomes steady.
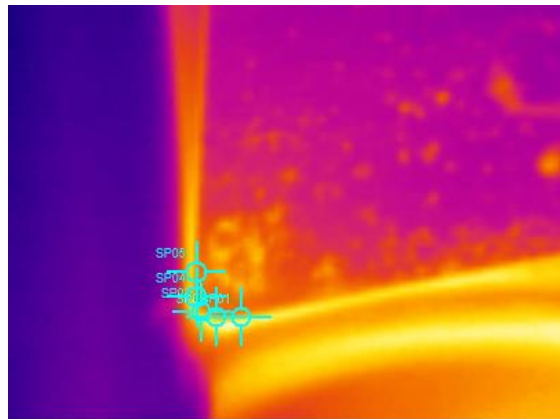
Figure 2.27. Data points along tool tip for 60 µm hone radiused tool.
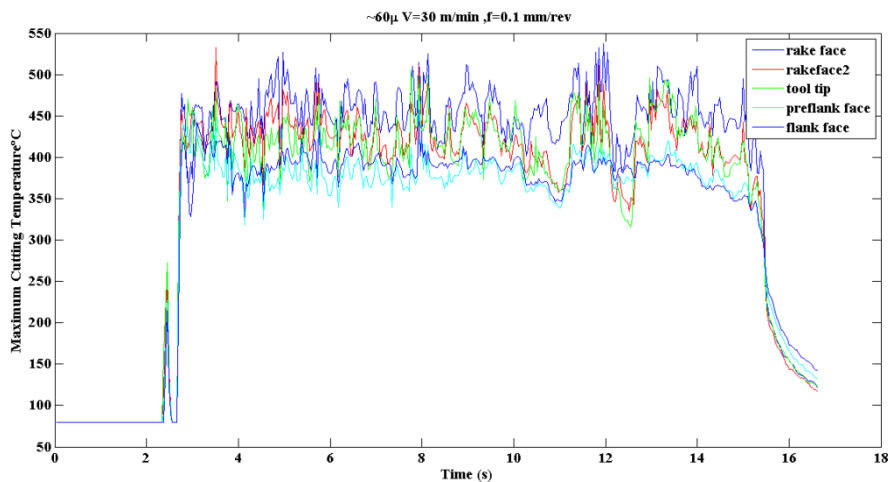
Figure 2.28. Temperatures at different points during cutting process with 30 m/min cutting speed; 0.1 mm/rev feed rate and 60 µm hone radiused tool.

22

For a tool with sharp hone (~6 μm) 3 data points are fitted on tool tip (Figure 2.29). Data points and temperature distribution can be seen in the figures. It can be said that the maximum temperature difference is around 50 ˚C (Figure 2.30). The temperature behavior is seen more clearly without the vibrations; and the steady state temperature of the process can be accurately observed. Since the hone radius is smaller, the heat dissipation is lower than the large hone radiused tool. Thus the temperature difference is lower.
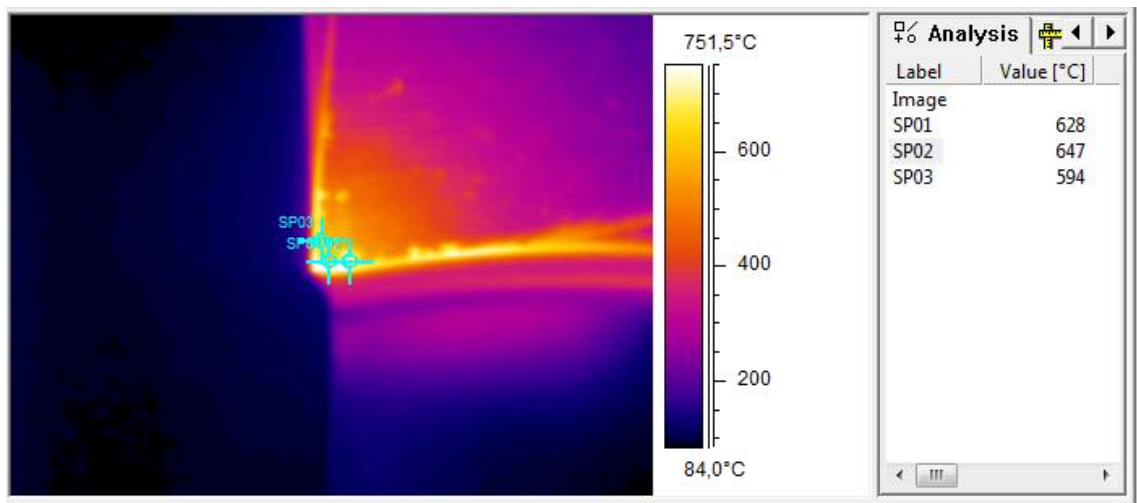
Figure 2.29. Data points along tool tip for sharp tool.
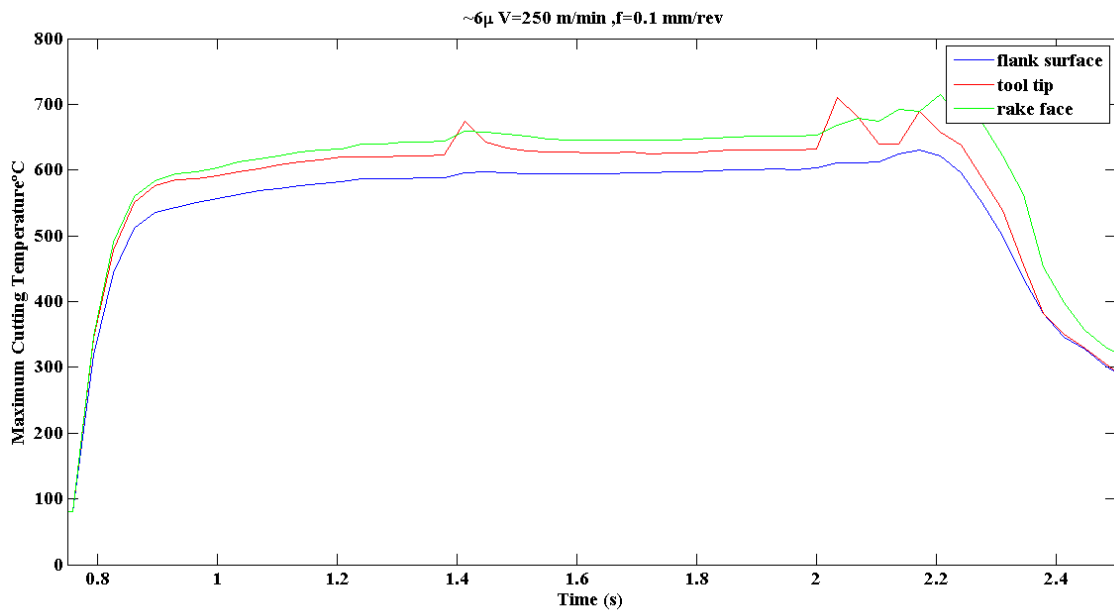
Figure 2.30. Temperatures at different points during cutting process with 250 m/min cutting speed, 0.1 mm/rev feed rate and sharp tool.

2.2.4. Effect of hone radius on cutting temperature at the hone

The change in temperature with increased hone radius is explicitly given for three different speeds in Figure 2.31, Figure 2.32 andFigure 2.33. It is observed that independent of cutting speed the temperatures are slightly increased with hone radii. The results are parallel with the ones of Yen et al. based on their FEA with a similar workpiece material [27]. This was explained by easier dissipation of heat on the large hone than smaller hone due to increased contact.
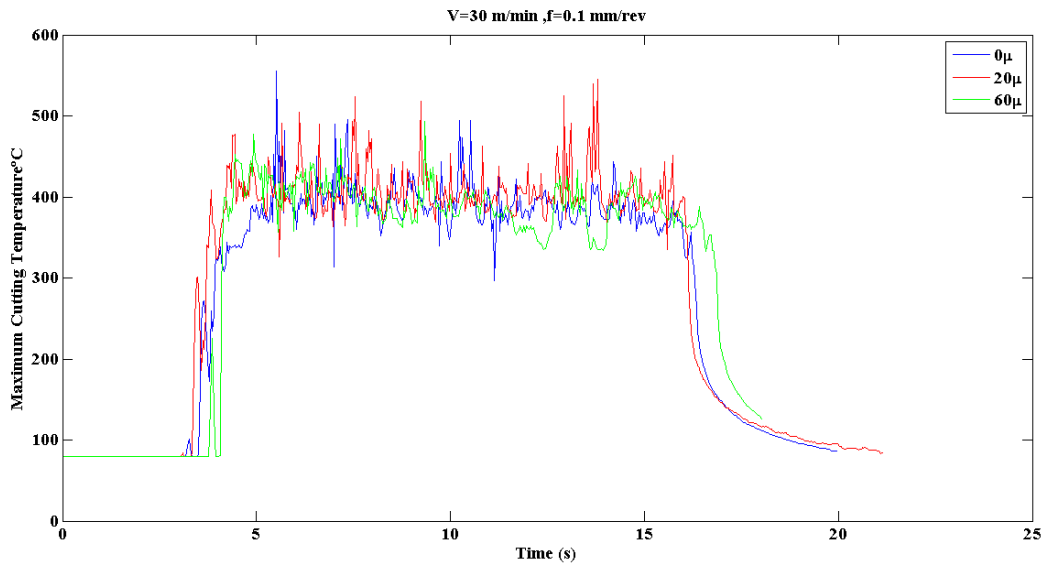
Figure 2.31. Temperature change with hone radius at 30 m/min cutting speed and 0.1 mm/rev feed rate.
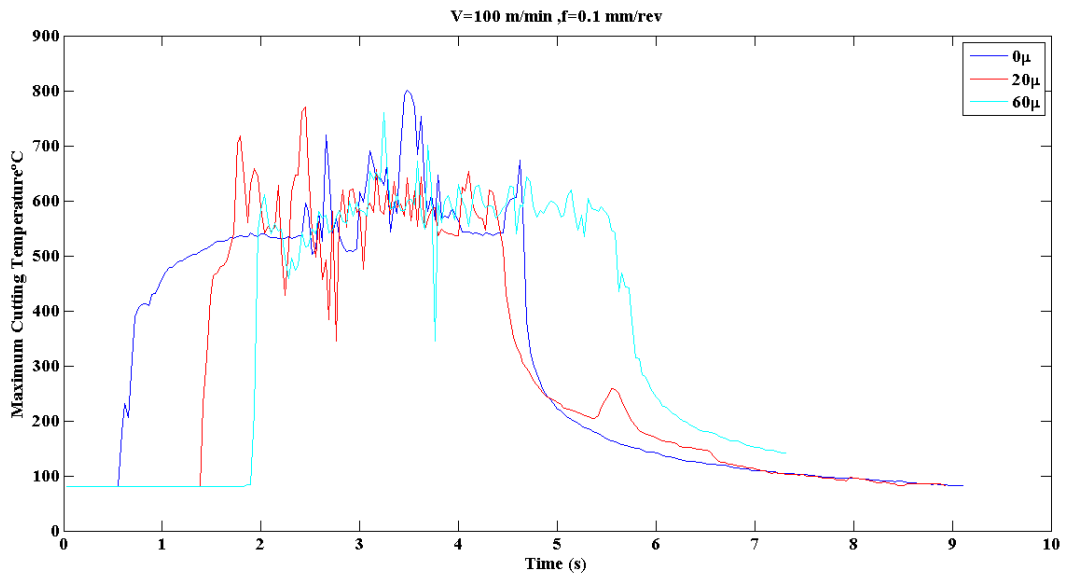
Figure 2.32. Temperature change with hone radius at 100 m/min cutting speed and 0.1 mm/rev feed rate

24
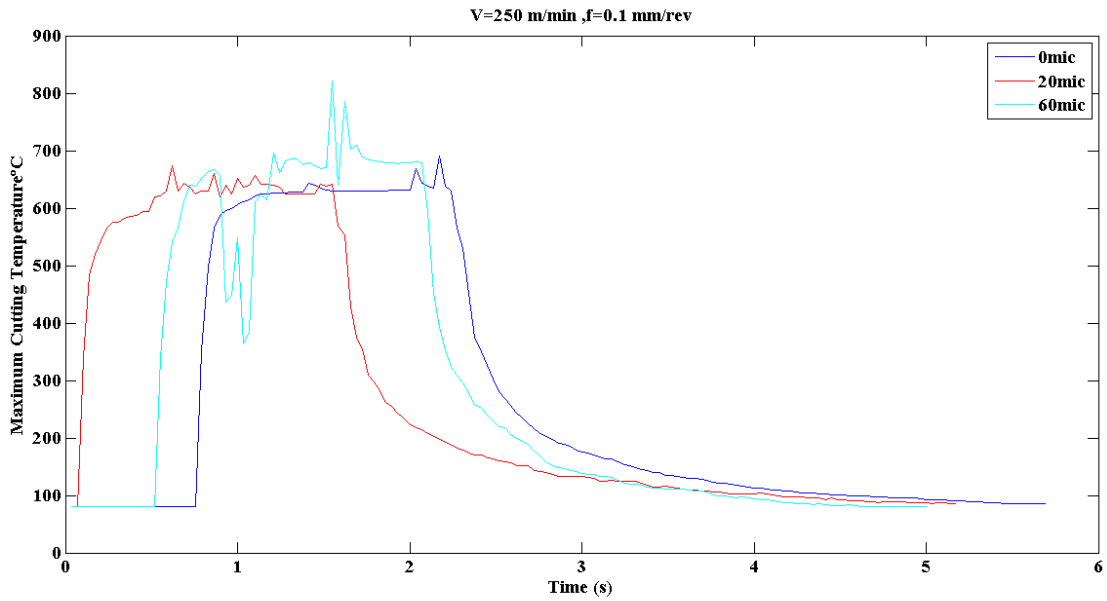
Figure 2.33. Temperature change with hone radius at 250 m/min cutting speed and 0.1 mm/rev feed rate

Effect of speed on cutting temperature at the hone can be seen in Figure 2.34, which confirms the common knowledge that increasing speed increases temperature; and this also applies for the tool tip.
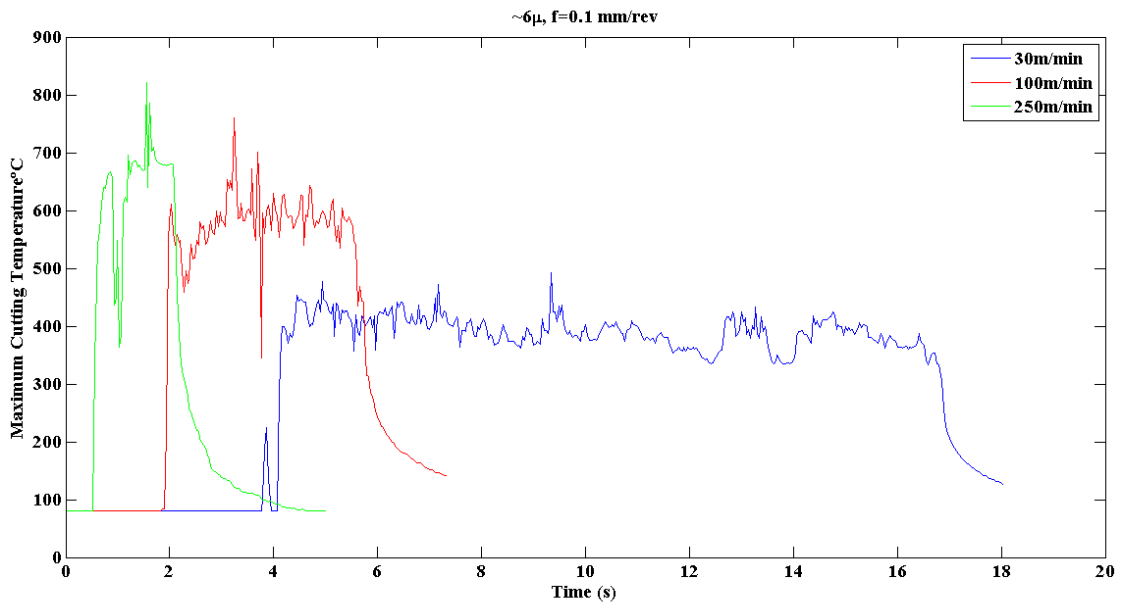
Figure 2.34. Effect of speed on temperature on the tool tip for 0.1 mm/rev feed rate and 60μm hone radiused tool.
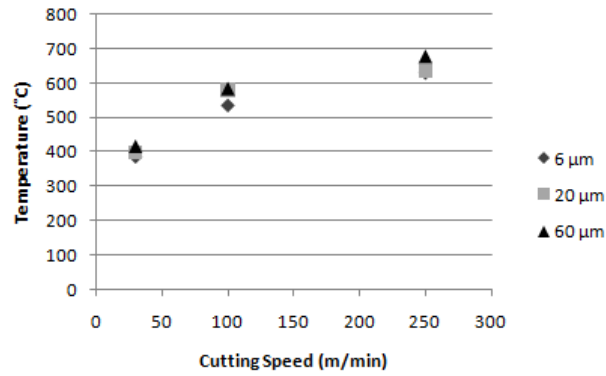
Figure 2.35. Change of temperature with speed and hone radius.

Measured temperatures of all tests can be seen in
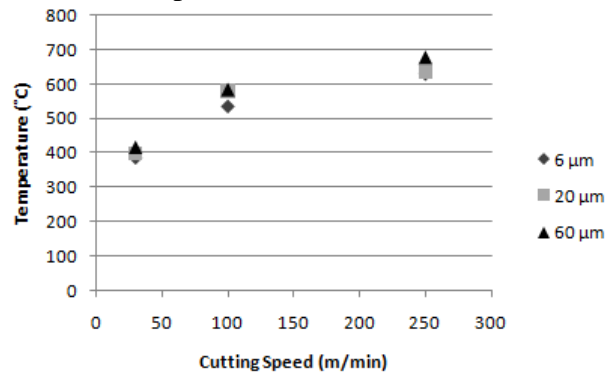
Figure 2.35. A study is available by Ceau et al.[24] where an empirical equation for temperature at the tool edge is presented for a similar workpiece material with lower carbon content (AISI 1045 Steel):

$$\theta = 243.283 \, v_c^{0.242} f^{0.078} a^{0.021} \tag{2.1}$$

where the temperature is θ (C˚), the cutting speed is vc (m/min), the rotation feed is f (mm/rev) and the cutting depth is a(mm). Experimental temperature data obtained from the cutting tests with the thermal camera are compared with the model. It is seen that the model is comparable with the measurements with a maximum difference of %20 (Table2.1.). The difference comes from the material properties and the measurement method, since at the research Ceau used thermocouples for measurements. Also the temperature measurements are all found to be lower than the calculated temperatures which pursue the effect of different conditions. Stress at the start of third deformation zone can be determined with JC model using this empirical equation for further model verification of the cutting model.

26

Table 2.1. Temperature data comparison with empirical model.

Hone Radius (μm)	Cutting Speed (m/min)	Measured Temperature (˚C)	Calculated Temperature (˚C)	Difference (%)
6	30	387	470	17.6
	100	536	629	14.7
	250	630	785	19.7
20	30	400	470	14.8
	100	582	629	7.4
	250	636	785	18.9
60	30	416	470	11.4
	100	585	629	6.9
	250	679	785	13.4

To sum up, the orthogonal cutting experiments are conducted to investigate mechanical and thermal behavior at different cutting conditions including the effect of the hone radius. General observations can be concluded as follows:

• Nonlinear increase of forces with increasing hone radii is observed; and it is seen that the affect of hone radius on total forces is very little.

• Experimental results are used to find edge forces. Forces obtained from the small feed tests did not give compatible results. Thus regression model is used on measured forces. It is observed that hone radius has a visible nonlinear effect on edge forces; which are also affected by cutting speed.

• Contact length on the flank contact including tool tip is introduced and will be used for modeling.

• To investigate thermal behavior infrared camera is used and it is observed that the temperature at the tool tip is lower than the temperature at the flank face. Also the hone radius has a little effect on temperatures at the tool tip whereas it is greatly affected by cutting speed.

CHAPTER 3 MODELING OF THE ORHOGONAL CUTTING PROCESS

In this chapter, the force model for the third deformation zone is presented. Firstly, the information about modeling of primary and secondary deformation zones is given briefly then stress, pressure and friction characteristics are discussed for the third deformation zone. Consecutively, the geometrical model for tool tip along with the contact length and mathematical model of force distributions are presented. Finally the solution procedure is explained.
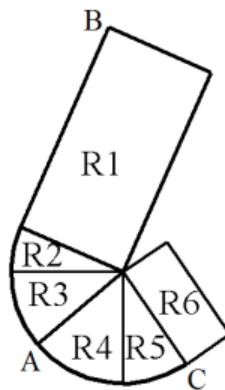
Figure 3.1.Hone-radiused cutting tool model with the divided regions.

Figure 3.1 gives a representation of hone radius divided into regions geometrically for mathematical simplicity. Region 1, 2 and 3 (R1, R2 and R3) denote primary and secondary shear zones which will be explained in Section 3.1. Region 4 (R4) begins with the stagnation point A, where the material ploughs under the tool and recovers elastically on the flank contact, which is denoted with Region 5 (R5) and Region 6 (R6). Flank contact is divided into two regions as R5 representing rounding of the tool tip on flank contact and R6 representing flat clearance face. Third deformation zone will be explained throughout this chapter.

28

3.1. Primary & Secondary Deformation Zones

Primary and secondary deformation zones are responsible for chip formation; the modeling approach for these two zones is acquired from Özlü's work [3]. For primary shear zone, material behavior is represented with the Johnson-Cook constitutive model [35], and the minimum energy approach is used for the shear angle prediction [36].

Johnson- Cook constitutive model is represented as follows while the material parameters are presented in Table 3.1.

$$\tau = \frac{1}{\sqrt{3}}\left[A + B \times 10^6 \left(\frac{Y}{\sqrt{3}}\right)^n\right]\left[1 + \ln\left(\frac{\dot{Y}}{\dot{Y}_0}\right)^m\right]\left[1 - \left(\frac{T - T_{ref}}{T_m - T_{ref}}\right)^v\right] \qquad (3.1)$$

where Y is the shear strain, $\dot{Y}$ is the shear strain rate, $\dot{Y}_0$ is the reference shear strain rate, A, B, n, m, and v are material constants, T_m is the melting temperature of the material and T_{ref} is the reference temperature. Absolute temperature T is obtained from the conservation of energy.

Table 3.1. JC material parameters and thermal properties for AISI 1050 Steel [3].

A	B	n	m	v	Tm (K°)	Tref (K°)
880	500	0.234	0.0134	1	1733	300

For the secondary shear zone, the dual-zone model developed by Özlü et al. [36] is applied. Briefly, the rake face is divided into two friction zones, where the regions close to the tool-tip are represented by sticking friction and the rest is modeled by sliding friction model.

For third deformation zone pressure and shear distributions are adapted from the secondary shear zone. All modeling details for primary and secondary shear zones can be seen in [3].

3.2. Third Deformation Zone

Third deformation zone is responsible for material ploughing that forms the flank contact. As in the primary and secondary shear zone modeling, thermomechanical model is used for material model due to its simplicity and functionality. In addition, considering that the beginning of the shear band is also the beginning of third deformation zone; obtained shear stress from the JC model can be adopted for the shear

stress distribution. For the validity of this assumption, sensitivity analyses for JC model parameters are done. Dual zone approach is also adapted from the aforementioned model, where the contact at the hone and flank surfaces are divided as sticking and sliding friction contact. For stagnation angle it is taken as equal to shear angle for the following reasons. Firstly, it is stated in [3] that there would be a conflict between the hone radius and the shear band when shear angle is bigger than stagnation angle. Therefore the minimum value of the stagnation angle must be equal to shear angle. Shear angle measurements are found to be in the range of 25°-35° in that study. It is also shown that stagnation angle for metals are about 28° - 37° which is compatible with the shear angle values [15, 37]. Sensitivity analysis is performed to see the effect of stagnation angle on the third deformation zone forces.

3.2.1. Sensitivity Analysis

Sensitivity analysis is performed to see whether shear stress can be assumed to be equal to the stress at the beginning of the primary shear zone. Performed sensitivity analysis based on Johnson-Cook equation shows that while strain and temperature are kept constant, a 100% increase in strain rate results in 0.74% change in shear stress. Similarly a 100% increase in strain results in 6% increase of the stress. Change of shear stress with strain and strain rate can be seen Figure 3.2(a) and Figure 3.2(b). Based on the sensitivity analysis it was concluded that the effects of strain and strain rate on the shear stress are not significant for the material and parameter ranges considered in this work. Thus, strain and strain rate from the primary shear zone can be adopted.
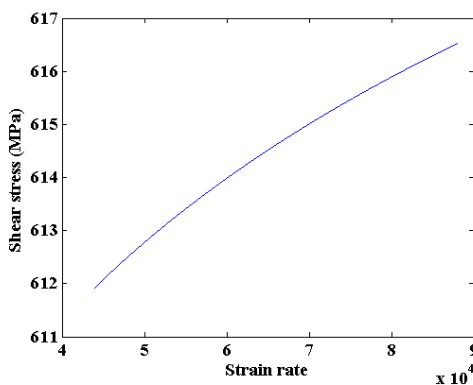
(a) Shear Stress vs. Strain rate   (b) Shear Stress vs. Strain
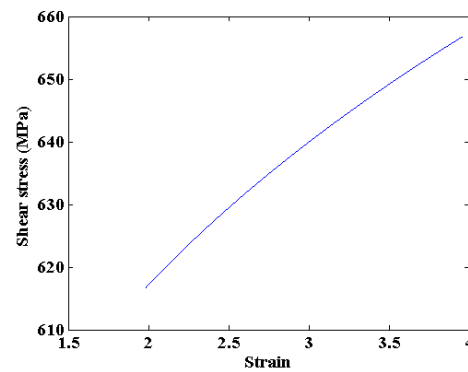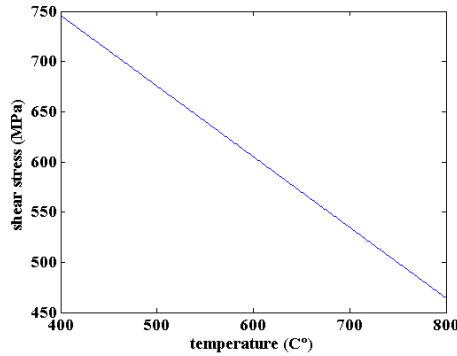
(c)Shear Stress vs. Temperature

Figure 3.2.(a) Change of shear stress obtained from JC model with (a) strain rate (b) strain (c) temperature for AISI 1050 Steel model parameters.

Sensitivity analysis of thermal behavior is also essential for adaptation of the Johnson Cook model. From the simulation results it is seen in Figure 3.2(c) that increasing temperature 100% decreases the shear stress 37%, while the strain and strain rate are kept constant. The change cannot be ignored. However, initially this change is not taken into consideration in the model because of the fact that the temperature difference found from the experiments (Chapter 2) is at most 80 degrees from rake face to hone radius; and the temperature around hone is about 600 degrees. Thus the temperature range is smaller. In the verification chapter (Chapter 4) temperature obtained from the Ceau's model [24] will be used in JC model to obtain shear stress, and the results will be compared to the initial model results.
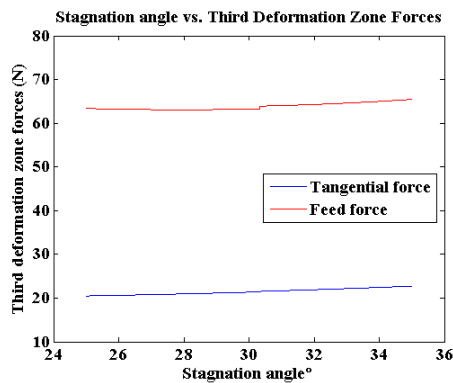
Figure 3.3.(Third deformation forces changing with stagnation angle for 30µm hone radius at 250 m/min speed and 0.1mm/rev feed rate.

In addition sensitivity analysis of stagnation angle is conducted since the stagnation angle effects the assumed amount of material ploughed under the tool. It also affects the contact length of the Region 4 of the third deformation zone. Model results for 30µm hone radiused tool, 250 m/min cutting speed and 0.1mm/rev feed rate are shown in

31

Figure 3.3. When stagnation angle is increased from 25˚ to 35˚ due to shear angle values acquired from [3] (28%); tangential edge forces increase by5.6% whereas feed edge forces decrease by 7.9%. It is then decided that the effect of stagnation angle on third deformation zone forces is not significant for the discrepancy ranges considered in this work.

3.2.2. Normal pressure and shear stress distributions

Normal pressure and shear stress distributions initially assumed similar to secondary shear zone; which can be seen in Figure 3.4 along with the sticking and sliding zones, and are defined as follows:

$$P(\chi) = P_0 \left(1 - \frac{\chi}{l_{ce}}\right)^{\zeta} \quad 0 \leq \chi \leq l_{ce} \tag{3.5}$$

$$\tau = \tau_0 \quad 0 \leq \chi \leq l_{pe}$$

$$\tau = \mu P(\chi) \qquad l_{pe} \leq \chi \leq l_{ce} \tag{3.6}$$

where P is the normal pressure distribution, $P_0$is the normal pressure constant, which is defined as normal stress on the rake face at the tool tip,χ is the distance from the stagnation point, l_{ce} is the contact length after stagnation point, ζ is the stress distribution exponent, τ_0 is the shear stress at the beginning of the primary shear zone, μ is the sliding friction coefficient between tool and workpiece, and l_{pe} is the sticking contact length. Sliding friction coefficient is determined from calibration tests for 1050 steel [3] in the form of:

$$\mu = 6.12 \times 10^{-4} V_c + 0.398 \tag{3.7}$$

whereV_c is the cutting speed in m/min.
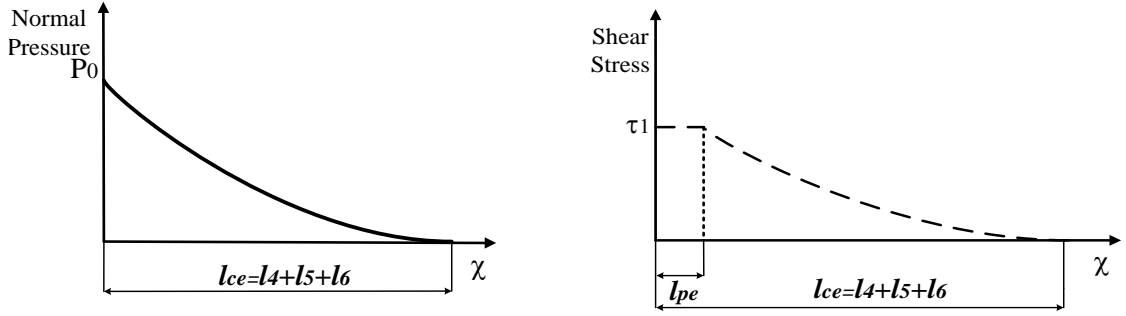
Figure 3.4. (a) The normal pressure and (b) the shear stress distributions in the third deformation zone where l_4, l_5 and l_6 denote the arc and line lengths of R4,R5 and R6 of Figure 3.1.

3.2.3. Contact Length in the Third Deformation Zone

Four different approaches are used for contact length determination. First one is the full recovery case; where it is assumed that the material below the stagnation point compressed under the tool hone will fully recover itself to its original height which is named ploughing depth. In Figure 3.5 the ploughing depth and the recovery of the material on the flank contact are shown.

Ploughing depth and the regarding contact length are calculated as follows:

$$h_p = r(1 - \cos\theta_s) \tag{3.8}$$

$$l_{ce} = \theta_s r + \gamma r + \frac{h_f}{\sin\gamma} \tag{3.9}$$

where h_p is the ploughing depth obtained from the geometry, h_f is the final height which is equal to ploughing depth, l_{ce} is the contact length, θ_s is the stagnation angle, and γ is the clearance angle.

Second approach is partial elastic recovery, where the material volume compressed under the hone is staying as the same, and the elastic recovery height is found from the elastic strain as:

$$h_f = h_p e^{-2Y/\sqrt{3}} \tag{3.10}$$
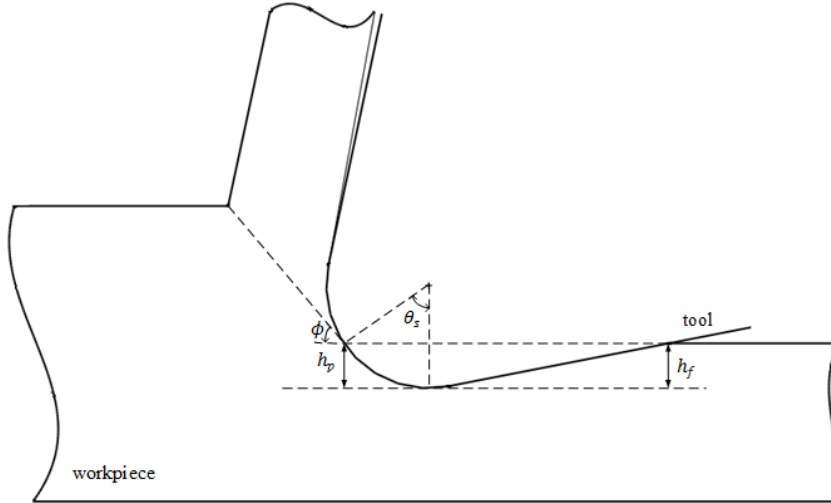
Figure 3.5. Ploughing depth and the recovery of the material on the flank contact.

For the third and fourth approach, measured contact lengths are used in modeling. Empirical model is very feasible to be used for any cutting process after calibration, and using measured contact length is expected to give the most realistic results. The details of the contact length measurements can be found in the Chapter 2. Since the measured contact length, ℓ_{ce}', is the projection seen on the flank face, actual contact length has to be determined. The geometrical representation of projections is shown in Figure 3.6and calculated as follows:

$$p_1 = 2r \cos\left(\frac{\pi}{4} + \frac{\mathrm{y} + \theta_s}{2}\right) \cos\left(\frac{\mathrm{y} + \theta_s}{2}\right) \tag{3.11}$$

$$p_2 = 2r \sin\left(\frac{\theta_s}{2}\right) \cos\left(\mathrm{y} + \frac{\theta_s}{2}\right) \tag{3.12}$$

$$p_3 = 2r \sin\left(\frac{\mathrm{y}}{2}\right) \cos\left(\frac{\mathrm{y}}{2}\right) \tag{3.13}$$

$$\ell_6 = \ell_{ce}' - (p_1 + p_2 + p_3) \tag{3.14}$$

34
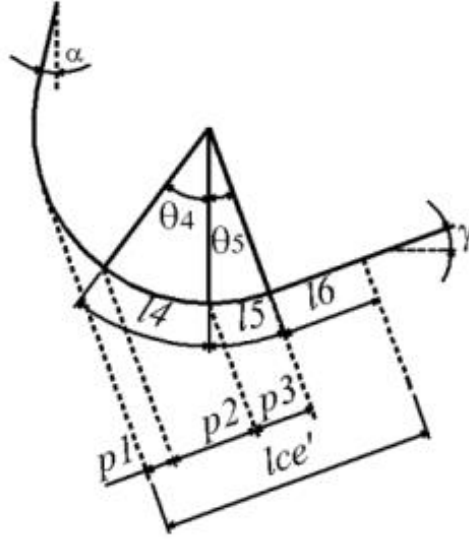
Figure 3.6. Contact length and length projections on the clearance face.

Projected contact length l_{ce}' is obtained from experiments for different hone radii, feed and speed. With the obtained data from Aksu's study [34], an empirical model is developed representing the effect of feed rate, cutting speed and hone radius using regression analysis for l_{ce}' as follows:

$$l_{ce}' = -0.459V_c + 0.4356r + 121.01f + 150.6 \qquad (3.15)$$

where, l_{ce}' is the total projected contact length of the third deformation zone in mm, V_c is the cutting speed (m/min), r is hone radius (μm) and f is the feed rate (mm/rev). Afterwards actual total contact length l_{ce} is obtained by finding corresponding angle, θ, yielding:

$$l_{ce} = \theta r \qquad (3.16)$$

As in the secondary deformation zone [ref] the tangential stress on the third deformation zone is equal to shear yield stress at the end of the sticking zone, sticking contact length ℓ_{pe} is obtained by:

$$l_{pe} = -l_{ce}\left(\left(\frac{\tau_1}{\mu P_0}\right)^{\frac{1}{\zeta}} - 1\right) \qquad (3.17)$$

35

3.2.4. The Forces Acting on Regions
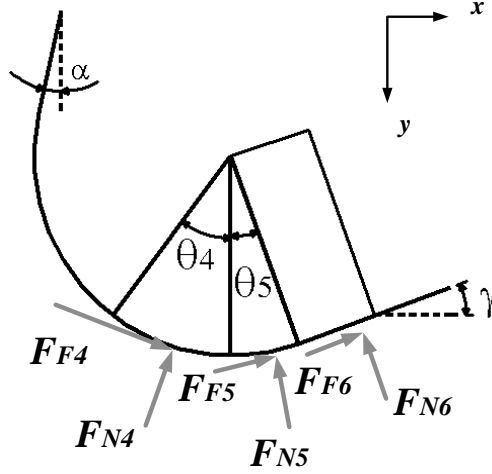
Figure 3.7. Force orientations along hone on the third deformation zone and flank face.

3.2.4.1 Forces acting on region 4

Region 4 is the first region after stagnation point, where the material is plastically deformed before entering the flank contact region. The angle sweeping through this region is represented by θ_4 (Figure 3.7) since contact is an arc, and calculated as follows:

$$\theta_4 = \frac{\chi}{r}$$

(3.18)

where, r is the hone radius. If the contact length is shorter than the projected length of the 4th region then the normal forces can be calculated as follows:

$$F_{N4x} = \int_0^{ul_1} wP_0 \left(1 - \frac{\chi}{l_{ce}}\right)^\zeta \sin\frac{\chi}{r} d\chi$$

$$F_{N4y} = \int_0^{ul_1} wP_0 \left(1 - \frac{\chi}{l_{ce}}\right)^\zeta \cos\frac{\chi}{r} d\chi$$

(3.19)

where, w is the depth of cut, ul_1 is the upper integral limit calculated using equation (3.21), by solving equation (3.20) for θ.

36

$$l_{ce}{}' - p_1 = r\cos(\text{y} + \theta_s)\sin\theta + r\sin(\text{y} + \theta_s)\,\cos\theta - r\sin(\text{y} + \theta_s) \qquad (3.20)$$

$$ul_1 = r\theta \qquad (3.21)$$

There may be three conditions for the frictional forces: only sliding, only sticking, and both sliding and sticking contact. If the contact condition in region 4 is only sliding, frictional forces are calculated as follows:

$$F_{F4x} = \int_0^{ul_1} \mu w P_0 \left(1 - \frac{\chi}{l_{ce}}\right)^{\zeta} \sin\frac{\chi}{r}\,d\chi$$

$$F_{F4y} = \int_0^{ul_1} \mu w P_0 \left(1 - \frac{\chi}{l_{ce}}\right)^{\zeta} \cos\frac{\chi}{r}\,d\chi \qquad (3.22)$$

If the contact condition in region 4 is only sticking then friction forces are given as:

$$F_{F4x} = \int_0^{ul_1} \tau_0 w \cos\frac{\chi}{r}\,d\chi$$

$$F_{F4y} = \int_0^{ul_1} \tau_0 w \sin\frac{\chi}{r}\,d\chi \qquad (3.23)$$

If contact conditions involve both sticking and sliding, then the frictional forces become:

$$F_{F4x} = \int_0^{l_{pe}} \tau_0 w \cos\frac{\chi}{r}\,d\chi + \int_{l_{pe}}^{ul_1} \mu w P_0 \left(1 - \frac{\chi}{l_{ce}}\right)^{\zeta} \sin\frac{\chi}{r}\,d\chi$$

$$F_{F4y} = \int_0^{l_{pe}} \tau_0 w \sin\frac{\chi}{r}\,d\chi + \int_{l_{pe}}^{ul_1} \mu w P_0 \left(1 - \frac{\chi}{l_{ce}}\right)^{\zeta} \cos\frac{\chi}{r}\,d\chi \qquad (3.24)$$

Orientation of forces for all regions is shown in Figure 3.7.

If the contact length is longer than the fourth region, ul_1 can be calculated as follows:

$$ul_1 = r\theta_s$$

$$(3.25)$$

3.2.4.2 Forces acting on region 5

Region 5 is responsible for the beginning of flank contact which is a result of the elastic recovery of the material deformed in front of region 4. Angle sweeping through this region (Figure 3.7) is defined by θ_5 which can be calculated as:

$$\theta_5 = \frac{\chi}{r} \tag{3.26}$$

Contact conditions in region 5 vary as in the 4th region, and forces are calculated similarly except that the lower limit of the integral is taken as the length of region 4 (equation (3.22)) and upper limit is taken as ul_2.

For instance, if the contact length is shorter than the length of region 5, then the normal forces can be calculated as follows:

$$F_{N5x} = \int_{ul_1}^{ul_2} wP_0\left(1 - \frac{\chi}{l_{ce}}\right)^{\zeta} \sin\frac{\chi}{r} d\chi$$

$$F_{N5y} = \int_{ul_1}^{ul_2} wP_0\left(1 - \frac{\chi}{l_{ce}}\right)^{\zeta} \cos\frac{\chi}{r} d\chi \tag{3.27}$$

where, ul_2 can be calculated using equation (3.29), by solving equation (3.28) for θ.

$$l_{ce}' - p_1 - p_2 = r\cos(\gamma)\sin\theta - r\sin(\gamma)\cos\theta + r\sin(\gamma) \tag{3.28}$$

$$ul_2 = l_4 + r\theta \tag{3.29}$$

If the contact conditions in region 5 involves only sliding, friction forces are:

$$F_{F5x} = \int_{l_4}^{ul_2} \mu P_0 w\left(1 - \frac{\chi}{lce}\right)^{\zeta} \cos\frac{\chi}{r} d\chi$$

$$F_{F5y} = -\int_{l_4}^{ul_2} \mu P_0 w\left(1 - \frac{\chi}{lce}\right)^{\zeta} \sin\frac{\chi}{r} d\chi \tag{3.30}$$

Friction forces if the contact conditions in region 5 involve only sticking are expressed as:

$$F_{F5x} = \int_{l_4}^{ul_2} \tau_0 w \cos\frac{\chi}{r} d\chi$$

$$F_{F5y} = -\int_{l_4}^{ul_2} \tau_0 w \sin\frac{\chi}{r} d\chi$$

(3.31)

If contact conditions involve both sticking and sliding:

$$F_{F5x} = \int_{l_4}^{l_{pe}} \tau_0 w \cos\frac{\chi}{r} d\chi + \int_{l_{pe}}^{ul_2} \mu P_0 w \left(1 - \frac{\chi}{lce}\right)^{\zeta} \cos\frac{\chi}{r} d\chi$$

$$F_{F5y} = -\int_{l_4}^{l_{pe}} \tau_0 w \sin\frac{\chi}{r} d\chi - \int_{l_{pe}}^{ul_2} \mu P_0 w \left(1 - \frac{\chi}{lce}\right)^{\zeta} \sin\frac{\chi}{r} d\chi$$

(3.32)

If the total contact length is longer than the length of region 5 then upper limits are calculated as follows:

$$ul_2 = l_4 + r\theta_s$$

(3.33)

3.2.4.3. Forces acting on region 6

Region 6 is also responsible for the flank contact. This contact region forms a line. Contact line makes an angle γ with the x axis; so that the force components are multiplied by *cosine* or *sine* according to the orientation.

Normal force components can be calculated as follows:

$$F_{N6x} = -\left(\int_{l_4+l_5}^{ul_3} P_0 w \left(1 - \frac{\chi}{lce}\right)^{\zeta} d\chi \right) \sin\gamma$$

$$F_{N6y} = -\left(\int_{l_4+l_5}^{ul_3} P_0 w \left(1 - \frac{\chi}{lce}\right)^{\zeta} d\chi \right) \cos\gamma$$

(3.34)

where, γ is clearance angle and ul_3 is the upper limit, which is equal to actual contact length ℓ_{ce}.

If the contact conditions in region 6 involve only sliding, the friction forces can be calculated as follows:

$$F_{F6x} = \left(\int_{l_4+l_5}^{ul_3} \mu P_0 w \left(1 - \frac{\chi}{lce}\right)^{\zeta} d\chi \right) \cos \gamma$$

$$F_{F6y} = -\left(\int_{l_4+l_5}^{ul_3} \mu P_0 w \left(1 - \frac{\chi}{lce}\right)^{\zeta} d\chi \right) \sin \gamma$$

(3.35)

If the contact conditions in region 6 involve only sticking, then the frictional forces become:

$$F_{F6x} = \left(\int_{l_4+l_5}^{ul_3} \tau_0 w d\chi \right) \cos \gamma$$

$$F_{F6y} = -\left(\int_{l_4+l_5}^{ul_3} \tau_0 w d\chi \right) \sin \gamma$$

(3.36)

If contact conditions involve both sticking and sliding, friction forces are given as:

$$F_{F6x} = \left(\int_{l_4+l_5}^{l_{pe}} \tau_0 w d\chi + \int_{l_{pe}}^{ul_3} \mu P_0 w \left(1 - \frac{\chi}{lce}\right)^{\zeta} d\chi \right) \cos \gamma$$

$$F_{F6y} = -\left(\int_{l_4+l_5}^{l_{pe}} \tau_0 w d\chi + \int_{l_{pe}}^{ul_3} \mu P_0 w \left(1 - \frac{\chi}{lce}\right)^{\zeta} d\chi \right) \sin \gamma$$

(3.37)

40

3.3. Solution Procedure

In this section, solution procedure for the proposed model is presented. Flow chart for solution procedure can be seen below:

Primary and secondary shear zones modeling [3].

↓

Determination of shear stress τ_0 and normal stress [3].

↓

Determination offriction model [3].

↓

Obtain Shear angle by minimum energy approach

&

Stagnation Point is taken as equal to shear angle.

↓

Determine total contact length & Sticking contact length
(3.15)-(3.17)- (3.20)-(3.28)

Region 4:	Region 5:	Region 6:
Normal forces: (3.19)	Normal forces:(3.27)	Normal forces: (3.34)
Friction forces if:	Friction forces if:	Friction forces if:
Only sliding:(3.22)	Only sliding:(3.30)	Only sliding:(3.35)
Only Sticking:(3.23)	Only Sticking:(3.31)	Only Sticking:(3.36)
Sticking &Sliding:(3.24)	Sticking &Sliding: (3.32)	Sticking &Sliding: (3.37)

Total Edge Forces (3.38)

Shear stress τ_0 and normal stress P_0 are obtained from the analysis of the primary and secondary shear zones [3]. Friction model is also taken from [3]. Shear angle is obtained by minimum energy approach and stagnation point is taken as equal to shear angle. Projected contact length l_{ce}' is obtained from experiments for different hone radii, feed and speed. With the measured data an empirical equation (3.15) is determined using regression analysis for projected contact length l_{ce}'. Afterwards, actual contact length l_{ce} is obtained by finding corresponding angle, θ, from the equations (3.20) and (3.28). Then, sticking contact length ℓ_{pe} is calculated by using the equation (3.17). With the knowledge of ℓ_{pe} friction conditions are known and the cutting forces can be calculated for each region. Upper limits for integrals can be calculated by equations (3.21) and (3.27). For region 4 normal forces are obtained using equation (3.19). Friction forces are calculated using equation (3.22) if the contact conditions on the hone contact involve only sliding and using (3.23) if only sticking. If the contact conditions involve both sticking and sliding then equation (3.24) is used to calculate friction forces. For region 5, forces are calculated in a similar way using equations (3.27) and (3.30-3.32). Integral limits are changed for region 5 accordingly. For region 6 normal forces are obtained by (3.34) and friction forces are calculated using equations (3.35-3.37) with the contact conditions of only sliding, only sticking, or both sticking and sliding, respectively. Finally, tangential and feed edge forces are obtained as follows:

$$F_{ex} = F_{Njx} + F_{Fjx}$$

$$j=1,2,3 \qquad (3.38)$$

$$F_{ey} = F_{Njy} + F_{Fjy}$$

To sum up, in this chapter modeling of the third deformation zone is presented; including the material and friction behavior in a new way. To model the entire cutting process primary and secondary shear zone modeling are adapted from the previous work [3]. Also it is concluded that shear is not affected by strain and strain rate highly for the AISI 1050 material model. Thus material behavior assumed to be the same with the chip formation zones.

CHAPTER 4 VERIFICATION OF THE PROPOSED MODEL

In this section, model verification is presented. Model results involving different contact length estimations are discussed and compared to the experimental results. Model results are also discussed with data taken from the literature [34].

4.1. Model Verification

In Figure 4.1-Figure 4.8 comparisons of measured and predicted tangential and feed forces are shown together with the experimental data taken from the literature. Legends used in the graphs are listed as follows:

E.M.F.F: Empirical Model Tangential Force

E.M.T.F: Empirical Model Feed Force

P.R.T.F: Partial Recovery Model Tangential Force

P.R.F.F: Partial Recovery Model Feed Force

F.R.T.F: Full Recovery Model Tangential Force

F.R.F.F: Full Recovery Model Feed Force

R.CL.F.F: Measured Contact Length Feed Force

R.CL.T.F: Measured Contact Length Tangential Force

Figure 4.1. Different model results and measured data of tangential and feed forces for 6µm hone radius and 30 m/min cutting speed.

Figure 4.2. Different model results and measured data of tangential and feed forces for 6µm hone radius and 250 m/min cutting speed.

44

For the tool with 6 μm hone radius, it can be seen from Figure 4.1 and Figure 4.2 that although model with Full Recovery Assumption (FRA) and Elastic Recovery Assumption (ERA) provides close results the empirical model gives better results for both tangential and feed forces. When held separately, feed forces are better estimated than tangential forces and models give better results at slower speeds. The main reason for the misbehavior of the empirical model is the contact length underestimation at high forces. FRA and ERA give the contact lengths based on stagnation angle, which changes at most 2% with speed due its equality to the shear angle and minimum energy principle. It provides close results at all speeds, which in this case underestimated the larger forces with speed. There is a 17.7% average discrepancy between Empirical Model results and the experimental data of feed forces and 31.2% between tangential forces. The errors are 23.3% and 50.3%, respectively for FRA, whereas they are 24.4% and 53.3%, respectively for ERA.

Figure 4.3. Different model results and measured data of tangential and feed forces for 20μm hone radius and 30 m/min cutting speed.

Figure 4.4. Different model results and measured data of tangential and feed forces for 20µm hone radius and 250 m/min cutting speed.

For the tool with 20 µm hone radius (Figure 4.3 and Figure 4.4), model results show similar trends. FRA and ERA gives higher contact lengths with higher hone radius. Thus, the models have lower error with the experimental data compared to the results of smaller hone radius. Also empirical model estimates the contact lengths better. There is an 18.1% average error between Empirical Model results and the experimental data of feed forces and 28.2% between tangential forces. The errors are 20.3% and 34.7%, respectively for FRA, whereas they are 23.8% and 42.8%, respectively for ERA.

When the tools with 40 µm hone and 60 µm radii are considered (Figure 4.5Figure 4.8) it can be said that FRA and ERA give better model results than the previous one due to the increasing hone radius. However, Empirical Model underestimates the contact lengths and causes high errors. The average error between Empirical Model results and the experimental data of feed forces is 16.9% for 40 µm hone radiused tool and 17.5% for 60 µm hone radiused tool. For tangential forces these errors are 32.2% and 30.2%, respectively.

When feed rate is close to the hone radius or smaller, contributions of ploughing forces increase. Especially feed forces are affected by the process. As a result, due to the

minimum shear angle assumption on forces, higher shear angles and stagnation angles are obtained which affect strain and finally the contact lengths. That results in higher forces for large hone radiused tools (40 μm and 60 μm) at 0.05 mm/rev feed rate. This causes peaks at the beginning of the model results. Also it is observed that for high hone radii the forces are estimated better.
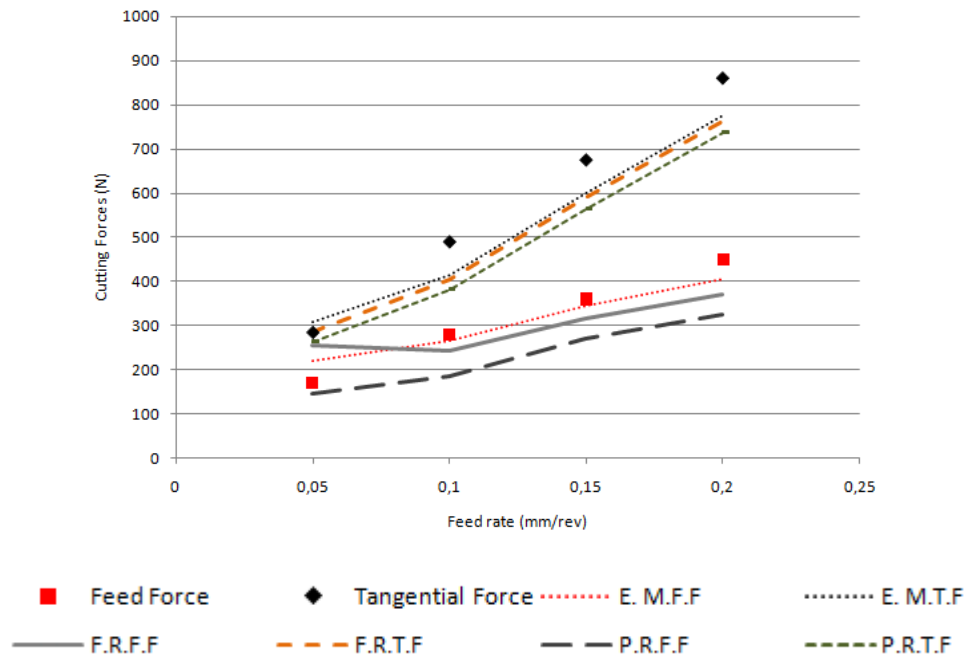
Figure 4.5. Different model results and measured data of tangential and feed forces for 40μm hone radius and 30 m/min cutting speed.

Figure 4.6. Different model results and measured data of tangential and feed forces for 40μm hone radius and 250 m/min cutting speed.
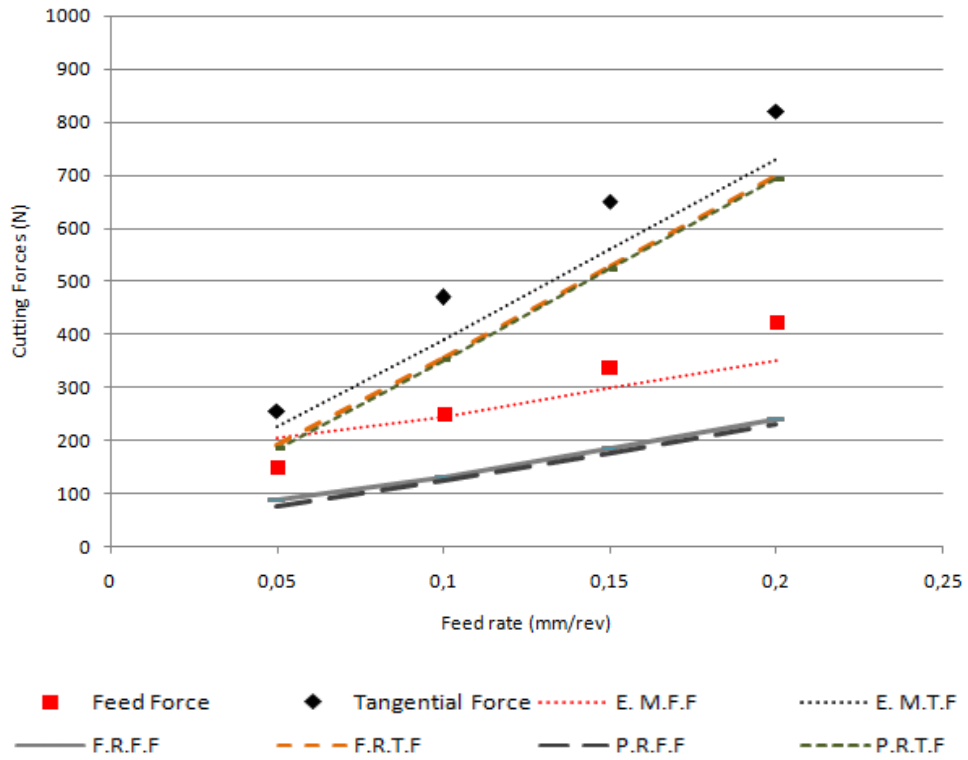
Figure 4.7. Different model results and measured data of tangential and feed forces for 60µm hone radius and 30 m/min cutting speed.
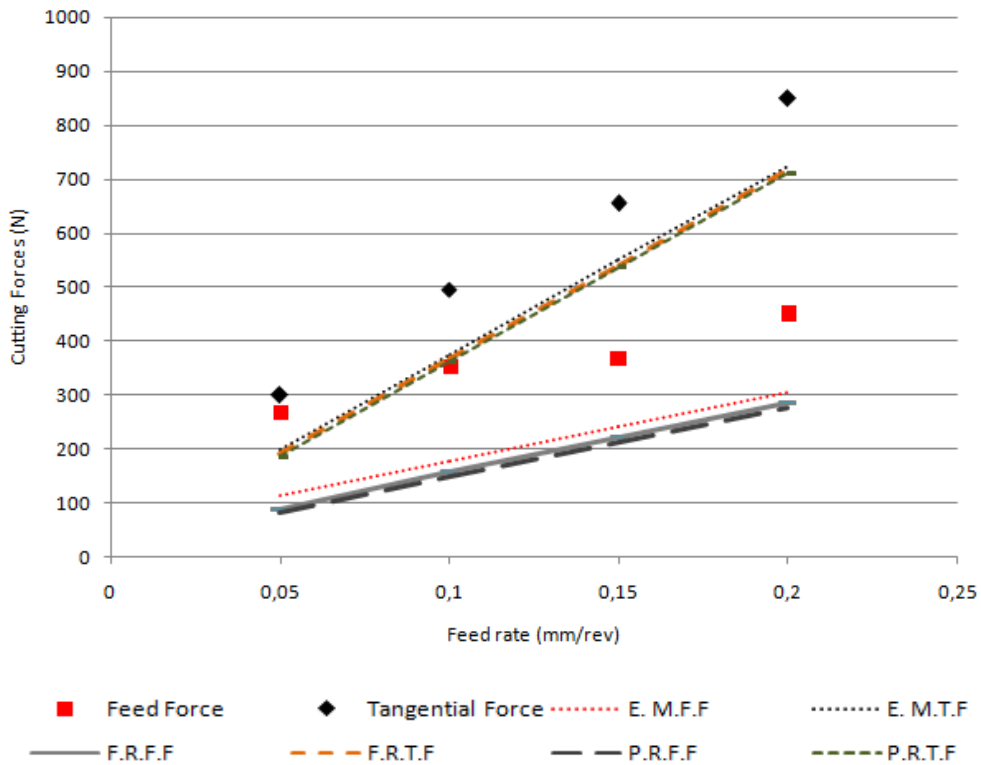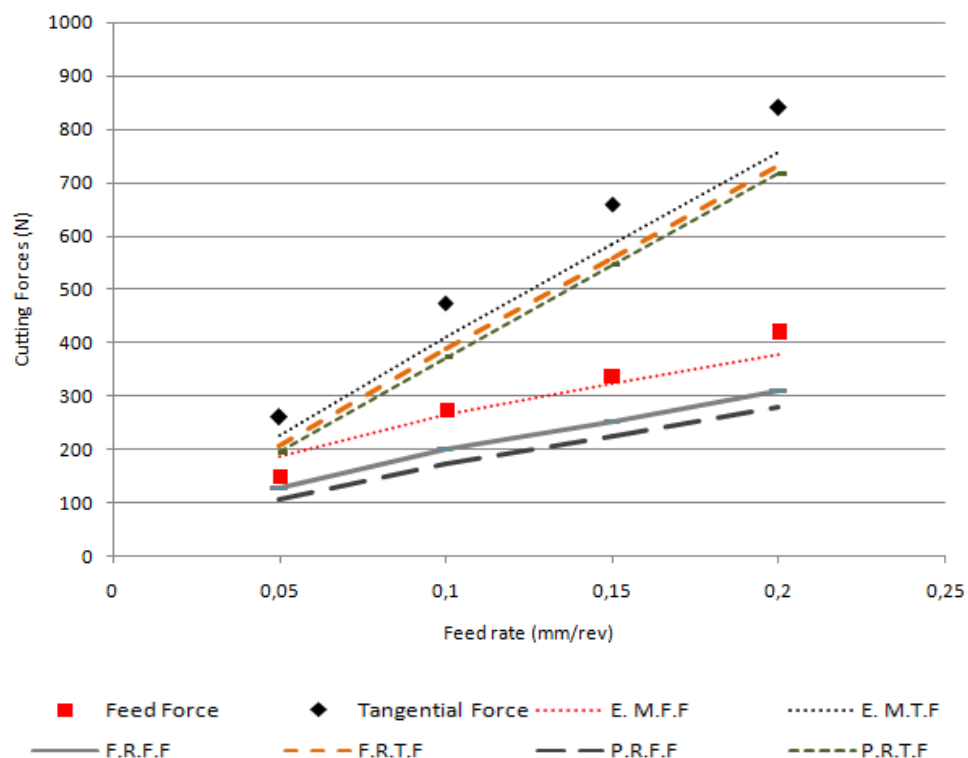

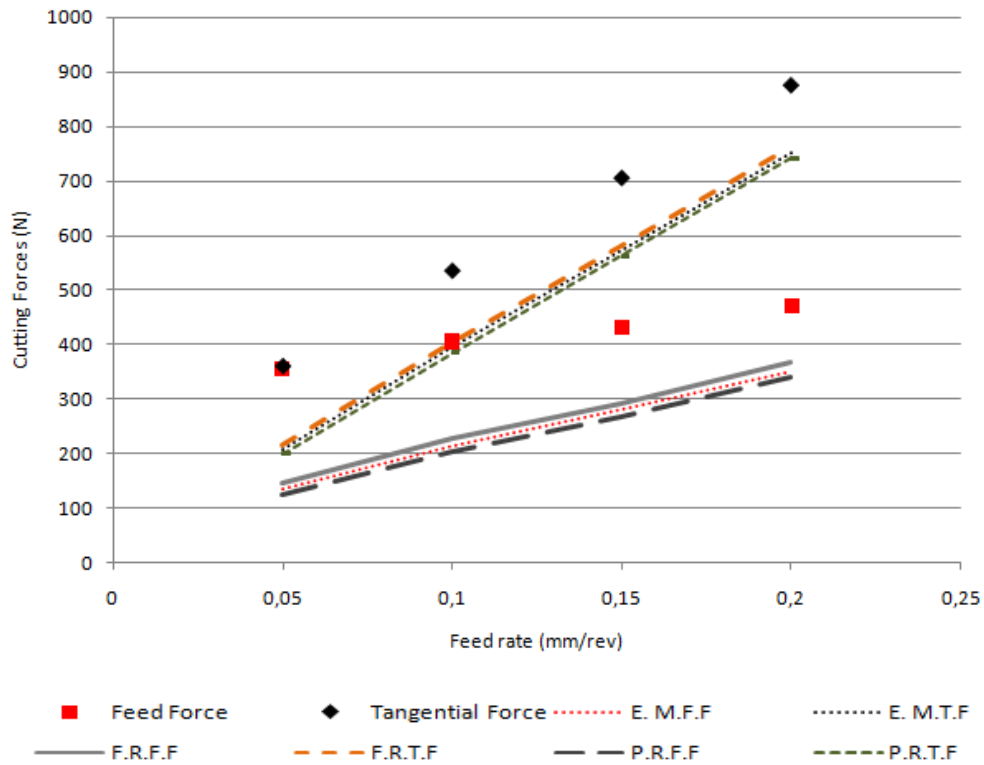Figure 4.8. Different model results and measured data of tangential and feed forces for 60µm hone radius and 250 m/min cutting speed.

48

Additionally, measured (real) contact lengths are used in the model for the tool with 60 µm hone radius which will be referred as RCL (real contact length). It can be seen that for 30 m/min the error is lower than that of250 m/min results. Also the results are compatible with FRA at 250 m/min. Overall errors of RCL are 28.7% for feed forces and 19% for tangential forces, which are better than other models and indicates that the correct assumption of contact length gives compatible model results.

Figure 4.9-Figure 4.13show the comparison of model results to experimental data obtained from [3]. Besides of the Empirical Model, FEA and ERA measured (real) contact lengths also used in the model.

As can be seen from the figures, RCL results are almost the same with empirical model, which implies that the empirical model evaluates contact lengths well. The average error between RCL results and the experimental data of tangential forces is 19.3% for 12 µm hone radiused tool, 19.1% for 30µm hone radiused tool and 16.6% for 60 µm hone radiused tool. For feed forces the error is 24.9%, 16.3% and 19.3% respectively. The average error between Empirical Model results and the experimental data of tangential forces is 20% for 12 µm hone radiused tool, 19.8% for 30µm hone radiused tool and 18% for 60 µm hone radiused tool. For feed forces the error is 22%, 20.3% and 20%, respectively. Another observation is that the models give better estimations at higher cutting speed, since forces have lower values then the experimental data above. It may be a result of different tool grade and higher clearance angle which is 11˚. Also similar to the above observations above forces are higher due to ploughing at 60 µm hone radiused tool for 0.05 mm/rev feed rate. When FRA is considered the average error of overall analysis is 19.3% for tangential forces while it is 34% for feed forces and it is 21.8% and 35.3%, respectively for ERA.

Figure 4.9. Comparison of different model results and measured data of tangential and feed forces from the literature for 12μm hone radius and 30 m/min cutting speed.

Figure 4.10. Comparison of different model results and measured data of tangential and feed forces from the literature for 12μm hone radius and 250 m/min cutting speed.

Figure 4.11. Comparison of different model results and measured data of tangential and feed forces from the literature for 30µm hone radius and 30 m/min cutting speed.
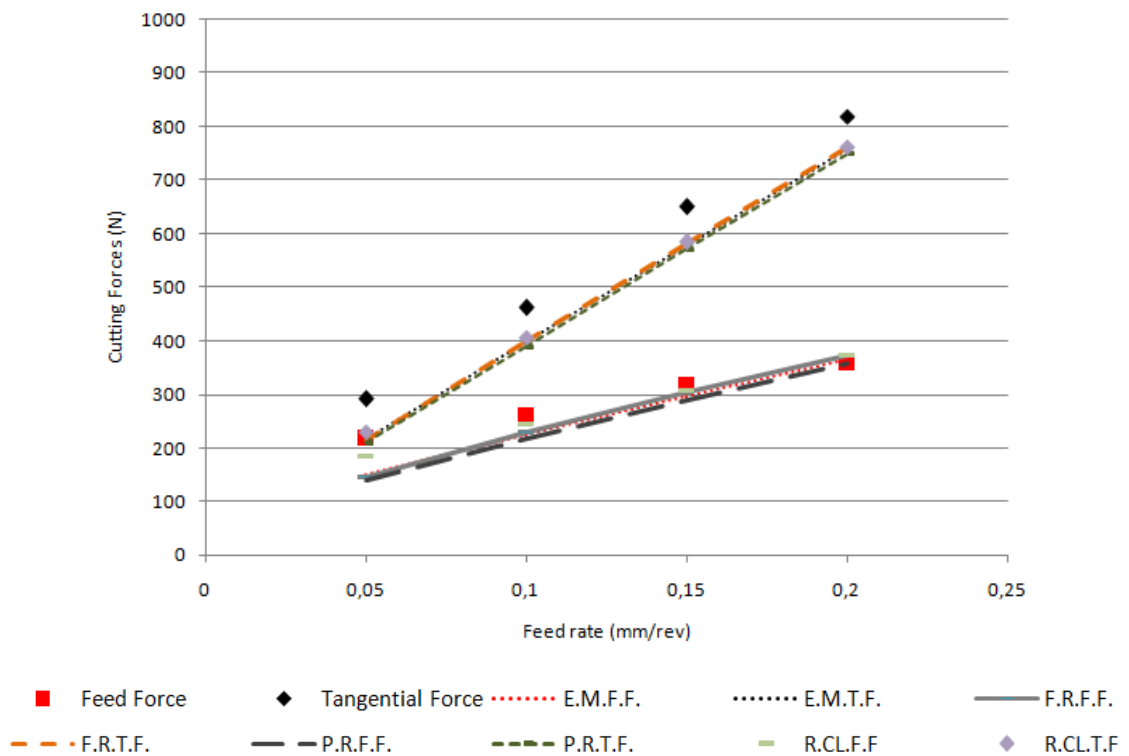
Figure 4.12. Comparison of different model results and measured data of tangential and feed forces from the literature for 30µm hone radius and 250 m/min cutting speed.
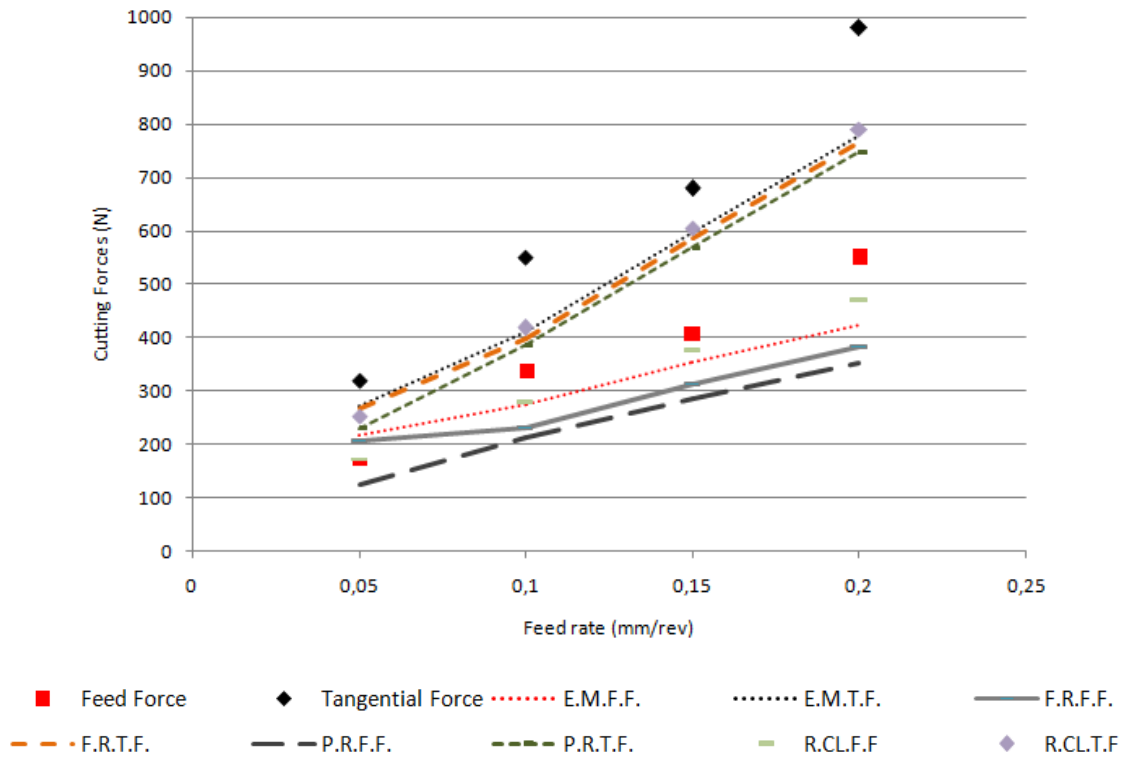
Figure 4.13. Comparison of different model results and measured data of tangential and feed forces from the literature for 60µm hone radius and 30 m/min cutting speed.
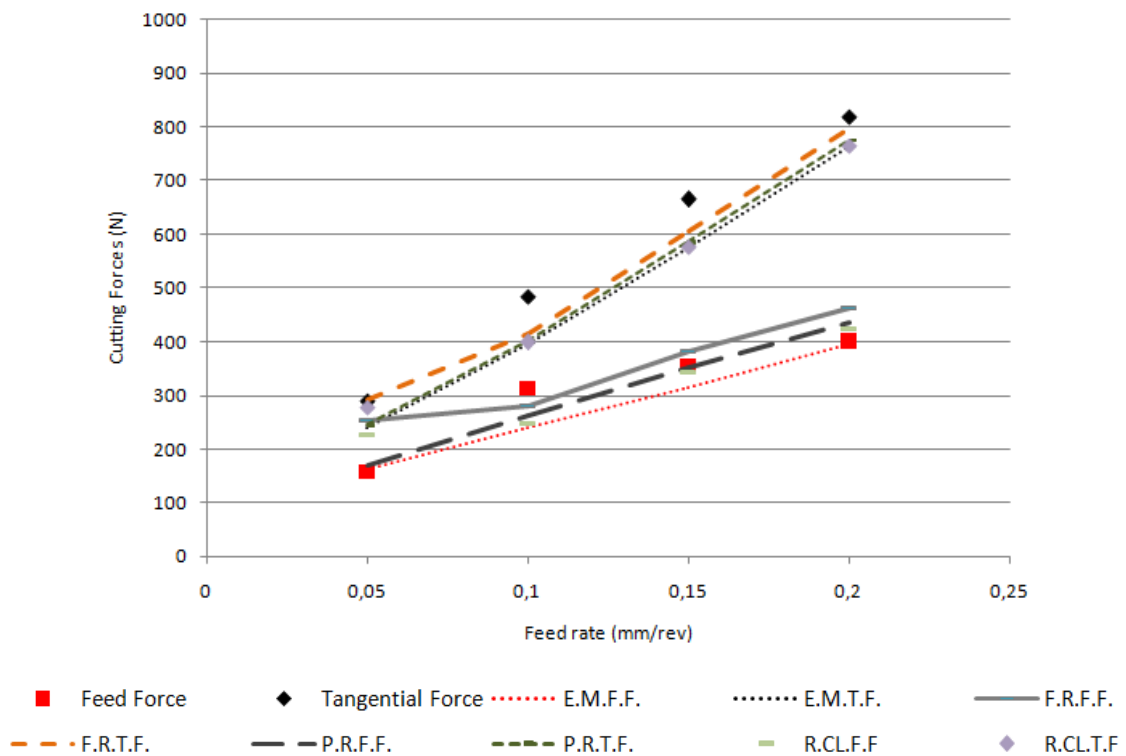
Figure 4.14. Comparison of different model results and measured data of tangential and feed forces from the literature for 60µm hone radius and 250 m/min cutting speed.

Edge forces obtained with linear regression are also compared with the third deformation zone forces obtained from different models. Edge force comparisons for sharp tool (6µm) and tool with large hone radius (60µm) are presented for 30 and 250 m/min cutting speeds.

When sharp tool (6µm) is considered (Figure 4.15 to Figure 4.19) it is seen that model forces are not changing with feed rate as in the linear regression method. However, all models underestimate the forces and the errors are high. For FRA at third deformation zone 4th region forces cancel out 5th and 6th region forces because of the small rounding of the tool tip; which result in forces around 10N. ERA also gives similar results for edge forces due to small hone radius. Only empirical model at 30 m/min overestimates feed edge force while underestimating tangential edge force. Edge forces are dependent of the slope of the regression line; if the forces are highly affected by the increase of the feed rate; the slope of the regression line becomes steeper and the fees forces are found to be lower. Average errors for forces are 60% for empirical model, 80% for FRA, 90% for ERA and 70% for RCL.
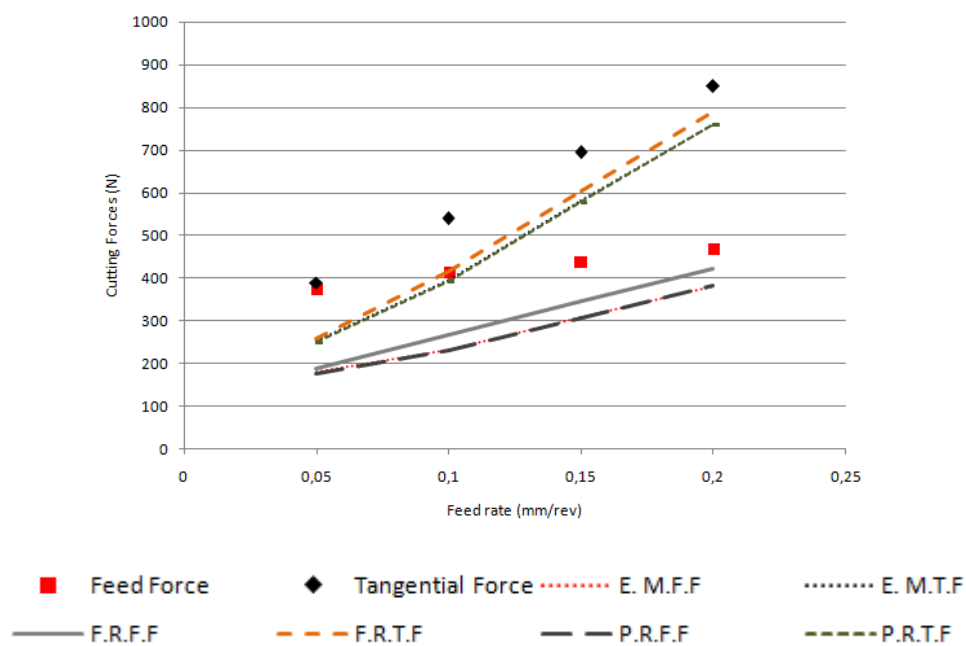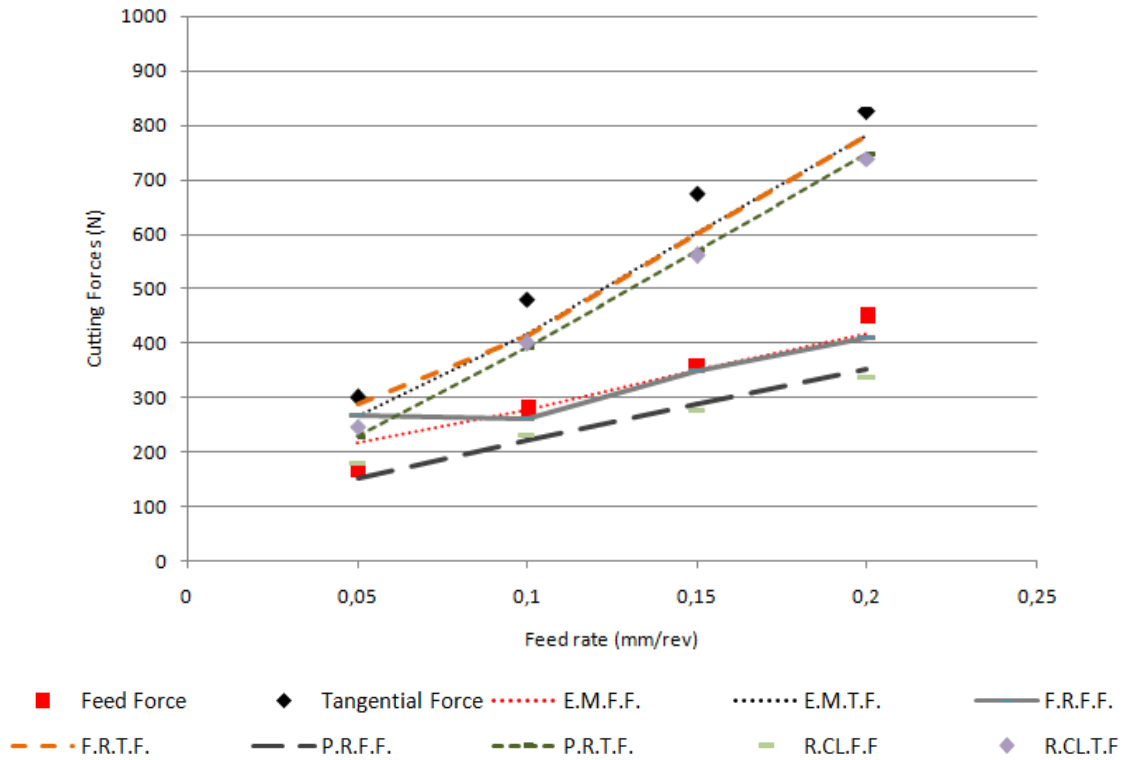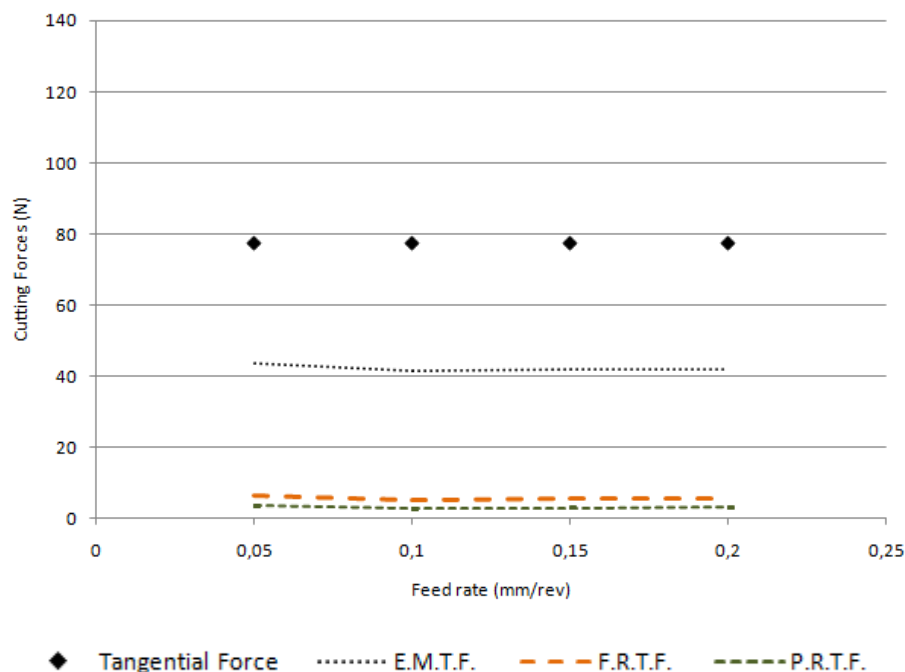

Figure 4.15. Comparison of different model results and measured data of tangential edge forces for 6µm hone radius and 30 m/min cutting speed.
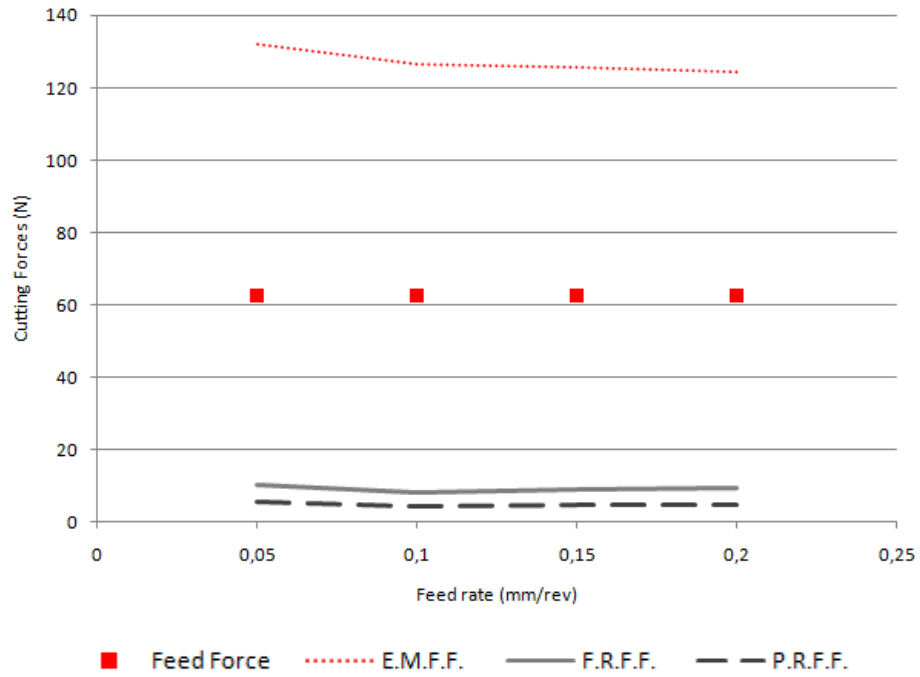
Figure 4.16. Comparison of different model results and measured data of feed edge forces for 6μm hone radius and 30 m/min cutting speed.
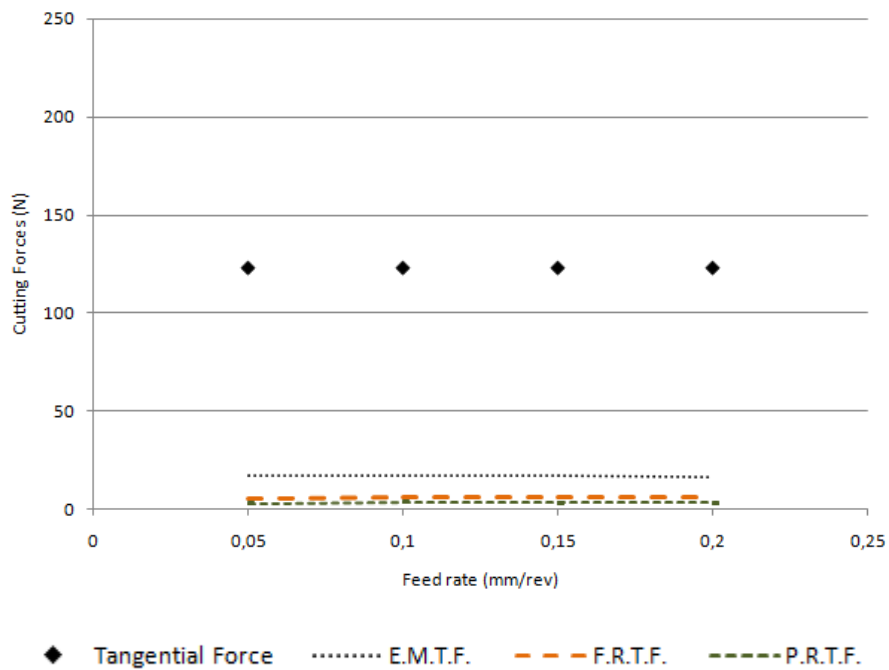
Figure 4.17. Comparison of different model results and measured data of tangential edge forces for 6μm hone radius and 250 m/min cutting speed.
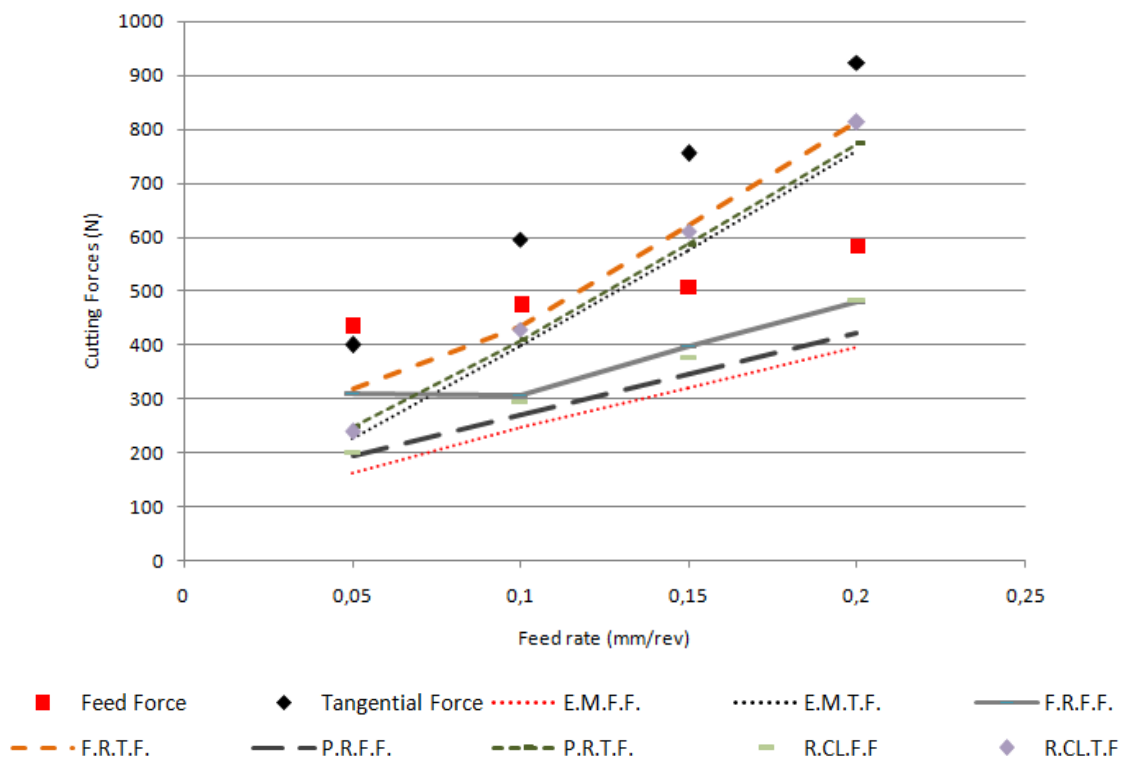
54
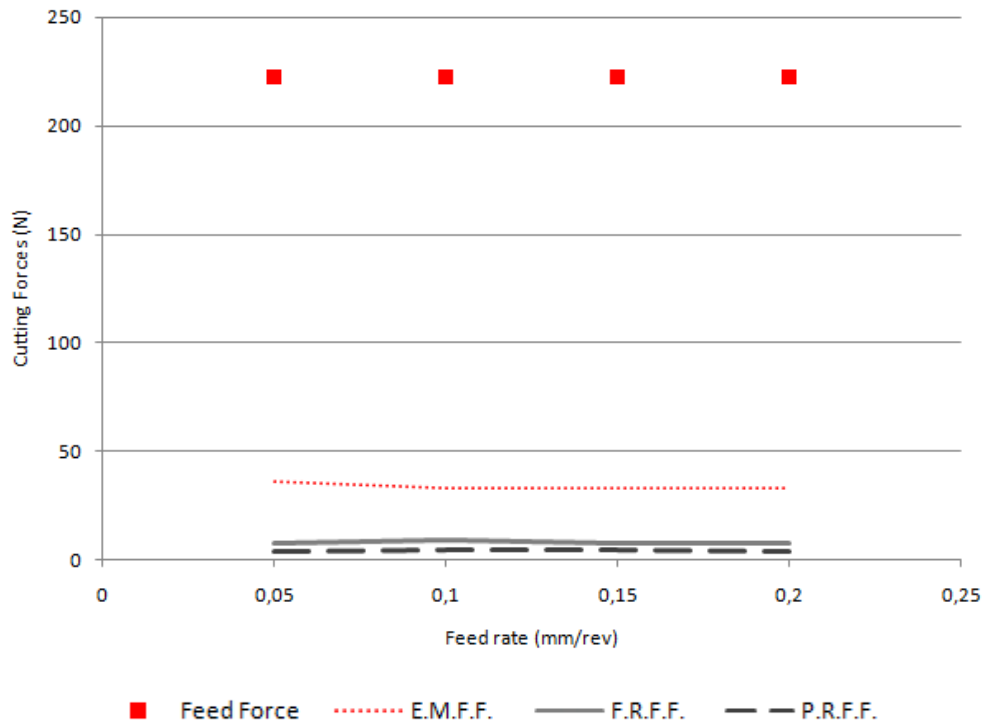
Figure 4.18. Comparison of different model results and measured data of feed edge forces for 6µm hone radius and 250 m/min cutting speed.
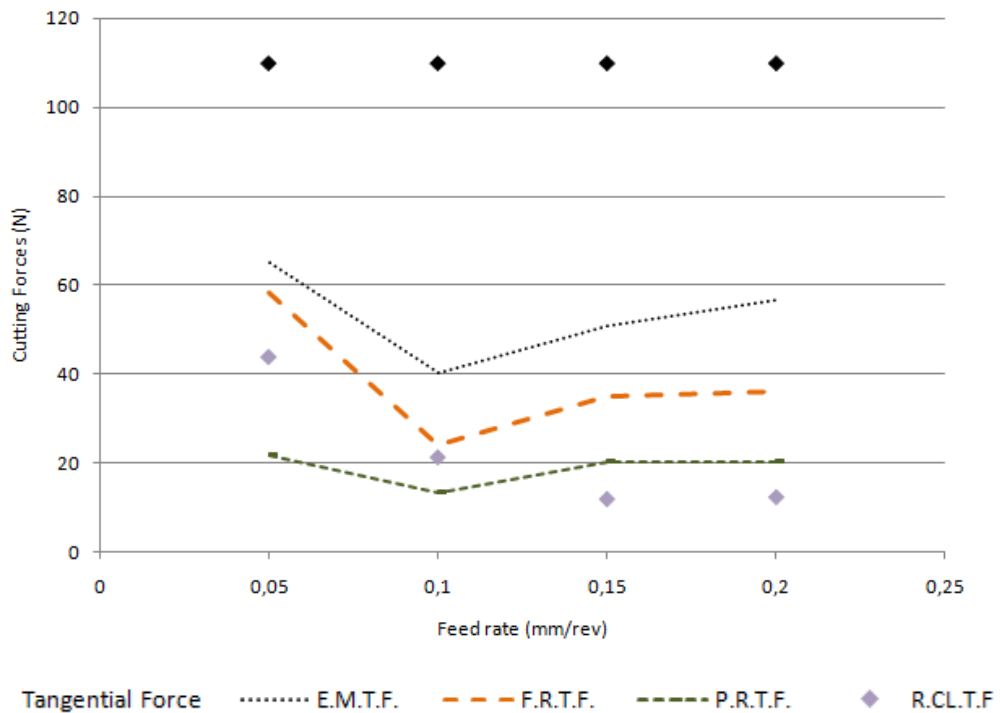
Figure 4.19. Comparison of different model results and measured data of tangential edge forces for 60µm hone radius and 30 m/min cutting speed.
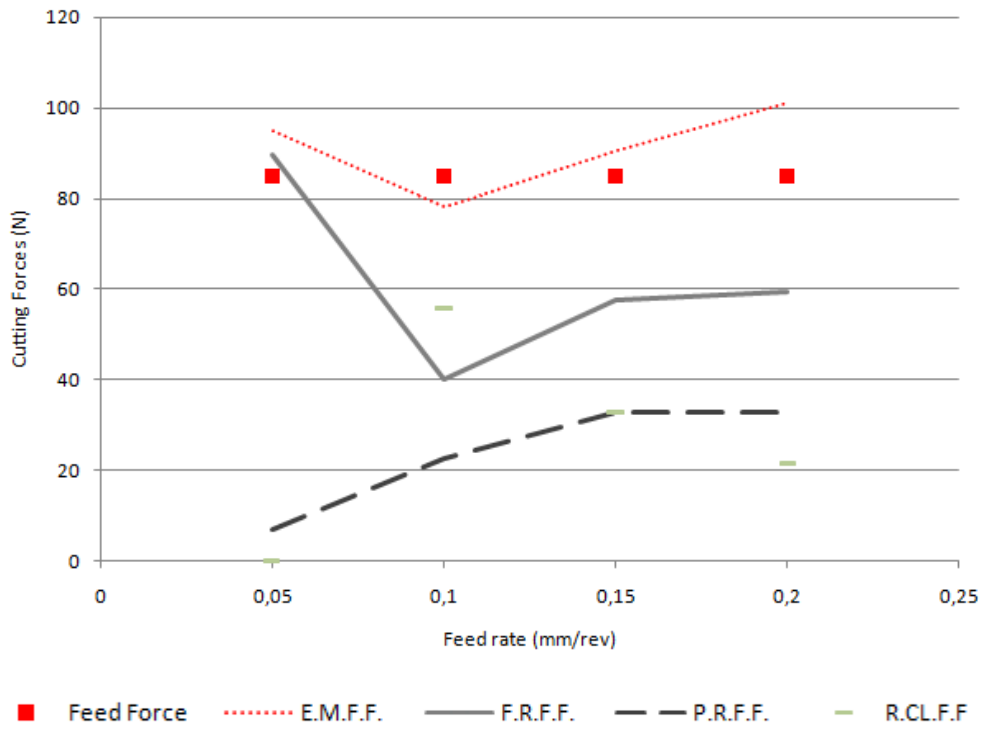
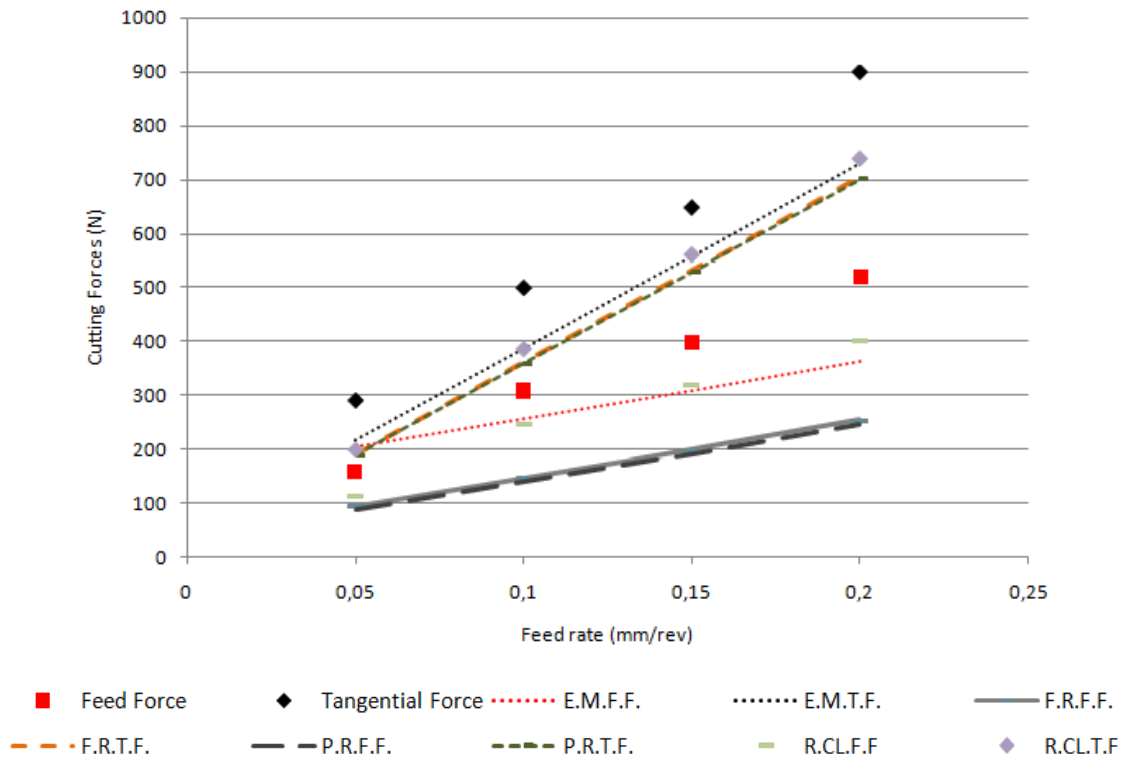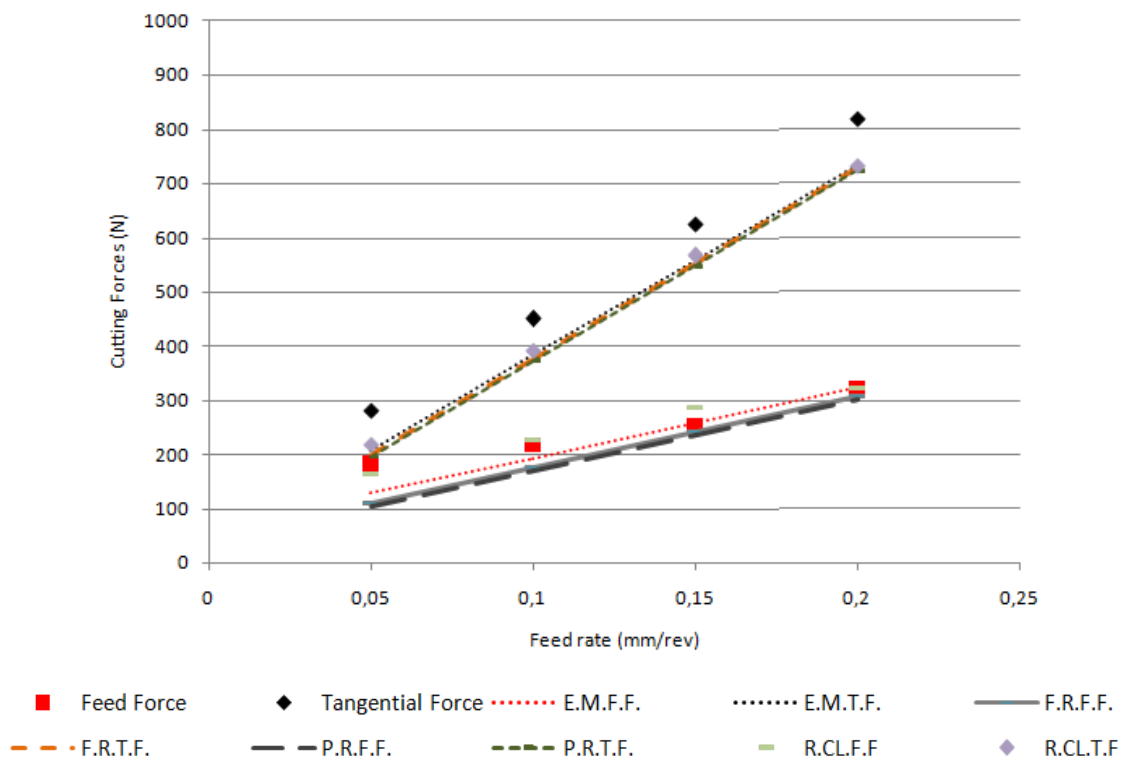Figure 4.20. Comparison of different model results and measured data of feed edge forces for 60µm hone radius and 30 m/min cutting speed.
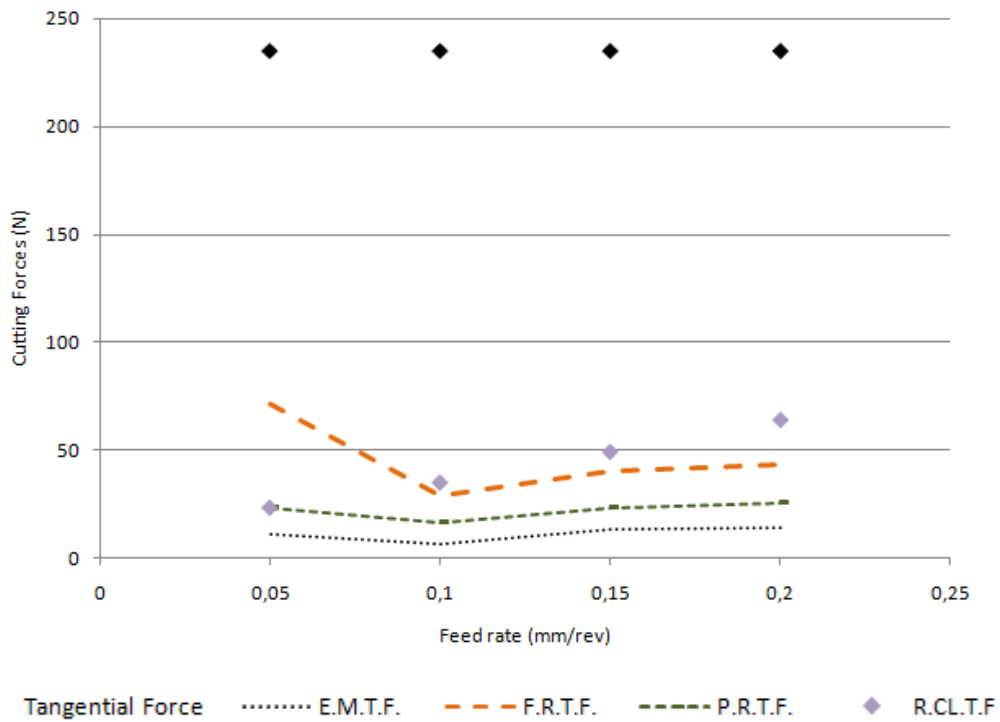
Figure 4.21. Comparison of different model results and measured data of tangential edge forces for 60µm hone radius and 250 m/min cutting speed.

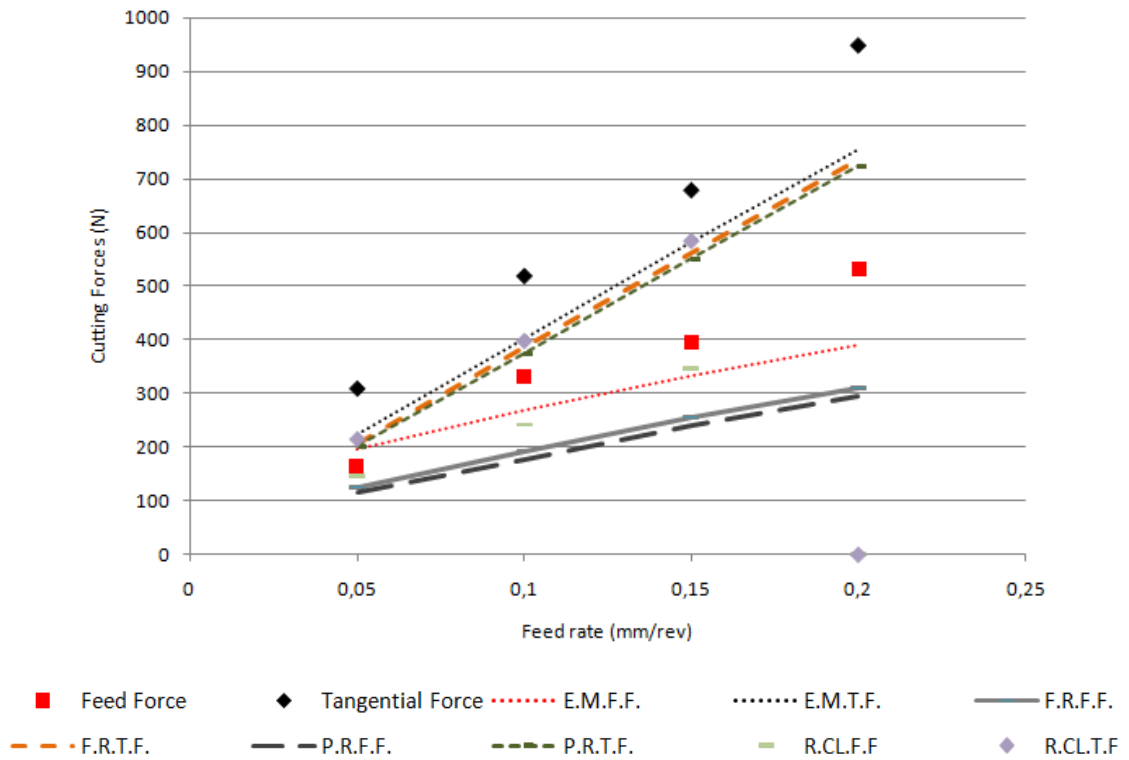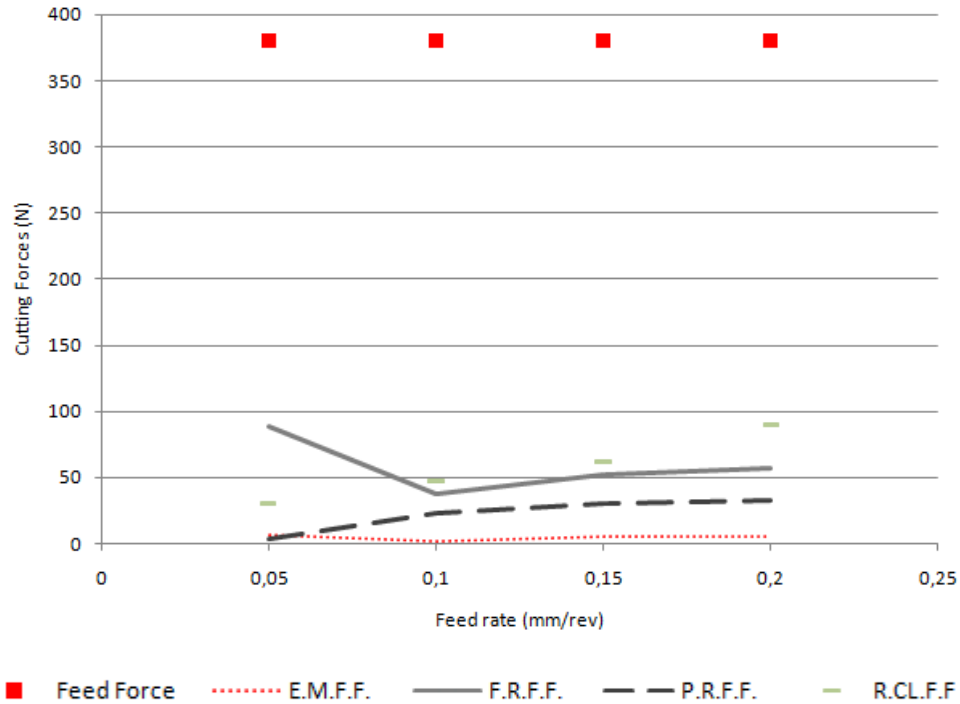Figure 4.22. Comparison of different model results and measured data of feed edge forces for 60μm hone radius and 250 m/min cutting speed.

When tool with large hone radius (60μm) is considered (Figure 4.20, Figure 4.21andFigure 4.22) it is seen that with increased hone radius higher edge forces are obtained from ERA and FRA. This is the result of increased force components in the 5th and 6th regions with higher hone radius. Also, it can be observed that, ERA results in larger edge forces at 0.05 mm/rev feed rate due to the high stagnation angle obtained from the simulations; which can be explained by the comparable feed rate with hone radius. For instance; it is observed from Figure 4.19 to Figure 4.22; high stagnation angle results in higher forces at 0.05 mm/rev feed rate.

Since the calculated edge forces are dependent on the contact length obtained directly by hone radius and stagnation angle for ERA and FRA; change in forces with feed rate is the result of small changes in hone radius in each test; whereas it is a result of changed contact length for RCL and empirical model.

It is observed that at 250 m/min the difference is very high (90%) between model and linear regression results while at 30 m/min models predict edge forces fairly (30%) with linear regression model. However, there is no uniformity in the trend of model results. It can be indicated that the results are not consistent since linear regression model results have their own discrepancies due to the effect of the feed rate on forces.

4.2. Further Investigation and Analysis on the Parameters of the Proposed Model

Originally pressure distribution and the stress were assumed as the same of first deformation zone; and as a result of sensitivity analysis, strain, strain rate and stagnation angle were taken from the first deformation zone. In this section various changes to the elements of the model are proposed for better estimation of third deformation forces.

4.2.1. Friction Behavior Analysis

In the model the friction behavior is based on combined sticking and sliding contact zones. For error minimization purposes the conditions of all sliding contact and all sticking contact are also investigated and compared with the experimental data. Figure 4.23 shows model results for a nearly sharp tool. It can be observed that the model with all sliding contact assumption and the dual zone approach gives nearly the same results, whereas model with all sticking contact assumption provides higher forces due to the increased shear stress. For small hone radiused tools the contact length is also smaller. Thus total sticking forces are not much higher than the forces of sticking and sliding zones combined. However, as the contact length increases with hone radius, sticking will be effective on a larger area and will result in much higher forces due to increased shear stress.
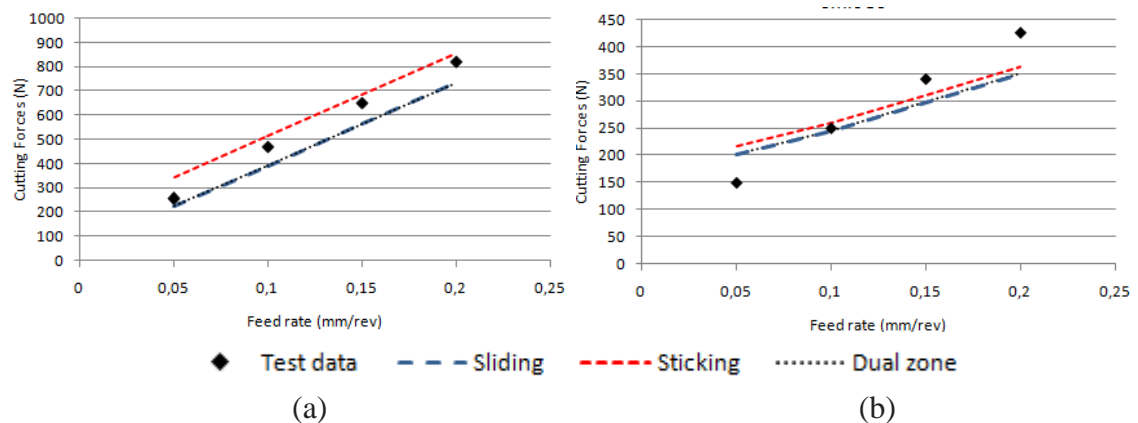
Figure 4.23. (a) Tangential (b) Feed forces comparison of the model results with different friction behavior assumptions for 6μm hone radius and 30 m/min cutting speed.

When third deformation zone forces are considered (**Figure 4.24**), model with dual zone approach gives the best results. Also, when all data set is taken into consideration with different speeds and hone radii, the model with both sticking and sliding contact zones have the lowest average discrepancy.
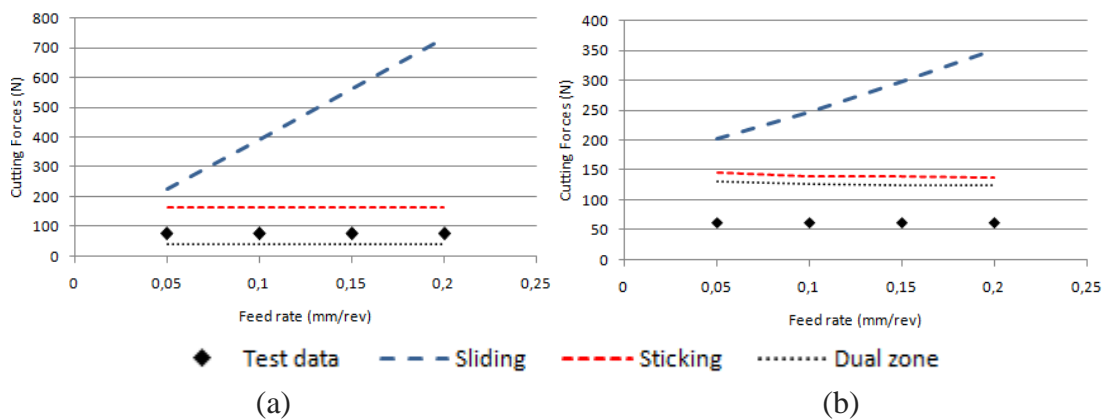
Figure 4.24. (a) Tangential (b) Feed edge forces comparison of the model results with different friction behavior assumptions for 6μm hone radius and 30 m/min cutting speed.

4.2.2. Shear Stress Analysis

The effect of the temperature is taken into consideration and the stress for third deformation zone is obtained by the Johnson Cook model. Temperature is obtained by Ceau's [24]empirical equation, which is explained in Chapter 2, strain is taken as the one in the secondary deformation zone and average strain rate is used which is confirmed by sensitivity analysis in Chapter 3. Comparison of stress with secondary shear zone stress can be seen in **Figure 4.25**and comparison of the results with the experimental data and empirical model data can be seen in

Figure 4.26.

It can be observed from the Figure 5.3. that difference between shear stress at the beginning of secondary shear zone and the calculated shear stress for the third deformation zone is at most 6% at 30 m/min cutting speed and 16% at 250 m/min cutting speed. However, due to sticking and sliding contact zone assumption, the difference between shear stresses affects only tangential edge forces of the empirical model by 1N. The shear stress formulation and the empirical formula for temperature can be used for making the model more analytical. ERA and FRA are not taken into consideration since the normal discrepancies are higher than the empirical model.
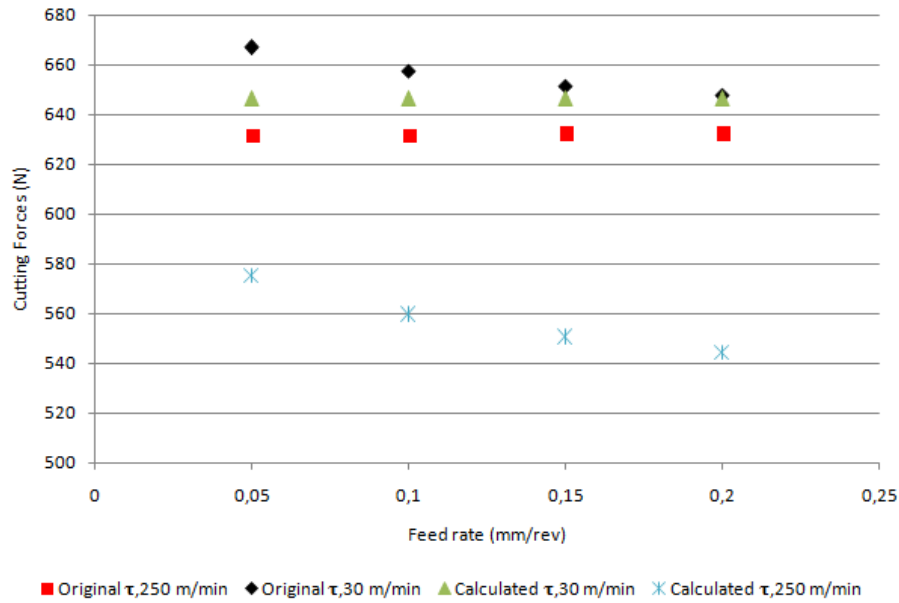
Figure 4.25. Shear stress comparison for 6μm hone radius at different speeds.
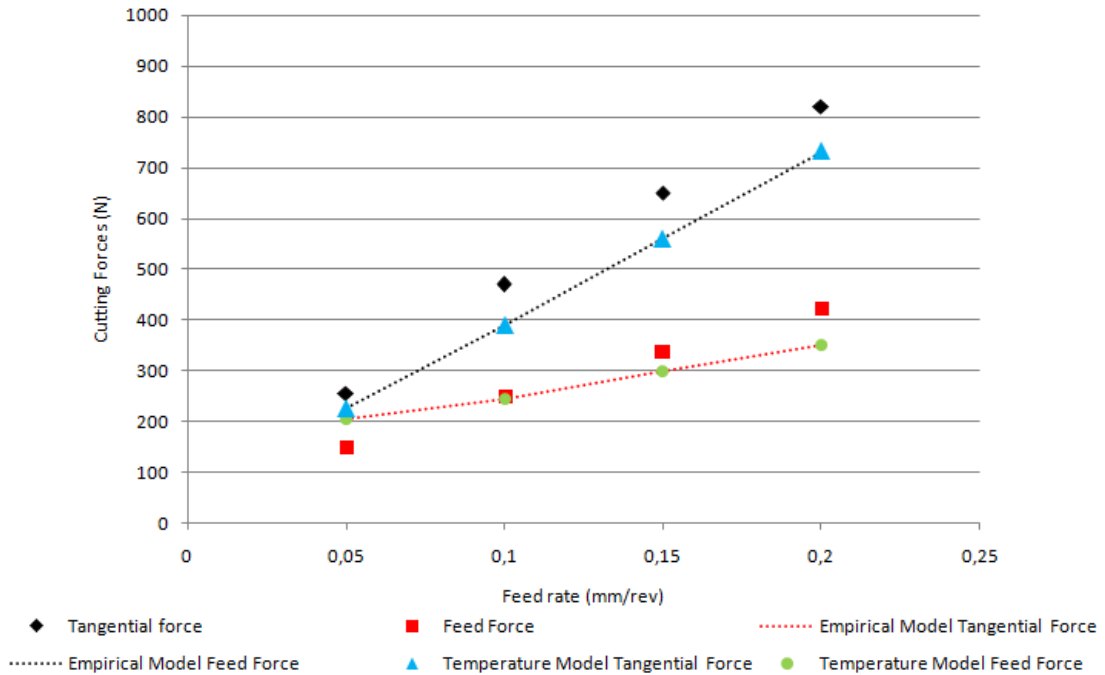
Figure 4.26. Total force comparison for 6μm hone radius and 30 m/min speed, empirical model.

4.2.3. Pressure Distribution Analysis

The pressure distribution is given in the previous chapter, and the distribution coefficient (ζ) is assumed to be the same as the one in the primary and secondary shear zones. In this section, total and third deformation force results from different pressure distributions are compared. It is observed from the analysis that for different speeds and

hone radii different pressure distributions yield better results where for 6µm hone radius and 30 m/min speed, model results are shown in Figure 4.27andFigure 4.28.
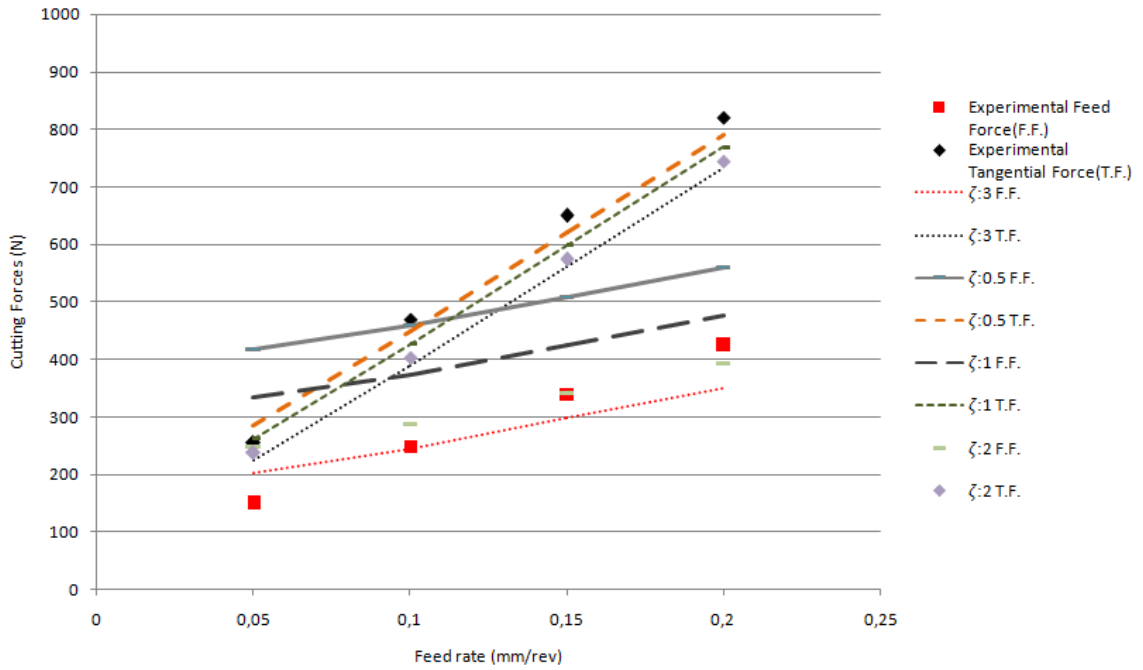
Figure 4.27. Tangential and feed force comparison for different pressure distribution for 6µm hone radius and 30 m/min speed, empirical model.
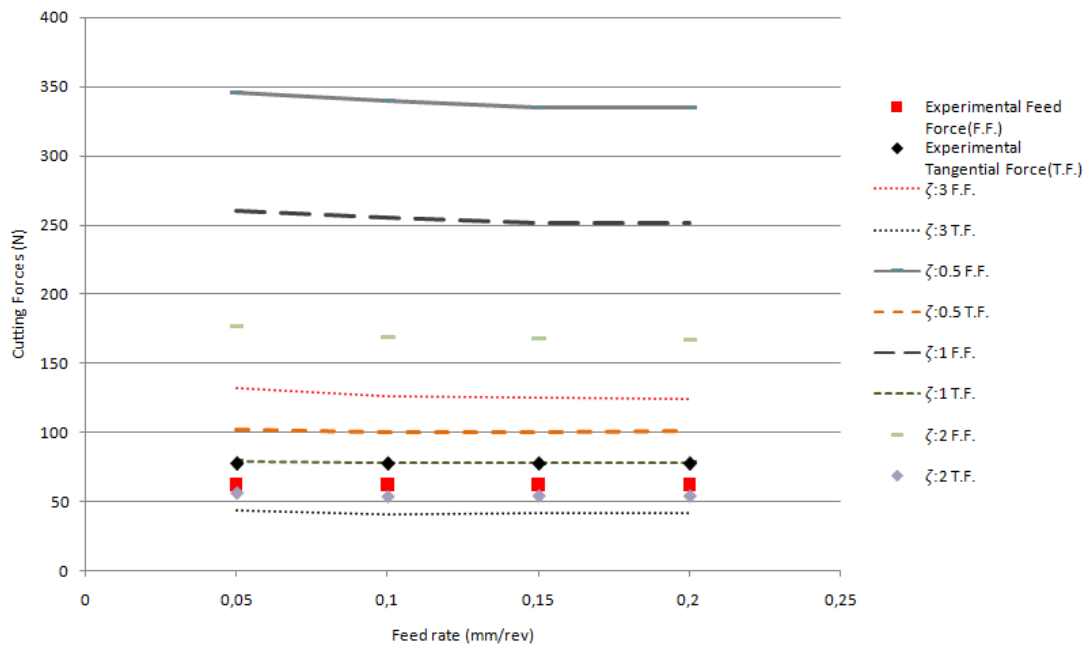
Figure 4.28. Tangential and feed third deformation zone force comparison for different pressure distribution for 6µm hone radius and 250 m/min speed, empirical model.

Tangential forces are estimated with lowest discrepancy when ζ=0.5 while feed forces are estimated with the lowest discrepancy when ζ=2. Tangential third deformation zone

forces are estimated with lowest discrepancy when ζ=3 while feed third deformation zone forces are estimated with lowest discrepancy when ζ=2. When all data set is taken into consideration, first degree distribution (ζ=1) gives the lowest average discrepancy for total forces whereas the original pressure distribution (ζ=3) has the similar discrepancy. Since the difference is not very high original pressure distribution coefficient is maintained.

4.2.4. Contact Length Analysis

In the previous chapter, different contact length estimations are used in the model and total and third deformation zone forces are discussed. Some models gave compatible results with total forces however discrepancy between third deformation zone forces and the models were very high. For that matter, contact lengths giving accurate third deformation zone forces are obtained using linear regression model in this section. For comparison both contact length and forces data from the literature are used [34]. Firstly material model is investigated. To obtain higher third deformation forces higher stress should be obtained. Therefore strain and strain rate are increased in the simulations while temperature is decreased. Initial values of strain, strain rate and temperature are calculated from analytical and empirical equations given in the previous chapters. Simulations were run for 12µm hone radiused tool at 30, 60, 100 and 250 m/min cutting speeds and 0.05, 0.1, 0.15 and 0.2 mm/rev feed rates. Third deformation forces are taken as reference.

Figure 4.29 andFigure 4.30show the errors for the contact length calibration. Lowest error combination for all tangential, feed forces and contact length is selected and the corresponding stress, strain and temperature values are obtained. (See Appendix 1) The results are not presented for 30 m/min since force discrepancies are found to be higher than 40%. For 60 m/min cutting speed, simulations provides contact lengths corresponding to lower discrepancies between forces however the discrepancy between measured contact lengths and the simulation results are around 70-90% which is not compatible and again not presented. For 100 m/min and 250 m/min cutting speeds it is observed from the figures that error for forces are around 30%- 40 %. The forces obtained with lower discrepancy are often a result of very low temperature, which is not compatible. Also, there is no unity in the results of this method as it is not able to find similar results at the same strain, strain rate for different feeds and speeds.
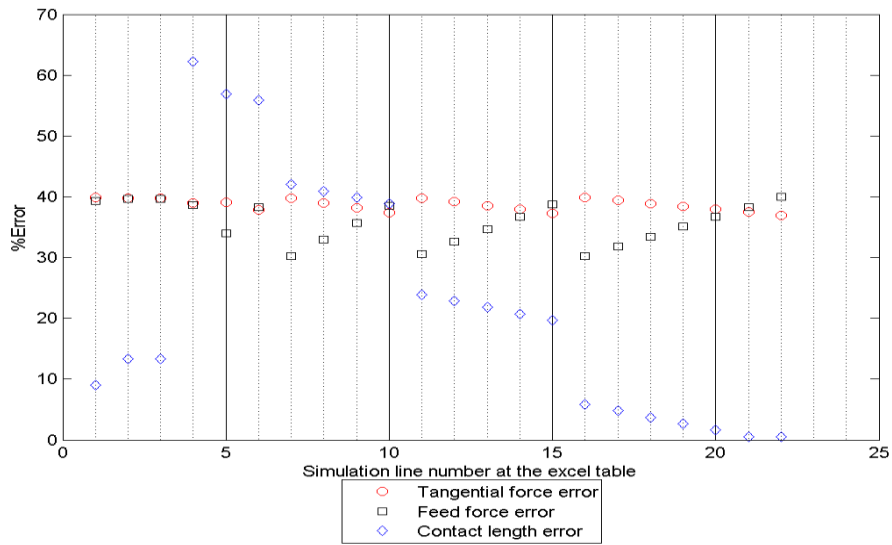
Figure 4.29. Contact length calibration simulation results for 12μm hone radiused tool, 100 m/min cutting speed and 0.1 mm/rev feed rate.
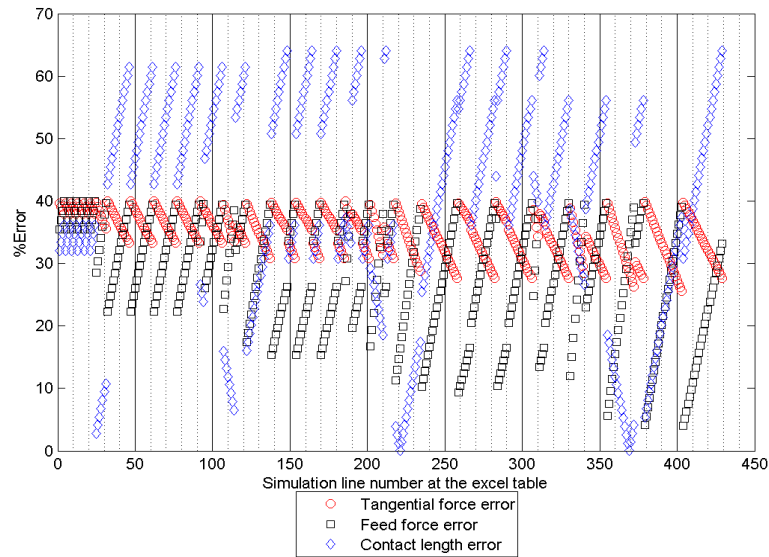
Figure 4.30. Contact length calibration simulation results for 12μm hone radiused tool, 250 m/min cutting speed and 0.1 mm/rev feed rate.

For the last approach, pressure distribution is changed while the rest of the model remains same. (Figure 4.31) Then the effect of contact length is investigated to see if there exists a contact length satisfying both tangential and feed forces.

63

(a)

(b)
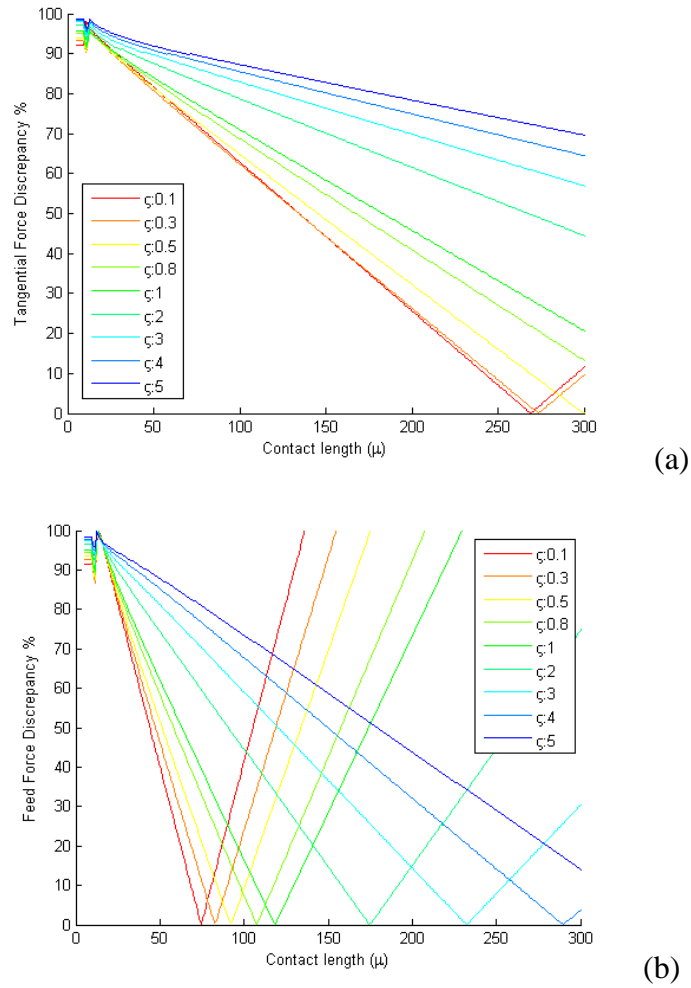
Figure 4.31. (a) Tangential (b) Feed force results with changing contact length for 12µm hone radiused tool, 100 m/min cutting speed and 0.1 mm/rev feed rate and different pressure distributions.

It can be seen from the results that contact length corresponds to the tangential forces with low discrepancy has feed forces with very high discrepancy with the experimental data.

There are several reasons for the both simulations not giving compatible results. First of all linear regression model is used for third deformation forces which has contradictions at the model itself such as giving negative forces due to the slope of the fit. Another reason is that material model between the tool and the workpiece may not be constructed well enough since there are different grades of the tool and the microstructure of the ploughed material may behave differently. Finally inaccuracies in the measurements can cause such discrepancies.

64

4.2.4. Edge Force Determination with Secondary and Third Degree Regression

To introduce an alternative regression approach, second degree and third degree regression is investigated. Second and third degree regressions take feed rate into consideration more than linear regression model. However, the resulting edge forces are independent from the feed rate as before. Figure 4.32 shows the two different regression approaches. It is observed that third degree regression often result in negative forces thus an example for the second degree regression results comparison with the Empirical Model and linear regression model results.

(a)   (b)
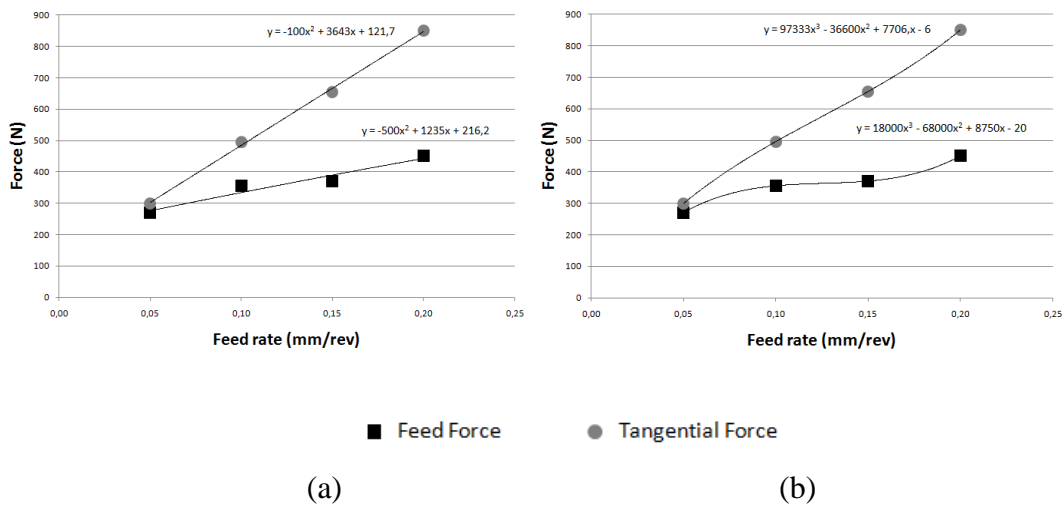
Figure 4.32. (a)Second degree (b) third degree regression for 6μm hone radius and 250 m/min cutting speed

(a)   (b)
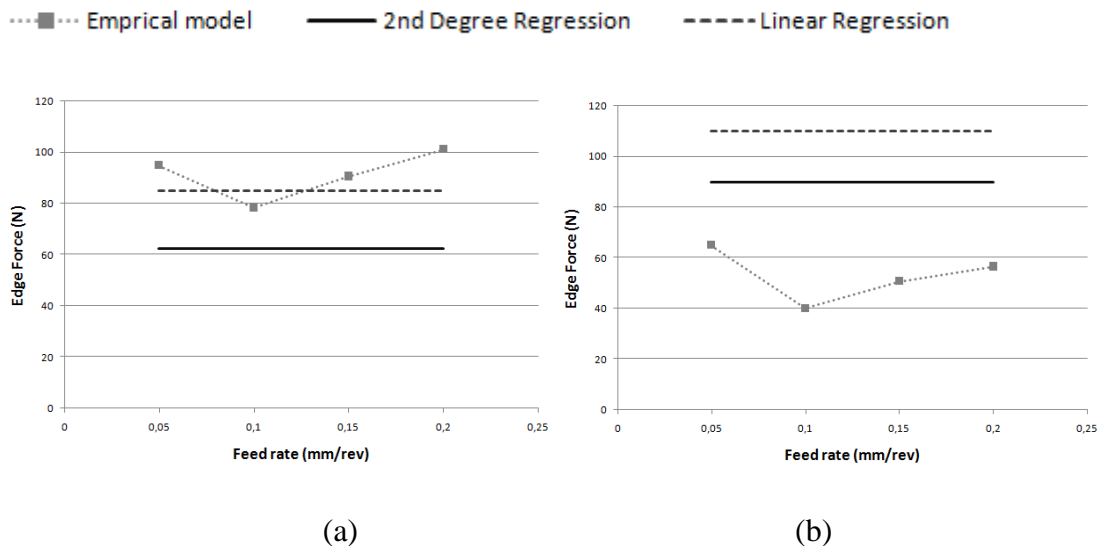
Figure 4.33 (a) Feed (b) tangential edge forces 60μm hone radius and 30 m/min cutting speed.

65

It is observed from

Figure 4.33 that linear regression model estimates the feed edge force better whereas for tangential force second degree regression is more suitable. When overall data is investigated second degree regression results in lower forces which are more compatible with the empirical model results. However, at high speeds due to the underestimation of the contact length; the error between the model results and regression results are very high. Second degree regression can be considered with a different contact length approach of the model.

To sum up, in this chapter proposed model with different contact length estimations are verified with the experimental data. General observations can be concluded as follows:

• Empirical Model and RCL gives the best total force results among the proposed model due to better contact length estimation. However, for third deformation zone the errors are high due to the linear regression model.

• Different approaches for model components are investigated for better estimation. Initial approaches gave better estimations except that the shear stress can be obtained by an empirical model for a more computable model.

• Different regression methods for edge force determination are presented. It is concluded that second degree regression can be an alternative to linear regression model. However the discrepancy would be still high at high speeds.

CHAPTER 5 CONCLUSION& FUTURE RESEARCH

In this thesis, effect of the hone radius on total and third deformation zone forces and temperature is experimentally investigated with different cutting conditions. Also, total and third deformation zone forces are estimated with the proposed semi-analytical model, adopting the primary and secondary shear zone models by Özlü [30]. The following are the remarks for the experimental results, modeling and analysis done throughout this research:

- Total cutting forces generally increase with the hone radius; however the change is nonlinear and very small compared to the increase rate of hone radius.

- Two different approaches are considered to find edge forces. The forces obtained from the low feed cutting tests have contradictions; thus linear regression method is used for the edge force determination. It is seen that edge forces are increasing with increased hone radius similar to the total forces; and the change is nonlinear.

- Contact length on the flank face including tool tip is measured and compared with the data taken from the literature. It is seen that in both data sets the change of contact length with speed and feed are in opposite trends. This is believed to be the result measurement uncertainties and changes in the cutting process due to tool stiffness or cutting tool-workpiece material interaction.

- Temperature measurements are done with an infrared camera to investigate thermal behavior of the tool tip and compare temperatures with the rake and flank contacts. It is concluded that the hone radius slightly effects temperature of the tool tip due to higher heat dissipation on the bigger hone. Also it is observed that the temperature is lower at the tool tip than the rake face. Also flank face has the lowest temperatures. However the maximum difference is around 80 degrees which is by sensitivity analysis determined to be insignificant for the material properties in the

modeling. An empirical model is acquired from [24] which are in good agreement with the measured temperature data.

- For the third deformation zone modeling thermomechanical material model is used. Sensitivity analyses are done on JC material model parameters and found to be compatible with the ones in the secondary shear zone. Also an analysis of the shear stress with the empirical temperature model is presented. As a result it is concluded that the empirical model can be used to determine shear stress in the third deformation zone along with the strain and strain rate obtained from the secondary shear zone.

- For the friction behavior the dual zone model is adapted from the secondary shear zone where both sticking and sliding contacts are considered. The sticking zone model was found to be more effective for the sharp tool; however, model with both sticking and sliding contact zones is in better agreement with the overall data.

- The pressure distribution is investigated in order to determine the best representative model. It is seen that for overall data a third degree pressure distribution provides the best results similar to the secondary shear zone.

- Four different contact length estimation approaches are conducted and compared in the force model; full recovery, elastic recovery, empirical model and the measured data. It is seen that the material recovery models provide compatible results for high hone radiused tools, however, generally underestimate both total and the third deformation forces. Forces estimated with empirical and measured contact lengths are in better agreement with the force data obtained from the experiments and the literature [34]. It is also observed that the feed forces are estimated better.

- The model predictions for tangential and feed third deformation zone forces are compared with the edge forces identified from the measurements using the linear regression model. All four contact length models underestimate the edge forces. In addition, the forces obtained from the model are feed rate sensitive while the forces obtained through linear regression are not. However, for sharper tools the force trends

are compatible. Also it is observed that the feed edge forces are obtained as almost the double of the tangential edge forces from the empirical model.

- Studies for estimating the contact length satisfying edge forces are performed in terms of strain, strain rate, temperature and pressure distribution. The analyses for material parameters resulted in contact lengths giving feed and tangential edge forces with 30-40% discrepancy; however, temperature is reduced to unrealistic values to do so. Moreover, the contact length discrepancy with the measured data is around 70% in most of the results. When pressure distribution is changed and either the tangential or feed edge force is considered as the main parameter, the agreement is very good with the main parameter whereas the discrepancy is very high with the other. Another inconvenience is that the linear regression has also conflicts about edge forces since a sharp slope may result in negative forces.

- Second and third degree regression for the determination of edge forces is investigated. It is concluded that second degree regression may give more compatible results. However the error is still cannot be eradicated for the high speeds.

In future studies, due to the reasons stated above, another approach for the experimental determination of edge forces could be investigated. Also a different approach for contact length calculation could be implemented. Moreover, thermal investigation of the third deformation zone could be extended and an analytical model could be proposed. Furthermore; the model could be applied to practical machining processes especially micro cutting and precision turning where the cutting edge is very important.

Bibliography

[1] Waldorf, D. J., 2006, A Simplified Model for Ploughing Forces in Turning, Journal of Manufacturing Processes, Volume 8, Issue 2, pp. 76-82.

[2] Tunç, L.T., Budak, E., 2012, Effect of Cutting Conditions and Tool Geometry on Process Damping in Machining, International Journal of Machine Tools and Manufacture, Volume 57, pp. 10-19.

[3] Özlü E., 2008, Analytical Modeling of Cutting Process Mechanics and Dynamics for Simulation of Industrial Machining Operations, PhD Thesis, FENS Sabanci University, Istanbul.

[4] Altintas, Y.,2012, Manufacturing Automation. 2nd ed. Cambridge: Cambridge University Press.

[5] Merchant, E., 1945, Mechanics of the Metal Cutting Process I. Orthogonal Cutting and a Type 2 Chip, Journal of Applied Physics, 16/5:267-275.

[6] Albrecht, P., 1960, New Developments in the Theory of the Metal-Cutting Process: Part I. The Ploughing Process in Metal Cutting, J. Eng. for Industry 82, pp. 348-358.

[7] Endres, J. W., Manjunathaiah, J., 2000, A New Model and Analysis of Orthogonal Machining With an Edge-Radiused Tool, Manuf. Sci. Eng. 122, 384.

[8] Kountanya, R.K. , Endres, W.J., 2001, A High-Magnification Experimental Study of Orthogonal Cutting with Edge-honed Tools, ASME MED, v12, pp. 157–163.

[9] Waldorf D.J., DeVor, R. E., and Kapoor, S. G., 1999, An Evaluation of Ploughing Models for Orthogonal Machining, Journal of Manufacturing Science and Engineering, Volume 121.4, pp.550-558.

[10] Shatla, M., Kerk, C., Altan, T.,2001, Process Modeling in Machining. Part I: Determination of Flow Stress Data, International Journal of Machine Tools and Manufacture, Volume 41, Issue 10, pp. 1511-1534.

[11] Oxley, P. L. B., 1989, An Analytical Approach to Assessing Machinability, Mechanics of Machining, Halsted Press, New York.

[12] Shatla, M., Kerk, C., Altan, T.,2001, Process Modeling in Machining. Part II: Validation and Applications of the Determined Flow Stress Data, International Journal of Machine Tools and Manufacture, Volume 41, Issue 11, pp. 1659-1680.

70

[13] Guo. Y.B., Chou, Y.K., 2004, The determination of ploughing force and its influence on material properties in metal cutting, Journal of Materials Processing Technology, Vol. 148, pp. 368–375.

[14] Salvatore F., Mabrouki T., Hamdi H., 2011, Numerical simulation and analytical modeling of ploughing and elastic phenomena during machining processes, Int. Journal of Surface Science and Engineering, Volume 6-3, pp. 185-200.

[15] Fang, N., 2003, Slip-line Modeling of Machining with a Rounded-edge tool—Part I: New Model and Theory, Journal of the Mechanics and Physics of Solids, Volume 51, Issue 4, pp. 715-742.

[16] Karpat, Y., Özel, T., 2008, Analytical and Thermal Modeling of High-Speed Machining with Chamfered Tools, ASME Journal of Manufacturing Science and Engineering, Vol: 130.

[17] Karpat, Y., Özel, T., 2005, Predictive Modeling of Surface Roughness And Tool Wear in Hard Turning Using Regression and Neural Networks, International Journal of Machine Tools and Manufacture vol. 45 issue 4-5 April, pp. 467-479.

[18] Karpat, Y., Özel, T., 2008, Mechanics of High Speed Cutting with Curvilinear Edge Tools, International Journal of Machine Tools and Manufacture, Volume 48, Issue 2, pp. 195-208.

[19] Thiele, D. J., Melkote, S. N., 1999, Effect of Cutting Edge Geometry and Workpiece Hardness on Surface Generation in the Finish Hard Turning of AISI 52100 steel, Journal of Materials Processing Technology, Volume 94, Issues 2–3, pp. 216-226.

[20] Endres, W.J., Kountanya, R.K., 2002, The Effects of Corner Radius and Edge Radius on Tool Flank Wear, Transactions of NAMRI/SME, v30, pp. 401–407.

[21] Özel T., Hsu T-K., Zeren E., 2005, Effects of Cutting Edge Geometry, Workpiece Hardness, Feed Rate and Cutting Speed on Surface Roughness and Forces in Finish Turning of Hardened AISI H13 steel. Int J AdvManufTechnol 25:262-269.

[22] Özel, T., 2002, Modeling of Hard Part Machining: Effect of Insert Edge Preparation in CBN Cutting Tools, J. Mater.Proc.Technol, Volume 141, pp. 284-293.

[23] Ranganath, S., Campbell, A. B., Gorkiewicz, D. W., 2007, A Model to Calibrate and Predict Forces in Machining with Honed cutting Tools or Inserts, International Journal of Machine Tools and Manufacture, Volume 47, Issue 5, pp. 820-840.

[24] Ceau, G., Popovici, V., Croitoru, S.,2010, Researches About The Temperature of The Cutting Edge In Turning Of Unalloyed Steel, U.P.B. Sci. Bull., Series D, Vol. 72, Iss. 3.

[25] Wyen, C.-F., Wegener, K., 2010, Influence of Cutting Edge Radius on Cutting Forces in Machining Titanium, CIRP Annals - Manufacturing Technology, Volume 59, Issue 1, pp. 93-96.

[26] Bassett, E., Köhler, J., Denkena, B., 2012, On The Honed Cutting Edge and its Side Effects During Orthogonal Turning Operations of AISI1045 with Coated WC-Co Inserts, CIRP J. of Manuf. Sci. and Tech., Volume 5, Issue 2, pp. 108-126.

[27] Yen, Y.-Ch., Jain, A., Altan, T., 2004, A Finite Element Analysis of Orthogonal Machining Using Different Tool Edge Geometries, J. Mater.Proc.Technol., Vol. 146, pp. 72-81.

[28] Hua, J. et al., 2005, Effect of Feed Rate, Workpiece Hardness and Cutting Edge on Subsurface Residual Stress in the Hard Turning of Bearing Steel Using Chamfered; Hone Cutting Edge Geometry, Materials Science and Engineering: A, Volume 394, Issues 1–2, pp. 238-248.

[29] Umbrello, D., Ambrogio, G., Filice, L., Shivpuri, R., 2007, An ANN Approach for Predicting Subsurface Residual Stresses and the Desired Cutting Conditions During Hard Turning, Journal of Materials Processing Technology, Volume 189, Issues 1–3, pp. 143-152.

[30] Fang, N., Fang, G., 2007, Theoretical and experimental investigations of finish machining with a rounded edge tool, J. of Mat. Proc. Technology, Volume 191, Issues 1–3, pp. 331-334.

[31] Özel T., 2009, Computational Modelling of 3D Turning: Influence of Edge Micro-geometry on Forces, Stresses, Friction and Tool Wear in PcBN Tooling, Journal of Materials Processing Tech. vol. 209/11, pp. 5167-5177.

[32] Özel, T., Karpat, Y., Srivastava, A.K., 2008, Hard turning with variable micro-geometry PcBN tools. CIRP Annals—Manufacturing Technology 57, pp. 73–76.

[33] Kountanya, R., Al-Zkeri, I., Altan, T., 2009, Effect of Tool Edge Geometry and Cutting Conditions on Experimental and Simulated Chip Morphology in Orthogonal Hard Turning of 100Cr6 steel, Journal of Materials Processing Technology, Volume 209, Issue 11, pp. 5068-5076.

[34] Aksu, B.,Özlü, E. and Budak, E., 2008, Analysis and modeling of edge forces in orthogonal cutting, International Conference on Manufacturing Engineering, Greece.

[35] Johnson G. R. and Cook W. H., 1983, A constitutive model and data for metals subjected to large strains, high strain rates, and high temperatures, Proc. 7th Int. Symp. On Ballistics, Hague, Netherlands.

[36] Özlü, E., Budak, E., Molinari, A., 2007, Thermomechanical Modeling ofOrthogonal Cutting Including the Effect of Stick-Slide Regions on the Rake Face,10th CIRP International Workshop on Modeling of Machining Operations, Calabria, Italy, August.

[37] Basuray, P.K., Misra, B.K. and Lal, G.K., 1977, Transition From Ploughing to Cutting During Machining With Blunt Tools, Wear, Vol. 43, pp 341-349.

[38] Çakır,E., Karagüzel, U., Olgun, U., Özlü, E., Bakkal, M., Budak, E., 2013 Modeling of Temperature Distribution in Orthogonal Cutting and Experimental Verfication, 4th UTIS Proceedings, pp 129-138.

Appendix 1

An example of contact length calibration simulation results for 12μm hone radiused tool, 250 m/min cutting speed and 0.1 mm/rev feed rate. (Original table is 643 rows)

Tangential Force Error (%)	Feed Force Error (%)	Contact Length Error (%)	Total Force Error Tangential (%)	Total Force Error Feed (%)	ζ	Strain Rate (1/s)	C°	Shear Stress (MPa)	Speed (m/s)	Feed (mm/rev)
39,99	36,35	22,09	26,74	28,46	2,00	43999,03	199,22	648,83	100,00	0,10
39,60	37,65	23,15	26,69	28,12	2,00	43999,03	199,22	648,83	100,00	0,10
39,21	38,94	24,21	26,63	27,79	2,00	43999,03	199,22	648,83	100,00	0,10
39,83	36,97	16,21	26,72	28,30	1,00	43999,03	199,22	648,83	100,00	0,10
39,24	38,96	15,15	26,64	27,78	1,00	43999,03	199,22	648,83	100,00	0,10
39,21	38,94	24,21	26,63	27,79	1,00	43999,03	199,22	648,83	100,00	0,10
39,93	38,04	32,17	26,73	28,02	0,50	43999,03	199,22	648,83	100,00	0,10
39,24	38,96	15,15	26,64	27,78	0,50	43999,03	199,22	648,83	100,00	0,10
39,21	38,94	24,21	26,63	27,79	0,50	43999,03	199,22	648,83	100,00	0,10
39,93	38,04	32,17	26,73	28,02	0,10	43999,03	199,22	648,83	100,00	0,10
39,24	38,96	15,15	26,64	27,78	0,10	43999,03	199,22	648,83	100,00	0,10
39,21	38,94	24,21	26,63	27,79	0,10	43999,03	199,22	648,83	100,00	0,10
39,93	38,04	32,17	26,73	28,02	3,00	96797,87	907,55	185,13	100,00	0,10
39,24	38,96	15,15	26,64	27,78	3,00	96797,87	907,55	185,13	100,00	0,10
39,21	38,94	24,21	26,63	27,79	3,00	96797,87	907,55	185,13	100,00	0,10
39,93	38,04	32,17	26,73	28,02	2,00	96797,87	907,55	185,13	100,00	0,10
39,24	38,96	15,15	26,64	27,78	2,00	96797,87	907,55	185,13	100,00	0,10
39,21	38,94	24,21	26,63	27,79	2,00	96797,87	907,55	185,13	100,00	0,10
39,93	38,04	32,17	26,73	28,02	1,00	96797,87	907,55	185,13	100,00	0,10
39,24	38,96	15,15	26,64	27,78	1,00	96797,87	907,55	185,13	100,00	0,10
39,21	38,94	24,21	26,63	27,79	1,00	96797,87	907,55	185,13	100,00	0,10
39,93	38,04	32,17	26,73	28,02	0,50	96797,87	907,55	185,13	100,00	0,10
39,24	38,96	15,15	26,64	27,78	0,50	96797,87	907,55	185,13	100,00	0,10
39,21	38,94	24,21	26,63	27,79	0,50	96797,87	907,55	185,13	100,00	0,10
39,93	38,04	32,17	26,73	28,02	0,10	96797,87	907,55	185,13	100,00	0,10
39,24	38,96	15,15	26,64	27,78	0,10	96797,87	907,55	185,13	100,00	0,10
39,21	38,94	24,21	26,63	27,79	0,10	96797,87	907,55	185,13	100,00	0,10
39,93	38,04	32,17	26,73	28,02	3,00	96797,87	759,98	282,89	100,00	0,10
39,24	38,96	15,15	26,64	27,78	3,00	96797,87	759,98	282,89	100,00	0,10
39,21	38,94	24,21	26,63	27,79	3,00	96797,87	759,98	282,89	100,00	0,10
39,93	38,04	32,17	26,73	28,02	2,00	96797,87	759,98	282,89	100,00	0,10
39,24	38,96	15,15	26,64	27,78	2,00	96797,87	759,98	282,89	100,00	0,10
39,21	38,94	24,21	26,63	27,79	2,00	96797,87	759,98	282,89	100,00	0,10